THE RECOVERY OF TIN FROM SLAGS BY GASEOUS REDUCTION AND FUMING

by

Sringeri Ramaswamy Chandrashekar

A Thesis presented for the
Degree of Doctor of Philosophy
of the University of London

John Percy Research Group
in Process Metallurgy
Royal School of Mines
Imperial College of Science
& Technology,
LONDON SW7

DECEMBER 1977

ABSTRACT

Reduction of slags of compositions similar to those found in tin smelting practice has been carried out by bubbling pure hydrogen through the melt. The Silica/lime ratios and the FeO contents of the starting slag were varied systematically and it was found that increasing the Silica/lime ratio increased the rates of reduction considerably. However, increasing the FeO level in the starting slag had no effect on the rate of reduction of SnO but resulted in a metal phase richer in iron. The temperature of reduction was varied between 1250° and 1400°C (±5°C) and was found to have no effect on the rates of reduction of SnO or FeO from slags. Increasing the reducing gas flow rate resulted in higher reduction rates.

A mathematical model was developed to give an insight into the kinetics of reduction. Reduction of SnO from slags using hydrogen was shown to be a mixed transport controlled process. The predicted results from the mass transfer model were consistent with the experimental results. Also, slag reduction experiments with 10% H_2 (90% N_2) and pure CO were carried out and the rates were found to be slow. Reduction with 10% H_2 was shown to be a gas phase controlled process using the mass transfer model.

Fuming of SnO during reduction was studied using mass balances and fume losses were found to increase with the reduction potential of the gas used. Fuming of SnO, without reduction, was studied separately by bubbling argon through the melt. The results showed that fuming under an inert atmosphere was a slow process and possibly different in nature to the fuming that occurs during reduction. Quantitative metallography was used to study metal losses due to physical entrappment in slags. Gas flow rate, temperature and the positioning of the gas lance were shown to be important.

Recovery of tin from slags by sulfide fuming was studied by injecting SO_2 with natural gas and air (sub - stoichiometric) into the slag melt. This resulted in higher fuming rates than the more traditional pyrite fuming.

CONTENTS

CHAPTER 1

INTRODUCTION

CHAPTER 1

INTRODUCTION

The art and science of making and treating metals should strike harmony with the availability and cost of energy and raw materials. As the resources and their costs continually change, the search for new processes and attempts to improve the existing ones continue. The days of abundance are long gone and in modern times, larger amounts of less concentrated starting materials have to be processed through metallurgical treatments. Waste materials have even lower metal values and in processing these the emphasis has been on speed and selectivity of techniques to achieve economy and efficiency. The extractive metallurgy of tin offers a striking example of this trend and it was decided to examine a possible new process for the recovery of tin from oxide melts.

Tin is one of the rarest and most indispensable of the base metals. Its extraction embraces, mostly, pyrometallurgical methods. The hydrometallurgy of tin has not found any appreciable application because, cassiterite, the most important ore of tin, is practically insoluble even in concentrated solutions of acids and alkalies. The pyrometallurgical techniques used today are not efficient with regards to the use of energy and the amount of tin lost to waste products. This is partly because of a lack of complete understanding of the problems associated with tin smelting. The fundamental studies on the extractive metallurgy of tin are few and the technical literature available (especially on the thermodynamic and kinetic aspects) is exceedingly small. The comparatively small world output coupled with the tendency towards specialisation and secrecy of tin smelters is thought to be the cause of this situation.

Tin ores usually contain not more than 1·0 percent tin and they are beneficiated to obtain concentrates with 50-70 percent tin, often at very low recoveries of metal. The prevalent tendency of tin smelters to treat only high grade concentrates (60% tin upwards) forbids the production of low

grade concentrates, even though the latter can be produced at higher metal recoveries. Most commonly, the concentrate smelting is done in reverberatory furnaces although blast furnaces and electric furnaces can be used. Crude tin metal and tin rich slag containing up to 25 percent tin are the products of this concentrate or first stage smelting. This slag is re-treated in much the same way as the concentrates except that more reductant and fluxes are added and the temperature of reduction is higher (upto 1500°C as against 1250°C for the first stage smelting). Slag smelting or the second stage yields 'hardhead', a 20 wt.% iron-tin alloy and a slag still rich in tin (upto 5 wt.%). Economics permitting, a further treatment on this is carried out. The final slag may still have high tin values (more than 1%) and represent a serious metal loss.

The sulfides, chlorides and to a lesser extent, the monoxide of tin are volatile and this fact has been made use of to remove tin from the slags, most commonly from the slag from the second stage. A sulfidising agent like FeS_2 or ZnS is added and tin is fumed off in a blast furnace, reverbertory furnace or a converter. The chlorides tend to be corrosive. Tin monoxide fuming is, at present, a nuisance in conventional tin smelting operations and not an industrial process used to recover tin.

In sulfide fuming, the fume that is produced is difficult to handle and its smelting results in a large recycling dust load, due both to carry over of the fine material during smelting and to the production of further fume resulting from the sulfur content of the charge. Also, getting rid of sulfur dioxide could prove expensive if legislation does not allow its venting to the atmosphere. Generally the SO_2 concentrations in the flue gas are too low to make the production of sulphuric acid economical.

Tin pyrometallurgy faces two serious problems. The first of them is due to iron. The concentrates always contain appreciable quantities of Fe_2O_3 (upto 15 wt.%). This is reduced in the first stage and enters the slag as FeO.

All the unreduced tin in the first stage remains in the slag as SnO. By virtue of the fact that both SnO and FeO have similar free energies of formation, preferential reduction of SnO becomes difficult in the subsequent stages of smelting. With a view to win most of the tin if strong reducing conditions are used, a lot of FeO would be reduced as well and the product metal would be heavily contaminated with iron. While, in order to obtain a pure metal product if milder reducing conditions are sought, most of SnO remains unreduced and is lost to the slag.

Separation of iron from tin is difficult. When an iron-tin alloy is cooled a mushy dross of Fe-Sn intermetallic compounds is precipitated. If the original iron content of the alloy is high, then the yield of tin metal after skimming this dross is low. The dross is returned to the smelting but the iron recycles perpetually carrying a fixed amount of tin with it. The limiting factor is the iron content of the primary slag which is the sum of iron in concentrates and iron in hardhead.

The second major problem in tin extraction arises because of the inefficiency of the process used to carry out the smelting operations. In the reverberatory, heat transfer to the charge is by radiation from a source at a considerable distance. Once the slag is formed, the mode of heat transfer is by radiation and conduction through the slag layer. Also as the bath remains quiescent, mass transfer rates are low. Thus long smelting times (8-12 hours) are necessary. The practice of slag stockpiling in between different stages leads to serious losses of heat content of slags. To heat the stockpiled slags to the higher temperatures required for subsequent treatment involves tremendous energy costs.

All the above said troubles are more acute for treating low grade concentrates, because low grade concentrates produce more slag and hence the treatment of more unwanted material is required. But the production of low grade concentrates is far easier and the metal recoveries from

the ore are far higher. To treat the low grade concentrates economically, an efficient way of treating slags must be first found.

These problems were recognised in as long ago as 1957[1] and since then there have been many ventures to find alternative processes for slag treatment. Reduction with coke[2,3] and/or other solid reductants like ferrosilicon[(1)] were tried by different workers. Different kinds of furnaces (electric, rotary and laboratory furnaces) were tried to achieve good mixing of phases and the experiments were carried out on laboratory and pilot plant scales. Where good tin recovery was achieved[1] the alloy produced analysed 70 percent iron and in other cases[2,3] more than 6 percent of tin was left in the slag. Also, long times of reduction were needed. As there was not good slag/reductant contact (in the rotary furnace the coke floated on the slag) all the characteristic problems of reverberatory furnace smelting prevailed.

To obtain the necessary stirring and mixing of phases, bubbling gases through melts has been known for sometime. Kenworthy et al[1] tried gaseous reduction of tin slags to 'liberate tin from complex silicon molecules' and 'fixed' it with chlorine/sulfur to fume it off. More recently Floyd and Thurlby[4] demonstrated that tin slags can be reduced successfully by bubbling reducing gases through them.

All the work so far has been in search of alternative processes and so can indicate the feasibility of the new ideas. As such no firm conclusions regarding the effect of different parameters on tin slag reduction can be made. To appreciate more fully the problems associated with the tin extraction a more fundamental approach is called for.

In the present work, tin slag reduction has been studied through systematic variation of the different variables involved to elucidate their effects. Reduction has been carried out using pure hydrogen. Forming gas (10% Hydrogen) and pure carbon monoxide were also tried. Temperature was controlled accurately and its effect has been studied in the

range 1250°C-1400°C. For the first time, the 'nuisance' of tin extraction, the iron reduction from tin slags, has been looked at. Slag composition was varied systematically. A mathematical model is proposed which gives an insight into the complicated gas/slag reactions.

Tin recovery by slag fuming (sulfide fuming) was studied. Sulfidising gases were bubbled through the slag and this was compared with the traditional pyrite fuming.

Tin losses during extraction were also investigated into. Stannous oxide fuming represents a kind of tin loss and this was studied by bubbling pure Argon through the slag melt. By using a gas tight enclosure, fairly accurate mass balances have been written which allowed a study of 'fuming losses during reduction'. The problem of metal losses due to physical entrapment in slags has been briefly looked into.

CHAPTER 2

PREVIOUS WORK

CHAPTER 2

PREVIOUS WORK

2.1: STANNOUS OXIDE

2.1.1: Stability and Melting Point

SnO is known to decompose on heating. It undergoes a disproportionation reaction of the type

$$2SnO = Sn_{(l)} + SnO_{2(s)} \quad (1)$$

at temperatures above 175°C.

Carbo Nover and Richardson[5] have worked on the stability of SnO by holding an equilibrium mixture of SnO and Sn at temperatures between 900 and 1250°C. They found that SnO was stable above 1100°C. Other workers[6,7] suggest 1080°C to be the corresponding temperature. The more recent work of Seshadri[8] confirms the value of 1100°C. He found that SnO_2 content of "Stannous oxide" does not exceed 4·0 mole percent.

Carbo Nover and Richardson[5] calculate the melting point of SnO to be 977 ± 30°C. 1000°C[9], 1040°C[6] and 1075°C[10] have all been suggested as the melting point of SnO. Direct measurement of the melting point of SnO is difficult because of its instability around this temperature. Hence, the values quoted refer to the temperature at which $Sn_{(l)}$, $SnO_{(l)}$ and $SnO_{2(s)}$ coexist. From the above one could conclude that SnO is stable and liquid above 1100°C. In this work, however, it is SnO dissolved in slags that is primarily of interest.

2.1.2: Free Energy of Formation

There exist little data to calculate the free energy change for the reaction

$$Sn_{(l)} + \tfrac{1}{2}O_2 = SnO_{(l)} \quad (2)$$

P.A. Wright[11] has brought together some work related to the topic but only those valid for 1300°K or more, which are relevant to the present work are referred to here. Carbo Nover and Richardson[5] use the saturation solubilities of oxygen in tin in equilibrium with solid SnO_2 and liquid SnO, together with the free energy of formation of SnO_2 to

estimate that the free energy change of the reaction

$$Sn_{(1)} + \tfrac{1}{2}O_2 = SnO_{(1)} \qquad (2)$$

to be, $\Delta G^\circ = -64{,}400 + 21{\cdot}375T$ (± 280 cals) (3)

Assuming a value for the heat of fusion for SnO as 7·0 K.cals./mole (based on a comparison of ΔHf for similar oxides, PbO 6·2 K.cals./mole and FeO 7·4 K.cals./mole) Davey and Floyd[12] calculate the ΔG° value for the formation of $SnO_{(1)}$ at 1423°K to be - 33,950 cals./mole. Using the values for the ΔG° formation for $SnO_{(s)}$ at other temperatures taken from Elliott and Gleiser[13] and the above ΔH_f value for SnO, one can calculate for reaction (2)

$$\Delta G^\circ = -62{,}000 + 20{\cdot}00T \qquad (4)$$

Kozuka etal[14] give the expression

$$\Delta G^\circ = -64{,}300 + 21{\cdot}4T \text{ cals} \qquad (5)$$

to be valid in the temperature range 1050°- 1150°C, using an emf cell of the type

$$Ni, NiO/ZrO_2 - CaO/SnO,Sn$$

The three expressions given above for the free energy of formation per mole of liquid SnO agree with each other within experimental errors. Equation (6), an average of the above three equations, has been used in the present study.

$$\Delta G^\circ = -63{,}566{\cdot}7 + 20{\cdot}93 \ (\pm 250) \text{ cals./mole} \qquad (6)$$

2.1.3: Vapour pressure of SnO and SnS

Stannous oxide is volatile. Its vapour pressure has been measured by different workers and their results are not in complete agreement with each other[11]. Colin et al[15] have successfully explained this by proving the existence of the polymeric gas molecules Sn_2O_2, Sn_3O_3 and Sn_4O_4 using mass spectrometry. Exactly how $SnO_{(g)}$ forms from $SnO_{(1)}$ is still a matter of speculation. Kellogg[16] has proposed two ways; either by reduction of $SnO_{2(c)}$ or oxidation of $Sn_{(1)}$. He has argued that an optimum value of P_{SnO} at any temperature depends on the equilibrium

$$SnO_{2(c)} = Sn_{(1)} + 2SnO_{(g)} \qquad (7)$$

Stannous sulfide also has high vapour pressures and

this fact has been made use of in tin fuming processes. P.A. Wright[11] gives the following expression describing the partial pressure of SnS as a function of temperature

$$\log_{10} P_{mm} = \frac{-9980}{T} + 9{\cdot}551 \qquad (8)$$

The vapour pressures of $Sn_{(l)}$, $SnO_{(l)}$ and $SnS_{(l)}$ are plotted in Fig. 2.2 for temperatures greater than 1100°C. Equation (8) has been used to calculate P_{SnS}, while the works of Cochran and Foster[17] and Platteeuw and Meyer[18] have been used for P_{Sn} and P_{SnO} respectively.

2.2: TIN-IRON SYSTEM

This binary system is of great importance in tin metallurgy and a knowledge of the mutual solubilities, the phase diagram and the activities of the components is essential to understand and improve smelting and refining techniques. Experimental determinations of the thermodynamic properties of liquid tin-iron solutions are very few.

2.2.1: Phase diagram

Fig. 2.1 shows the phase diagram of the Sn-Fe system[11]. This diagram is based on that published by the Tin Research Institute[19] coupled with the liquidus of Campbell, Wood and Skinner[20] and adjusted above 1000°C to fit the work of Mills and Turkdogan[21] on the two liquid region. Davey[22], including additional low temperature liquidus points from Kakovskii and Smirnov[23], has plotted a graph of concentration of iron versus reciprocal of temperature. He noted that the solubility of iron in tin was not in doubt up to 1000°C, but that more accurate work above this temperature was necessary.

Shiraishi and Bell[24] have measured the solubility of iron in tin in the temperature range 1145°- 1490°C. Because the furnace used in their experiments did not withstand higher temperatures, they could not determine the consolute point. However, by assuming a sub-regular solution model, they calculate the consolute point as 1630°C. In fig. 2.1 the points shown are due to them.

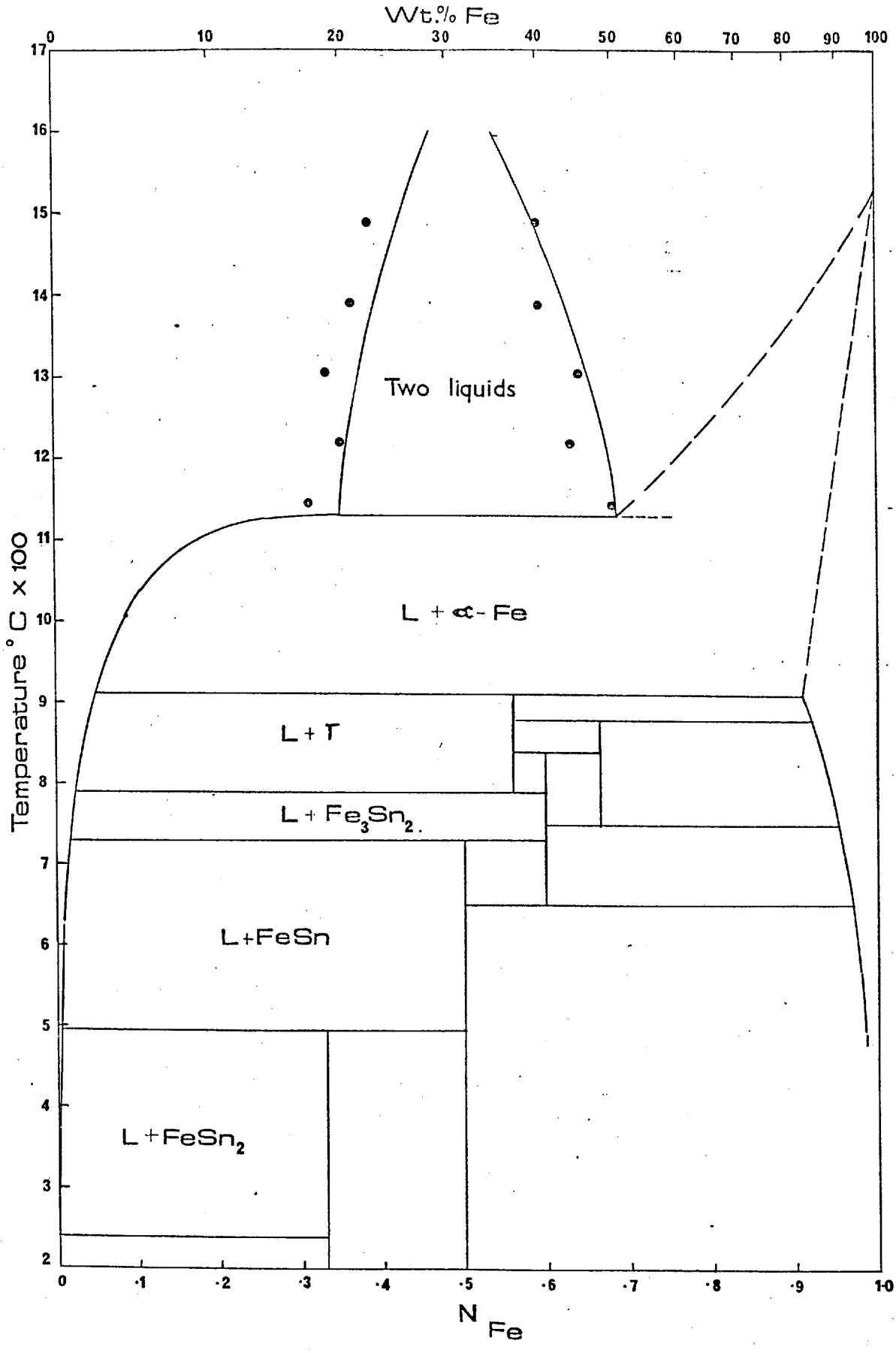

Fig. 2.1: The phase diagram for the Tin-Iron system.

• The experimental points of Shiraishi and Bell[24]

2.2.2: Activity of tin and iron in binary solutions

The only experimental determination, so far, of the activity of tin in the tin-iron binary is that done by Shiraishi and Bell[25]. In his excellent paper[26], Davey reviewed the previous estimates[11,12] and offered a new one. He made different estimates based on (1) regular solution behaviour, (2) sub-regular solution behaviour and (3) Lumsden's method (which is a refinement of the regular solution model taking into account (a) the difference in atomic size of pure components and (b) lack of perfect configurational randomness arising from deviation of AB bond energies from the mean of AA and BB bond energies).

Fig. 2.3 shows the relative agreement between the different models. Based on the fact that at the miscibility gap limit (tin-rich end) γ_{Fe} should be 1·95 (Appendix 1) Davey proposed the following expressions.

$$\log \gamma_{Fe} = -0{\cdot}072 + 0{\cdot}85N_{Sn}^2 \qquad (9)$$

$$\log \gamma_{Sn} = 0{\cdot}85N_{Fe}^2 \qquad (10)$$

Making use of the fact that there exists a large difference in vapour pressures between tin and iron in the temperature range 1200°- 1500°C (ratio is greater than 10^7) Shiraishi and Bell[25] determined the activity of tin in tin-iron alloys using the measurement of the vapour pressure of tin. Activities of iron in the system were calculated by Gibb's - Duhem integration. They give the following expressions for the activity coefficients.

$$\log \gamma_{Sn} = 0{\cdot}6125N_{Fe}^2 + 0{\cdot}3709N_{Fe}^3 \qquad (11)$$

$$\log \gamma_{Fe} = 1{\cdot}169N_{Sn}^2 - 0{\cdot}371N_{Sn}^3 \qquad (12)$$

In Fig. 2.4 the activity values are plotted against composition using Davey's estimate (equations 9 and 10) and the above expressions for the activity coefficients. Both sets strictly apply only to the high tin region. The values used in this work are due to Shiraishi and Bell.

2.3: TIN SLAGS

2.3.1: Composition and Properties

The most common impurities in tin ores are Silica,

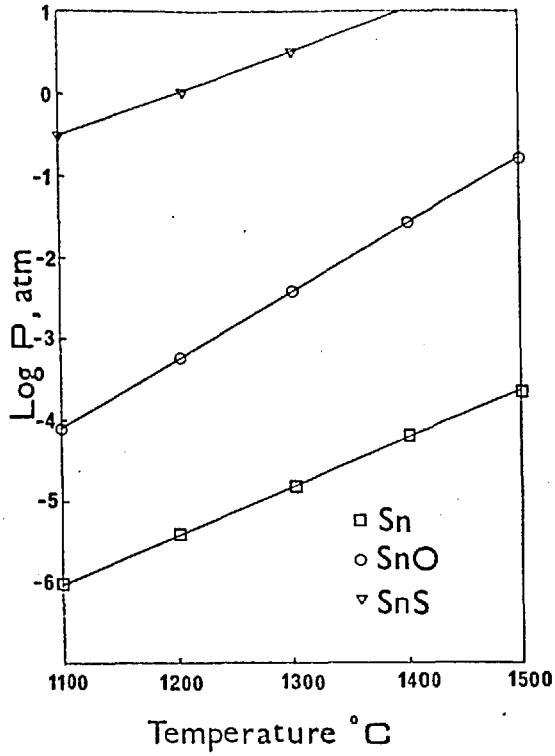

Fig. 2.2: Comparison of volatility of different species of tin.

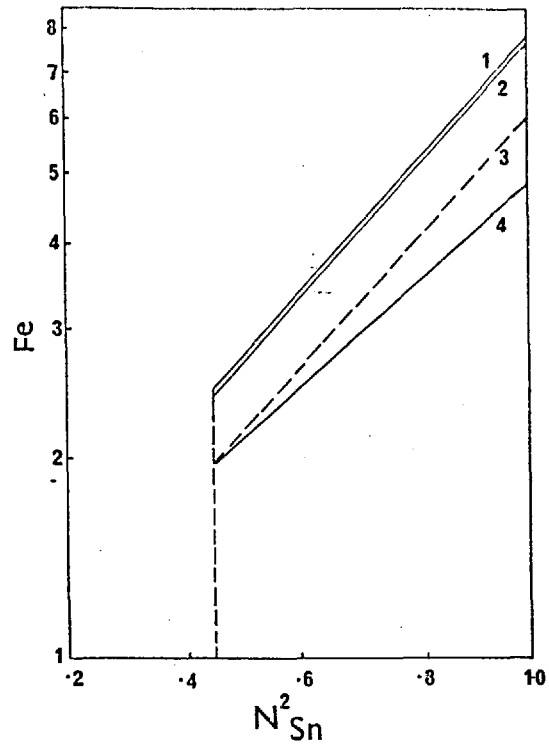

Fig. 2.3: Different solution models for γ_{Fe}.
1. Lumsden's method
2. Sub-regular solution
3. Davey's estimate
4. Regular solution.

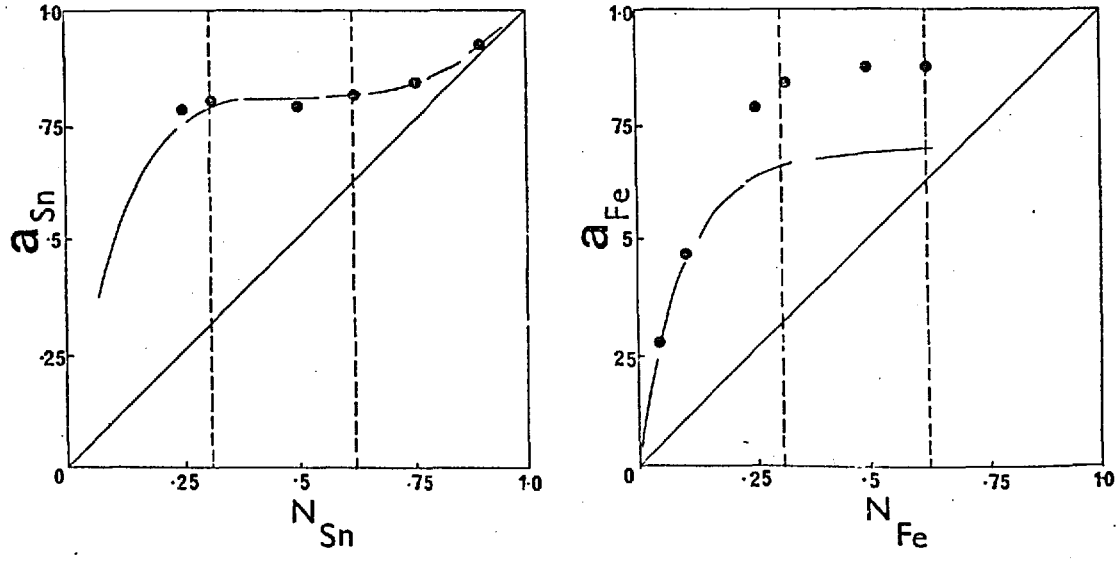

— Davey[26]
• Shiraishi and Bell[25]

Fig. 2.4: Activities of tin and iron in the binary

alumina and the oxides of iron. Lime is added as a flux during smelting. Generally, the slag compositions fall in the following range (in weight percent).

SnO	FeO	CaO	SiO_2	Al_2O_3
3-25	10-40	5-30	20-40	up to 10

Other oxides may also be present. Tin and iron are present predominantly as stannous and ferrous ions. SnO_2 has a low solubility in slags[27].

Keysselitz and Kohlmeyer[9] determined the melting point of stannous meta-silicate (SnO - SiO_2) as 890°C. Tin slags start melting around this temperature and melting is complete by 1150°C (the first stage of tin smelting is carried out at about this temperature). In alumina-containing slags, compositions containing about 10 wt. % alumina have the lowest melting points[28]. FeO also decreases the liquidus temperature.

The viscosity of slags is an important parameter. A knowledge of the viscosity and the effect of other variables on it is useful in achieving good results during reduction[2] and to reduce metal losses in slags. The few slag viscosity measurements that are available are for steelmaking slags. FeO is known to increase the fluidity of silicate melts[30,33,34]. SnO and FeO behave similarly in silicate melts (Fig. 2.5) and their charges and even the cationic radii (0·83Å and 0·81Å respectively) are the same[32]. Hence it is reasonable to assume that SnO has the same effect on the viscosity of slags as FeO. To get an idea of the viscosity of tin slags all SnO can be considered to be FeO on a molar basis. Many models[29,30] relating composition to viscosity are available. The values are likely to fall between 2 and 9P for low FeO (10 wt. %) and between 2 and 6P for high FeO slags (40 wt. %) in the temperature range 1250 - 1400°C.

Tin slags are highly corrosive and the difficulty of finding a suitable containing material has been experienced by all workers in the field. Also difficulties arise due to the volatile nature of SnO.

2.3.2: Slag-Metal Equilibrium

The equilibrium distribution of tin and iron between metal and slag phases is governed by the reaction

$$SnO_{(s)} + Fe_{[M]} = FeO_{(s)} + Sn_{[M]} \qquad (13)$$

(s) and [M] denoting slag and metal phases respectively. The importance of this reaction can not be overstressed as the final tin contents of the slag and metal depend on it. The standard free energy change of this reaction is given by

$$\Delta G^\circ = 7946{\cdot}7 - 10{\cdot}1T \ (\pm 500) \text{cals.} \qquad (14)$$

The calculations are shown in Appendix 2. The variation of the equilibrium constant with temperature is small.

The work of Davey and Floyd[12] seems to be the first important study of the above equilibrium. They contacted slag-metal samples and approached equilibrium from both (high tin slag - high iron metal, low tin slag - pure tin metal) sides. Generally the slag compositions were similar to the ones found in tin smelting practice. The experiments were conducted at 1150°C in ceramic crucibles. The stirring of the phases was only occasional, using an iron rod. After finding that 30 minutes of contacting time was insufficient they equilibrated slag and metal phases for upto 90 minutes.

After analysing the final slag and metal phases for tin and iron, they expressed their results in terms of an empirical distribution coefficient

$$K = \left[\frac{\%\ Sn}{\%\ Fe}\right]_{metal} \times \left(\frac{\%\ Fe}{\%\ Sn}\right)_{slag} \qquad (15)$$

This varied from 300 for metal which was pure tin (representing the first stage tin smelting) to about 100 for metal of miscibility gap composition (second stage tin smelting). The distribution coefficient was a useful parameter to characterise the efficiency of any smelting operation and its dependence on metal composition was as expected from thermodynamic considerations. They worked mostly on high iron slags and metal high in tin for which, any failure to achieve equilibrium would give optimistic values for K.

Harris and Hallett[31] conducted similar experiments

and confirmed the κ values of about 300 for the first stage smelting. However, they observed κ values nearer to 50 for metal compositions found in the miscibility gap region (as opposed to 100 of Davey and Floyd).

Davey and Floyd[12] correlated the distribution coefficient κ and the equilibrium constant K_{eq} for reaction 13 by the equation

$$\log \kappa = \log \frac{K_{eq}}{S} + \beta(1 - 2N_{Fe}) \qquad (16)$$

where,

S is the ratio of the activity coefficients of FeO and SnO $\left(\frac{\gamma FeO}{\gamma SnO}\right)$

and β is the interaction coefficient (regular solution model).

In deriving equation (16) they assumed that S remained a constant with respect to tin and iron concentrations in the slag and that the alloy was a regular solution. Thus a plot of $(1-2N_{Fe})$ Vs log κ would be a straight line, from the intercept of which K_{eq} could be calculated if S were known. They found that the ΔG° values for reaction 13, calculated using the intercept (taking S = 1) and an independent set of calculations (similar to those in Appendix 2) agreed within experimental errors and the errors in the ΔG° values used for FeO and SnO in the calculations. There was no appreciable difference in the experimental results for high and low iron (low and high tin) slags. The lime/silica ratio in the slag did not seem to have any notable influence on the tin-iron equilibria. It was fairly clear that equilibrium between slag and metal had been achieved during the 1½ hours of contacting.

Harris and Hallett[31] have demonstrated that while equilibrium can be easily achieved (within half an hour of contacting) from the high tin (in slag) side, it was uneven and slow in the case of high iron slags. Recognising the fluidity of slags as a major factor, they attributed the large differences in times to approach equilibrium (½ hour for tin rich slags and 18 hours or more for iron rich slags)

to the difference in fluidities between tin rich and iron rich slags. They suggested that the diffusion of SnO away from the metal/slag interface into the slag was the rate controlling step.

2.3.3: Activity of SnO in slags

Fig. 2.5 shows the relative 'affinities' of SnO, FeO and lime towards silica. A small increase in the activity of SnO would be expected when FeO is added to a binary melt of SnO and silica,and the increase would be very much larger if lime is added instead. However, a more interesting situation exists if lime is added to a ternary of SnO + FeO + SiO_2. Both a_{SnO} and a_{FeO} would be expected to increase. To have reliable quantitative data, however, activity measurements on the quaternary slags should be made.

Seshadri[8] has measured the activity of SnO in ternary melts (SnO + FeO + SiO_2 and SnO + CaO + SiO_2) by equilibrating them with pure liquid tin via the gas phase. By measuring the oxygen content of the equilibrated tin and using "pure" liquid SnO(a = 0·9, ref.5) as the standard, he has calcul- the a_{SnO} in slags. It can be seen from his results that the values for γ_{SnO} are nearly 1·0 in FeO-containing melts and 2·0 in lime-containing melts. It is perhaps significant that γ_{SnO} does not vary appreciably with N_{SnO}, in the range of N_{SnO} values used (0·25 to 0·4 and 0·2 to 0·53). Whether this is true for very low N_{SnO} values (0·1 and well below 0·1, as in industrial slags) is difficult to know.

While the experimental temperature (1250°C) was near the tin smelting temperatures, the SnO levels in the slags used in the above work were very much higher than those found in practice. If this was because low SnO slags did not give measurable oxygen transfer to tin metal, a different method of activity determination should be used for industrial slags. Also, activity determinations on melts containing both lime and FeO would have been helpful in knowing the effect of the 'competition' between SnO and FeO.

From Watanabe's work[35], Wright[11] has shown that lime

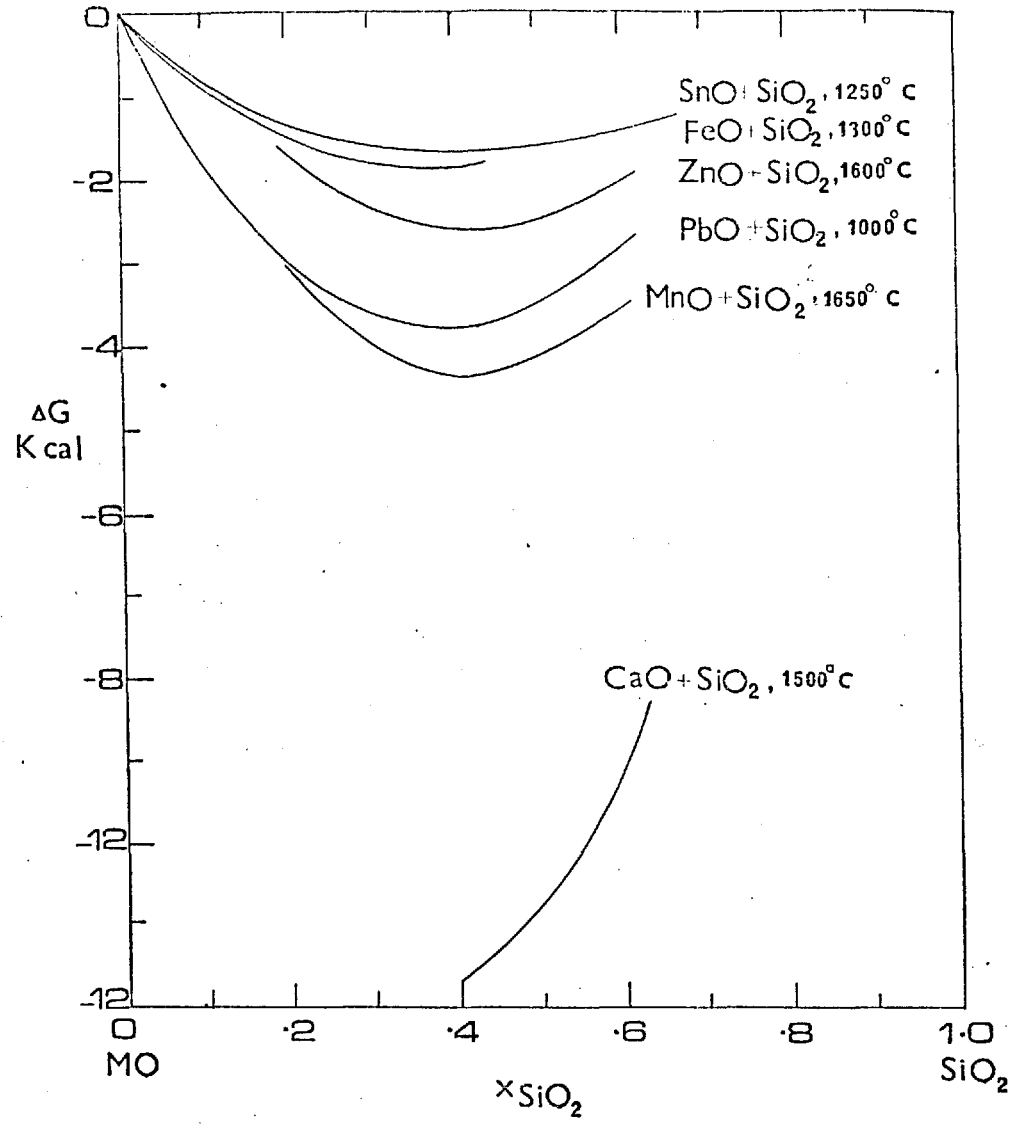

Fig. 2.5: Integral free energy of mixing curves for binary silicates.

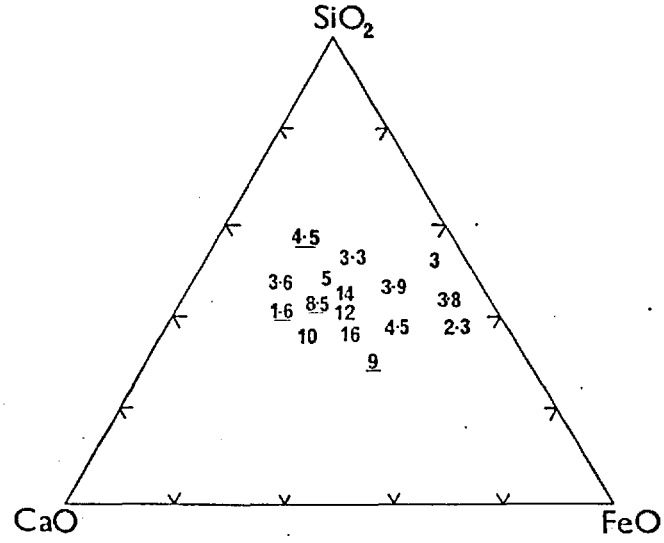

Fig. 2.6: Activity coefficient of SnO (less than 10 wt.%) in slags. The values underlined were estimated by the investigator. The rest are due to P.A. Wright[11]

increases the activity coefficient of SnO more than that of FeO. Chizikov and Khazanov[36] equilibrated synthetic CaO-FeO-SiO_2 slags with metallic tin in alumina crucibles at 1200°C. They have determined the tin and iron contents of the equilibrated slag and metal phases. P.A. Wright[11], making certain simplifying assumptions, taking the activity values for FeO at 1260°C from Bodsworth's[37] work, has calculated a_{SnO} and γ_{SnO}. From his own account, the approximations were too numerous and the γ_{SnO} estimated cannot be expected to do more than show the order of magnitude (Fig. 2.6). This approach is believed to be valid and would give correct values if it can be shown that equilibrium between the slag and metal had been reached and/or more accurate values for K_{eq} were available.

This was the method chosen by Biswas and Rankin[38] who plotted K, the empirical distribution coefficient versus $(1 - 2N_{Fe})$. (See section 2.3.2). From the intercept they calculated the ratio of the activity coefficients of FeO and SnO. However the slags used in their work did not contain lime. The comparison of their results with that of Davey and Floyd[12] shows that lime increases the ratio $\gamma_{SnO}/\gamma_{FeO}$.

Using the tabulation of S values from Davey and Floyd's work given by Biswas and Rankin in conjection with the a_{FeO} from Bodsworth's work[37], γ_{SnO} values have been calculated. These values, along with P.A. Wright's[11] estimates are shown in Fig. 2.6. This again is thought only to show the approximate values. It is interesting that the γ_{SnO} values (SnO contents of these slags are from 1 - 10 wt. %) seem to be very high at the centre of the triangle. In view of the approximations involved in arriving at this diagram, it is thought best if no firm conclusions are drawn from it.

2.4: RECOVERY OF TIN FROM SLAGS

2.4.1: Reduction

The need to process slags efficiently and reduce the tin content of discard slags has always existed. Not surprisingly, it was thought that this could simply be done by intensifying the reduction process through which the

slag had previously passed. Kenworthy et al[1] tried to win tin and tungsten from tin slags by "fusion reduction". Slags (1·3% tin, 0·8% tungsten and 7 - 10% iron) were reduced in graphite crucibles at 1600°C using coke and/or other reductants (ferrosilicon, calcium carbide, silicon, silicomanganese, ferromanganese etc.). While the metal recoveries were high (slags after reduction had no more than 0·1% tin or tungsten) the metal contamination was too high for economic refining. Tin and tungsten together did not total more than 20% in the alloy while the iron content was more than 70%. Trials of repeated additions of reductant and flux in a reverberatory furnace did not reduce the tin content of slags below 3 wt. %[39].

Katkov[2] conducted reduction using coke with graphite rod stirring on slags containing 17 and 27% tin at various temperatures. He noted that coke floated on the melt and that reduction rates were appreciable only when the slag had good fluidity. Also, the tin losses to the gases as SnO decreased with increase in temperature. He advocated temperatures of 1500°C or more for slag reduction.

Davey[3] proposed the use of a rotary furnace to achieve good mixing of the constituents during smelting. In the trials it was found[41] that reduction did not proceed at reasonable rates and after 10 hours of smelting at 1200°C, more than 6% of tin remained in the slag. The reasons for the failure of the rotary furnace were that (a) coke floated on the melt and hence the rotary action of the furnace did not provide good mixing of the reductant and slag and, (b) the high temperatures necessary for slag reduction using solid reductants, could not be achieved in the rotary furnace.

Floyd and Thurlby[4] obtained good reduction of slags when they injected reducing gases into the melt. Large reductant/slag contact area was obtained by the introduction of bubbles and good mixing of slag resulted as the bubbles rose to the surface. They found that the entrainment of the solid reductant (char powder) with methane, Natural gas and hydrogen had no observable effect on reduction rates. They

clearly demonstrated the feasibility of the process (bringing the tin content from 8% to less than 1% in two hours of reduction). However, their conclusions regarding the effect of different parameters on reduction and fuming are open to doubt as they changed more than one variable from one experiment to the next. (They noted that increasing temperature reduced the tin content of slags rapidly while in a later work Floyd[40] found little effect of temperature on reduction rates). It is apparent that a more fundamental and careful study of the process is necessary.

Floyd[42] has described submerged combustion (partial burning of the reducing gases in the melt) to make up for heat losses and the endothermic nature of reduction reactions. The reduction reactions involved in tin smelting are only slightly endothermic (1700 cals per mole of SnO reduced for tin reduction with hydrogen and FeO reduction with hydrogen may not even be endothermic. Calculations are shown in Appendix 3 for hydrogen reduction). The reduction rates in submerged combustion do not appear any better than in gaseous reduction (Fig. 2, ref. 42). Thus, partial combustion of reducing gases is only useful as an efficient way of supplying heat to the reactants.

2.4.2: Fuming

The process of metal recovery from low tin slags (5% or less) is generally carried out by forming stannous sulfide. This is highly volatile (boils at 1230°C, Fig. 2.2) and fumes off liquid slags. A metal sulfide MS is added which reacts with the SnO in the slag as follows

$$MS_{(s\ or\ l)} + SnO_{(slag)} \rightarrow SnS_{(g)} + MO_{(slag)} \qquad (17)$$

FeS_2, ZnS, CaS are used for this purpose. Pyrite (FeS_2) is the most common as it has the highest Sulfur potential. Reaction 17 follows first order reaction kinetics[11] with respect to SnO concentration.

Reverberatory furnaces, Converters, Blast furances or other kinds of shaft furnaces[11] are used for the fuming process. The tin recoveries are usually 70 to 90% and the

pyrite requirements are about 5 - 10% of the charge. The reverberatory furnace fuming is different, requiring 10 - 20% pyrite addition and producing 50% tin recovery. For shaft furnace fuming, improved charge distribution[11], (composition and size), oxygen enrichment of the blast[43] and fuel injection[44] have all had the desired effects of better utilization of the reductant and optimum fuel requirements. Fluidity of slags was important and pyrite added as lumps was found to have better utilization than powder[45].

Kenworthy et al[1] carried out laboratory fuming tests holding slags in graphite crucibles at around 1550°C and providing sulfur in various forms - elemental sulfur, pyrite, methyl mercaptan (CH_3SH) and Hydrogen Sulfide. All provided more or less the same efficiency of fuming, 85% recovery on 1·3% tin starting slags, except elemental sulfur which gave about 70% recovery. They recognised the need for a reducing agent e.g. coke, "to liberate tin from the complex molecules in slag" before fixing it with sulfur. Mattes containing less than 0·2 wt. % tin were obtained when excess sulfur was used. A metal layer containing less than 0·2 wt. % tin (mostly iron) was always obtained. They bubbled the gases through the melts in most cases and this gave high fuming rates.

2.5: TIN LOSSES

2.5.1: Stannous Oxide fuming

While sulfide fuming is established as a method for beneficiating tin from slags, fuming of tin monoxide is yet to find an application as a method for tin recovery. Even though the possibility has received some attention[46,47,56-58] for the present at least, tin monoxide volatility is not made use of. It occurs in all tin smelting operations and represents a loss of tin from the main process stream.

The oxide fuming 'during reduction' deserves attention. Floyd and Thurlby[4] believe that addition of lime to slags and increase in reduction temperature increase SnO fume losses. Katkov[2] notes than an increase in temperature decreases the tin losses to gases. As their mass balances (from which the tin losses were determined) were not sufficiently accurate,

the observations are not thought to be reliable. Laboratory tests have shown[47] that, as the conditions are made more reducing the tin losses (from slags) to gases increase. Vigorous fuming of SnO from slags takes place under reduced pressure[46,47].

2.5.2: Metal Entrapment

Metal and matte losses in slags due to physical entrapment are a familiar, but serious kind of loss. It was first noticed in a reverberatory furnace during copper matte smelting when the matte was floated up into the slag phase by the rising SO_2 bubbles. The matte remained in the slag because of slow settling, due to high slag viscosities and/or tiny size of the droplets themselves. Formation of rafts of matte particles at the slag surface also prevented settling[48].

Metal losses in slags occur similarly and the flotation of metal upwards can happen in two ways. (1) The metal forms a thin film on the bubble and enters the slag phase. When the gas escapes at the slag/gas interface, the metal film ruptures and the tiny droplets formed during the process would be held in the slag. (2) If the wake behind the rising bubble is strong, droplets from the metal pool get caught in it and are forced upwards.

Minto and Davenport[49] define the following parameters characterising the mechanism of flotation.

$$\gamma_{G/S} - \gamma_{M/G} - \gamma_{M/S} = \Phi \text{ (film coefficient)} \qquad (18)$$

$$\gamma_{G/S} - \gamma_{M/G} + \gamma_{M/S} = \Delta \text{ (flotation coefficient)} \qquad (19)$$

where γ - interfacial tension, G, M and S are gas, metal and slag phases respectively. For an intact film Φ must be positive and for the flotation mechanism to operate Δ must be positive. Obviously a knowledge of interfacial tensions is necessary to find Φ and Δ and often these are not available. It can be noted that from the above equations

$$\Phi = \Delta - 2\gamma_{M/S} \qquad (20)$$

and hence, higher values of Δ also make Φ more positive. Thus film formation (or stability) represents the stronger,

ultimate case for flotation.

Once the metal is floated to the slag phase the physical properties of the slag and the fluid mechanics of the situation control settling. The effect of temperature, by reducing the slag viscosity and surface tension is obvious and super heating is advisable[50]. However, steep thermal gradients, if present, set up convective currents which, like turbulence in the melt, can hinder settling. Turbulence also increases the probability of collision between entrapped droplets which would help coalescence and settling. In tin slag reduction it was found[59] that, as the iron content of the metal increased the conditions for flotation became less favourable as iron increased the density and surface tension of the alloy.

CHAPTER 3

EXPERIMENTAL

CHAPTER 3

EXPERIMENTAL

Two kinds of experiments were performed in all, viz reduction and fuming experiments. The apparatus, techniques and the procedure used were nearly the same for both. Reduction was carried out using pure hydrogen, forming gas (10% H_2) and pure carbon monoxide. Tin recovery by fuming was studied using pyrite addition and by bubbling sulfur containing gases (SO_2 + CH_4 + air) through the melt.

Stannous oxide fuming (which represents tin losses) was studied by bubbling pure argon through the slag and this was very similar to the reduction runs in its experimental aspects. To study the metal losses due to physical entrapment in slags, quantitative metallography was used.

A gas tight enclosure and induction heating were used. A Pt-Pt/13%.Rh thermocouple was used to measure the temperature and the control was manual. The details for the reduction experiments are described first and in section 3.2.4, the relevant additional information for the fuming runs are given.

3.1: APPARATUS

3.1.1: Reaction Vessel

The schematic diagram is shown in Fig 3.1. The large pyrex vessel (55 cms. tall, 27·5 cms across with ·3 cm. thick wall) placed in the induction well had a flat ground glass flange (2·5 cms. wide) at the top; the bottom side of the water cooled brass lid was ground as well. High vacuum silicone grease used in between gave the necessary gas tightness. A graphite cylinder positioned inside the pyrex container acted as the high frequency susceptor and was the heat source. The refractory crucible holding slag was placed inside the graphite susceptor.

3.1.2: Brass Lid

The pyrex vessel was closed at the top using a

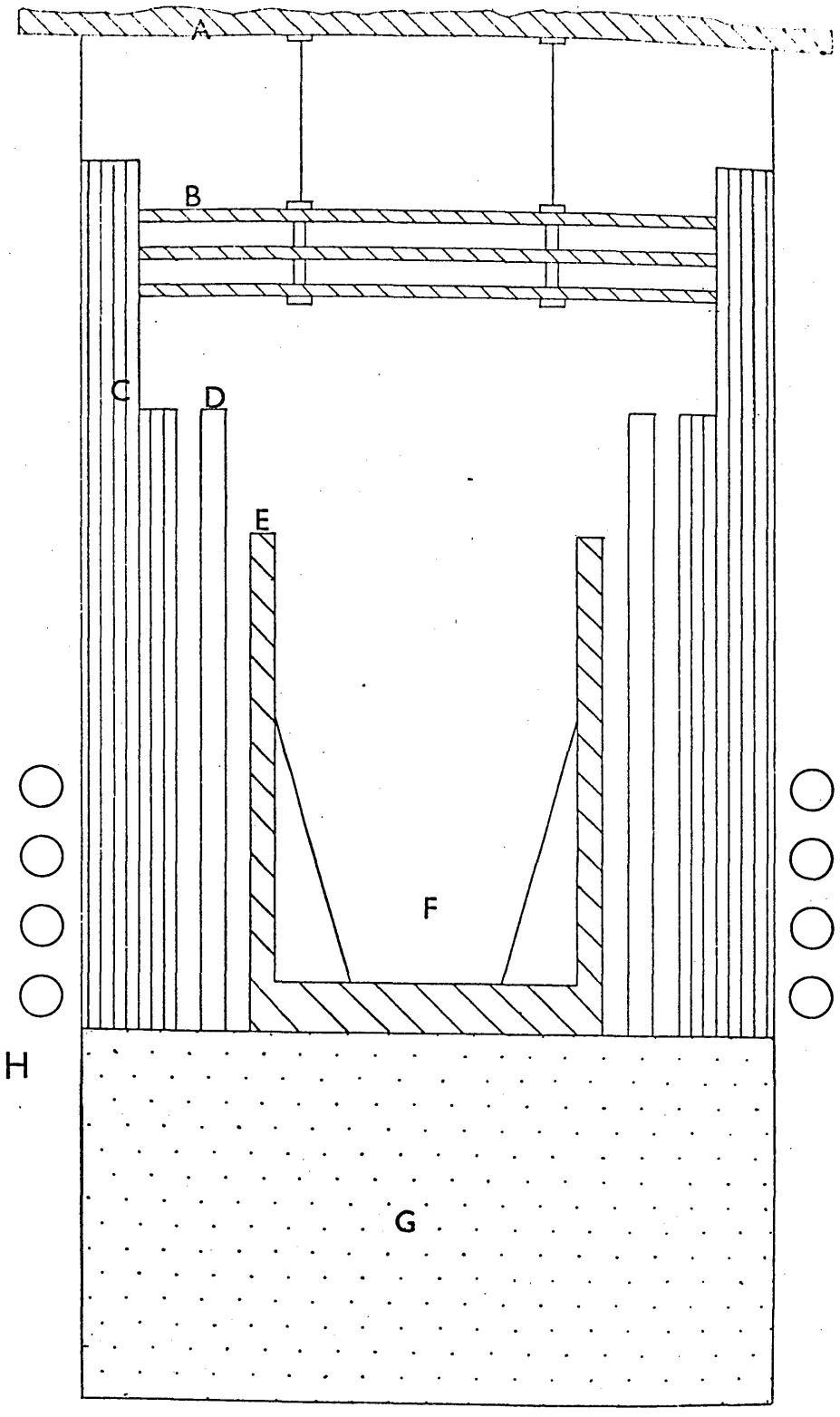

Fig. 3.1: The schematic diagram of the apparatus.

A - Brass lid B - Radiation shields
C - Kaowool blanket D - Silliminite tube
E - Graphite susceptor F - Alumina crucible
G - Calcined alumina powder.
H - Induction coil

water-cooled brass lid (Fig 3.2). It had a base (1·25 cm thick) carrying cold water around its periphery and, stems, through which passed different tubes (Gas lance, thermocouple sheath, gas outlet tube etc.) into the reaction zone. A turntable (section B-B, Fig 3.2) containing four stems facilitated drawing slag samples. Sampling rods could be brought to the sampling position (nearest to the center of the lid) one after the other, by rotating the turntable. All the stems had 'wilson' seals. As the crucible holding slag was small (a diameter of 9·5 cms) the stems and the turntable (sampling hole) had to be with in a radius of 4·75 cms. from the centre of the lid. Hence to provide enough room, the stems were made alternatively short and tall (11·25 and 14·0 cms).

3.1.3: Insulation

With the susceptor at around 1400°C (the experiments were conducted in the range 1250°-1400°C) insulation was needed to protect the gas seals and the pyrex walls. "Kaowool" blanket supplied by the Morgans, of about 4·0 cms. thick was placed between the susceptor and the pyrex walls. A tall silliminite tube of 1·0 cm thickness was placed between the graphite and the Kaowool to act as a further insulator. The bottom of the pyrex vessel was shielded from heat by filling the space between the graphite susceptor and the vessel bottom with calcined alumina powder.

Eventhough the brass lid had cold water flowing along its periphery all the time, to keep the 'O' rings providing the seals and the solder joints in the lid intact, it was found necessary to shield the lid from the hot zone. For this purpose mild steel radiation shields with the necessary holes (for window, sampling rods and other tubes to pass through) were hung from the bottom side of the brass lid (Fig 3.1). These had to be above the induction coils to prevent them from picking up any high frequency current. Three shields were found to be adequate.

3.1.4: Refractories

Gases were bubbled through pure thermally recrystallized

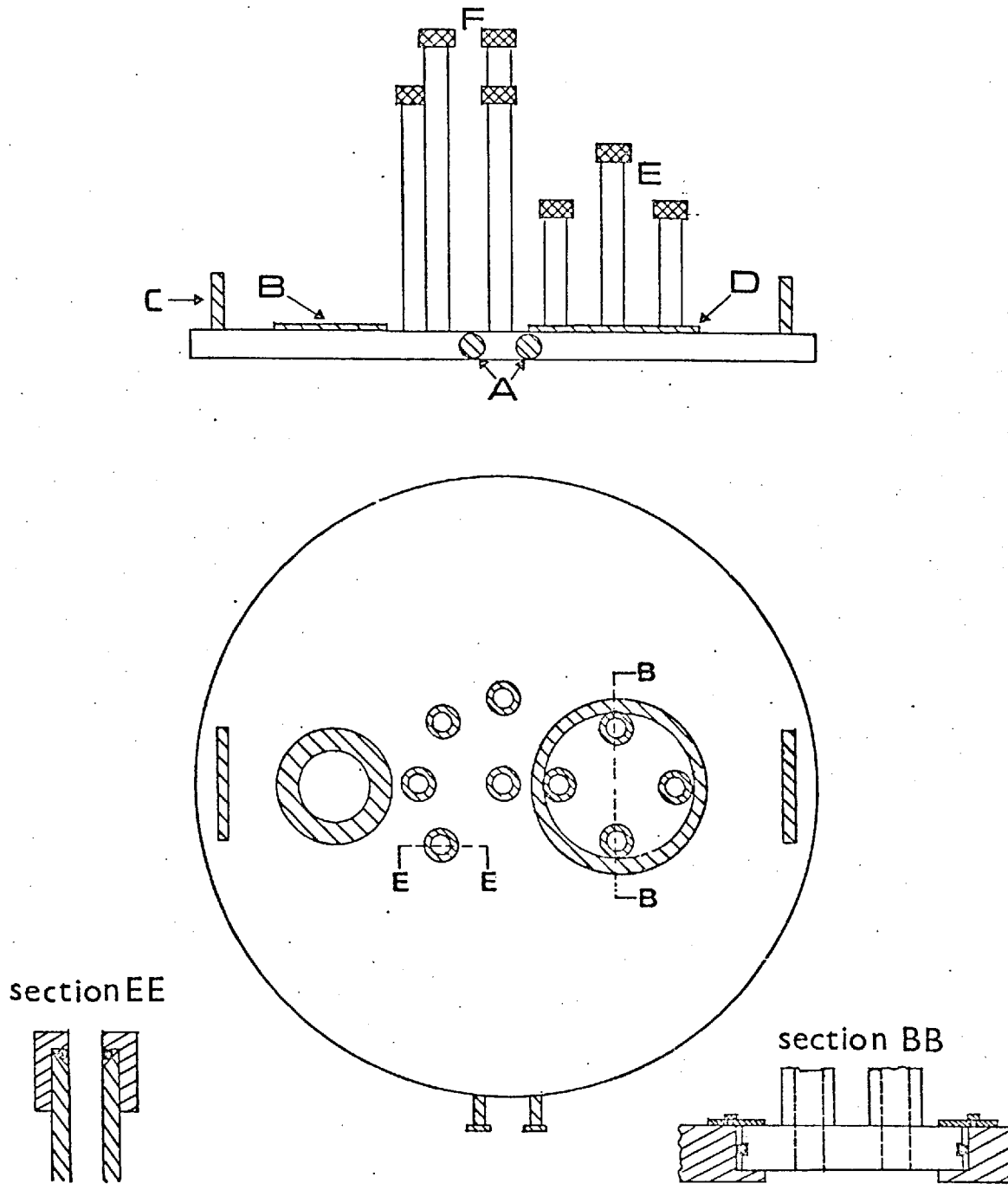

Fig. 3.2: The Brass lid

A - Water inlet and outlet B - Window
C - Handle D - Turn table
E - Stems for slag sampling
F - Stems for the gas lance, thermocouple sheath and the gas outlet.

alumina tubes (0·4 cm I.D. and 0·6 cm O.D.). Tubes of same size and material but with one end closed were used as thermocouple sheaths (for the Platinum, 13% Rhodium - platinum thermocouples that were used).

For holding slags, crucibles made of fireclay were tried in the beginning. It was found that the chemical attack on the fireclay walls was so severe that the slag started flowing out of the crucible towards the end of the experiment. Different kinds of refractory crucibles were tried but they all suffered the same fate. Figure 3.3(a) shows the severity of the attack. Only pure, thermally recrystallized alumina crucibles withstood the slag corrosion. Fig 3.3(b) shows the difference in the resistances of fireclay and pure alumina crucibles to chemical attack by slags. As can be seen, the fireclay is porous as well as being attacked.

Slag (black) can be seen inside the fireclay walls. The slag was found to be more corrosive as FeO content and the temperature of reaction increased. For this reason, the 1400°C runs were conducted for only one hour's duration while the majority of the experiments was carried out for two hours.

From chemical analysis it was found that the final slag compositions of high FeO slags had an alumina content of up to 3·7 wt.%.

3.1.5: Gas Train

In the reduction runs, high purity gases from cylinders were passed through a glass float flowmeter into the ceramic gas lance. The lance was always kept about 1·0 cm. above the bottom of the crucible. The outlet gases were passed through a drying column into a burner where they were completely oxidised before being exhausted into the atmosphere.

The drying column in the outlet gas circuit was weighed just before switching on the furnace and just before starting the actual experiment (i.e. before bubbling the reaction gas through the melt). During this (slag melting) period all the moisture in the starting oxide powders

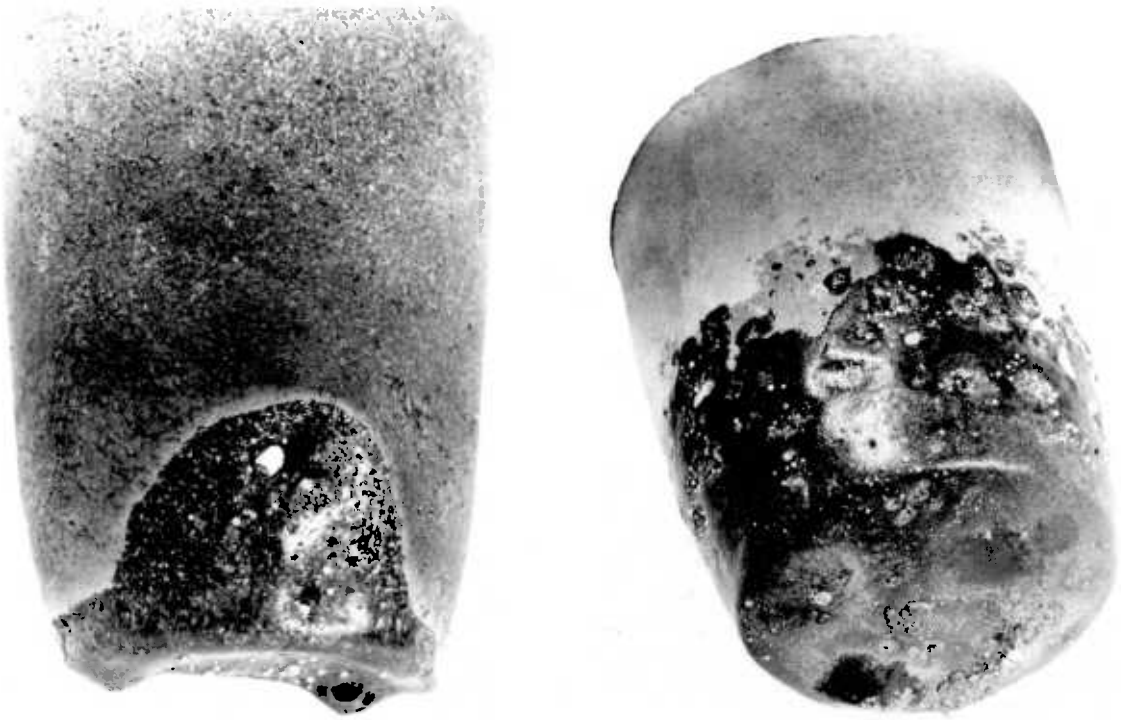

Fireclay Silliminite

Fig 3.3.(a) Slag attack on Crucibles.

Fireclay Alumina

Fig 3.3.(b) The difference in the resistances to slag attack.

vapourised and was collected in the drying column. Thus, the difference in the two weighings gave the moisture content of the slag. (This is different from the water produced during reduction). This value for the moisture content of the powders was used in the mass balance to calculate the amount of SnO fumed accurately.

3.2: TECHNIQUES USED

3·2·1: Slag Making

SnO and CaO (Analar grade) were used from bottles and pure quartz (fused silica) was specially bought. It was necessary to have only FeO in slags and not any higher oxide of iron. To be absolutely certain of this, ferrous oxide was prepared. Ferrous oxalate was decomposed in a tubular furnace at 850°C for four hours in an inert atmosphere. This FeO was used to make slags.

300 gms. of the powder mixture was prepared and thoroughly mixed. The powder mixture always had a volume of 450 ml. and the crucible capacity was only 250 ml. For this reason the powder slag was compacted before being put into the reaction crucible.

3.2.2: Sampling

Slag samples were taken intermittently during the experiment. For this purpose Copper rods (6 mm. dia.) were dipped in the slag bath and drawn up quickly. This not only quenched the samples but also prevented the melting of copper. For the high temperature runs (1400°C) nickel rods were used.

Copper and nickel were used for the reason that they did not react with the slag. In the early trials when steel rods were tried it was found that SnO had been reduced by iron and a white coating of tin on the sampling rods could be seen.

3.2.3: Chemical Analysis

The chemical analyses were carried out by the investigator and represented a substantial part of the work involved

in this project. It was decided to analyse the slags only for total tin and total iron contents, as the other constituents (SiO_2 and CaO) did not undergo appreciable changes during an experiment. Standard slags (i.e. specially melted slags of known composition) were made to find out the most suitable analytical technique. Instrumental methods tried, involved getting the slag into solution which formed the bulk of the work for the classical wet chemistry method. The latter gave good results and so was chosen, both for the analysis of slags and alloys.

SLAG

Tin: weighed slag samples, powdered to silky fineness, were thoroughly mixed with fresh sodium peroxide in a nickel crucible. The mixture was fused over a Mecker burner and the fused mass was completely extracted with water. To the extract was added 100ml. of conc. HCl and the solution was boiled. The boiling solution was reduced with a nickel coil for upto two hours.

The reduced solution was cooled under a tap and titrated against standard iodine solution using starch as indicator. A strong CO_2 atmosphere was maintained in the beaker both while the solution was cooled and titrated, by adding marble chips.

1 ml. of $N/_{20}$ Standard Iodine Solution ≡ 2·956 mgms. of Sn

Iron: The procedure for fusing the slag was the same as mentioned above for tin. Once the fused mass was extracted from the nickel crucible, the solution was filtered to separate tin and iron. The precipitate was extracted with hot distilled water and dissolved in conc. HCl. 1N Ammonia solution diluted in the ratio 1:1 was used to reprecipitate iron. Filtering and precipitation was repeated to ensure complete separation of tin and iron.

The precipitate was dissolved in conc. HCl and boiled to bring the volume down to about 25 ml. The hot solution was then reduced using freshly prepared 6 wt.% $SnCl_2$

solution and cooled quickly. About 10 ml. of 5 wt.% $HgCl_2$ was added to precipitate the excess $SnCl_2$. After adding a mixture of 20% H_2SO_4 + H_3PO_4 solution the ferrous iron was titrated against the standard dichromate solution using Sodium Diphenylamine Sulphonate as indicator.

1 ml. of $N/_{10}$ Standard $K_2Cr_2O_7 \equiv 5{\cdot}63$ mgs. of iron.

METAL

The same procedures were used for analysing the metal. The metal drillings (taken from 10-12 points on the solidified metal button to give the average composition) were dissolved in 1:1 conc. HCl; the next steps were exactly the same as for tin and iron in slag. The metal was always analysed both for tin and iron so that a check could be made.

3.2.4: Fuming runs

As noted earlier, the arrangements and procedure for the reduction and fuming runs were not very different from each other. Only in the sulfide fuming was there any difference and this is briefly described below.

The product gases from the apparatus, (as they contained SO_2) were passed through two sintered glass bubblers containing water before burning them. Every ten minutes the water was changed to ensure that it was always unsaturated with SO_2. In those experiments where the sulfidising gases (SO_2, air and methane) were used, a glass bead column was used to mix the gases from different gas cylinders.

Addition of Pyrite:

The pyrite fuming experiments, representing more traditional kind of fuming, were performed to be compared with the SO_2 + CH_4 + air fuming runs. For the comparison to be valid, it was necessary to add the pyrite continously or at least intermittently.

Pyrite was kindly provided by the Geology department of Imperial College. As feeding with an Archemides screw

was found difficult, a cruder method of addition, using a ceramic tube and a funnel was resorted to. Pyrite was coarsely powdered (300μ) and predetermined quantities (to give the same S potential as in SO_2 + CH_4 + air runs) were dropped onto the slag every twenty minutes. Fine powder was found to stick to the tube walls and caused an obstruction. Coarse powder also provided a more continous supply of S as the powder dissolved slowly.

The matte obtained was analysed for tin and iron using the same procedure that was used for the slag (section 3.2.3).

3.2.5: Quantitative Metallography

The cooled slag surface always contained tiny metal beads and it was known that metallic tin would be trapped inside the slag bulk as well. To study the effect of different parameters on the metal losses due to entrapment it was necessary to have a method of measuring the physically entrapped metal. It was felt that the chemical methods may not be suitable, as, most of the chemical agents would attack not only the physically entrapped metal in slag but the chemically dissolved metal as well. Hence a physical method was sought.

Conventional flotation was tried when the slag sample was crushed, the tin metal being soft, formed flakes and the hard slag particles impregnated on either side of it. Thus, the collector solution used could not reach the tin metal.

Quantitative metallography was used. A 'quantimet' was used to scan the sample. The different reflectivities of the metal and slag made them appear as bright white and darker regions on the television screen. Knowing the area percentage, volume percentage (which must be the same assuming the same distribution of metal in the 3rd dimension as in the first two) and hence the weight percentage could be calculated. A statistical survey of fifty or more sample regions was carried out before deriving the physically

entrapped tin content of the sample.

Fig 3.4 shows some photo micrographs of the entrapped metal in the slag.

3.3: PROCEDURE

The oxide powders mixed in requisite quantities were compacted and put into the alumina crucible. The crucible weight with and without the slag mixture was noted. The thermocouple sheath and the gas lance were weighed as well.

The crucible was then placed in the graphite susceptor and the apparatus was closed with the brass lid. Pure argon was passed for a minimum of 16 hours at a rate of about 200 ml/min before heating was started.

Once the slag was molten the drying column in the outlet gas circuit was removed, weighed and re-attached. (This to find the moisture content of the oxide powders). The thermocouple was dipped in the molten bath and left there till the end. The temperature was followed and recorded on a chart recorder. Use of the recorder helped towards better temperature control as the 'rate of heating' and the rate of approach to the desired temperature was known.

Once the required temperature was reached argon was bubbled into the bath for about 60 seconds. This was to homogenize the bath. It was found, during these experiments that the temperature gradient in these slag baths was about 25°C per cm. in the vertical direction (bottom hotter). However, stirring the melt (gas flow rate ≈ 600 ml/min) decreased the temperature gradient to about 3°C per cm. Usually, after argon mixing, heating was necessary to increase the bath temperature by about 20°C.

Hydrogen was then bubbled at a rate of 600 ml/min (except in the experiment where the effect of gas flow rate was studied). The first few minutes always provided vigorous fuming of SnO. Slag samples were drawn at regular intervals. After two hours of reduction (in most cases)

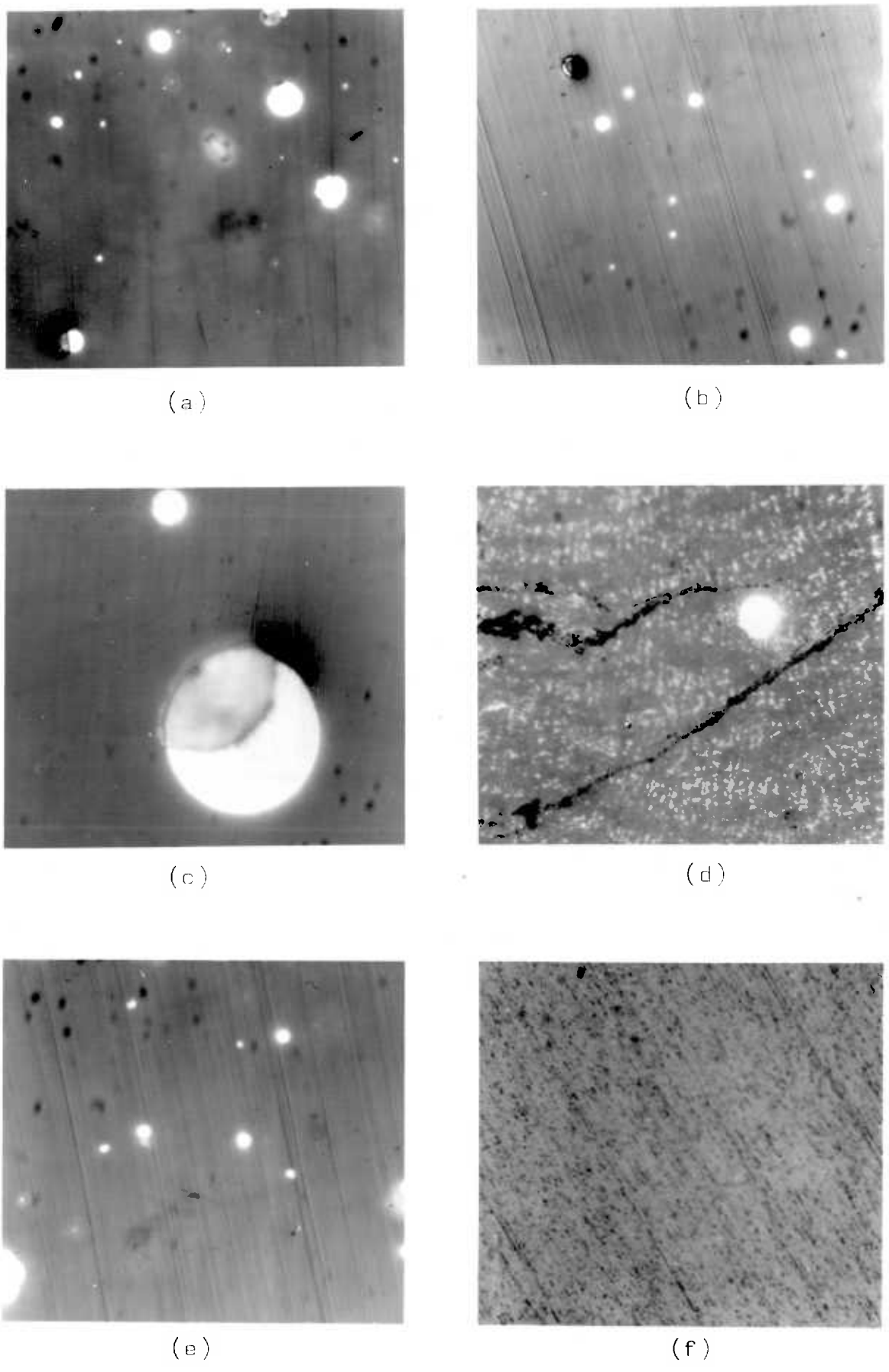

Fig 3.4: Photo Micrographs of the physically entrapped tin metal in slag (Magnification - x604) a, b, c - metal beads suspended from gas bubbles, f - slag free of entrapped metal.

the hydrogen bubbling was stopped and the bubbler was lifted up above the melt. Argon flow was maintained during cooling.

For all experiments a half an hour 'settling period' after the reduction was allowed at the reaction temperature. This was to facilitate the settling of metal droplets. Then the furnace was switched off and the apparatus cooled slowly.

The products taken out of the apparatus were all weighed (crucible with slag and alloy in it, thermocouple sheath, gas lance, the slag samples drawn etc.). The slag and the alloy (or the matte) were separated by breaking the crucible open. Tiny metal beads were always found at the top of the slag (Fig 3.5).

The slag samples, final slag and the alloy were then chemically analysed. Using the weight measurements the mass balance sheets were drawn up.

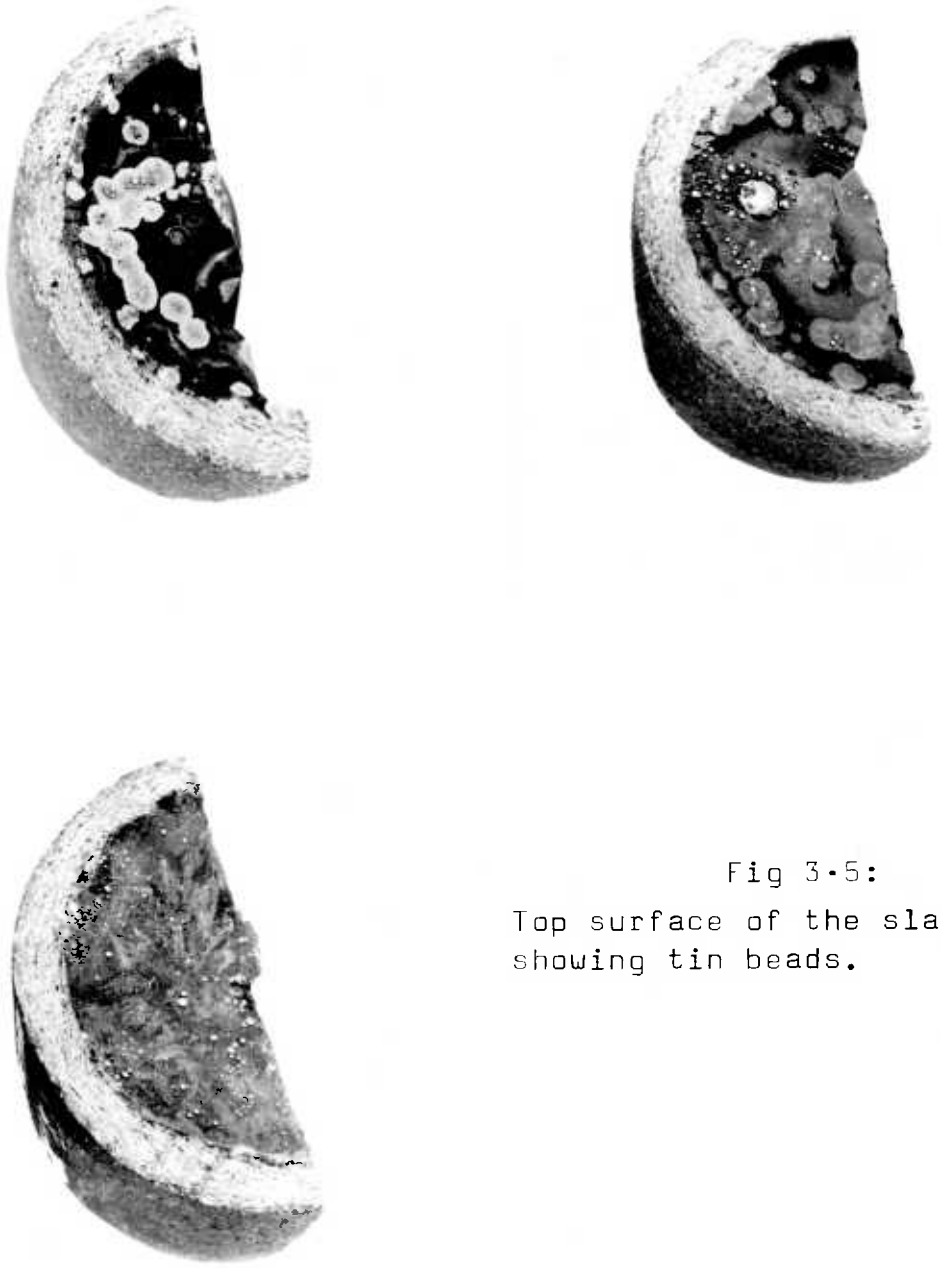

Fig 3·5:
Top surface of the slag showing tin beads.

CHAPTER 4

RESULTS

CHAPTER 4

RESULTS

4.1: Reduction

Reduction experiments were carried out between 1250° and 1400°C for one or two hours (with one exception of a three hour run) by bubbling reducing gases through the melt. 300 gms. of slag was used and the flowrate of the gas was 600ml/min. To facilitate settling and coalescence of the metal formed during reduction a half an hour settling time was allowed. When the apparatus had cooled down to room temperature under an argon atmosphere, the slag and metal phases were separated by breaking the crucible open. Chemical analysis was carried out on the slag and metal for their total tin and iron contents.

4.1.1: Pure hydrogen runs

Slag samples were drawn intermittently during the experiments with pure hydrogen. These were also analysed for total tin and iron contents. The effects of (a) slag composition, specifically the silica/lime ratio and FeO level in the starting slag, (b) temperature of reduction and (c) the gas flowrate,on tin and iron reduction rates, metal composition and tin losses were studied.

4.1.1A: Slag composition

The usual range of industrial slag compositions was identified and the slag compositions studied roughly covered this domain. Quaternary slags (SnO + FeO + CaO + SiO_2) were studied. Towards the end of an experiment the slag melt was a five component system because of the alumina dissolving from the refractories. (From chemical analysis it was found that a high FeO slag, after two hours of reduction had 3·7 wt.% alumina). The SnO content of the starting slag was the same (4·2 mol.%) in all slags studied,while the silica/lime ratio and the FeO content of the slag were varied systematically. Fig. 4.1 shows the working region and the different slags used. In Fig. 4.1, (mol.% FeO + constant mol.% SnO)forms one of the apices of

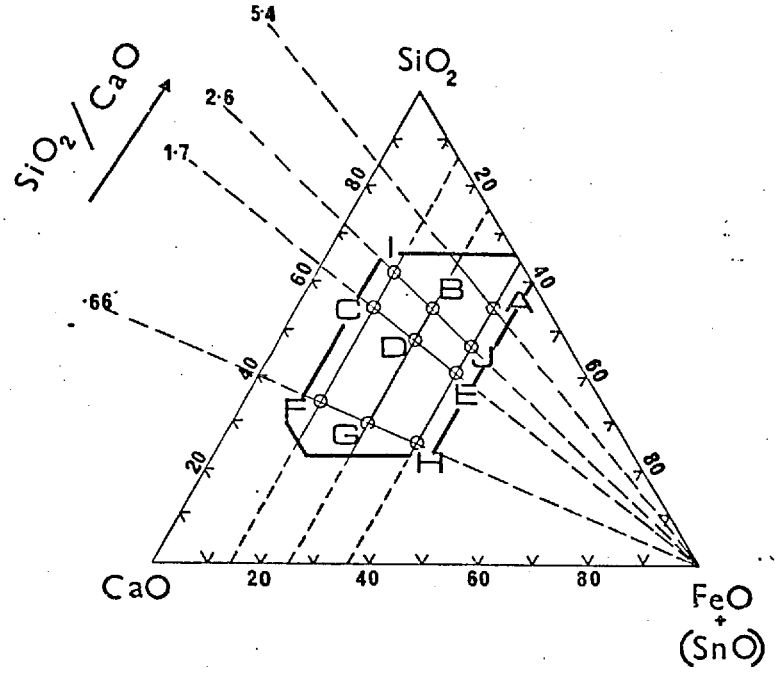

Fig. 4.1: Slag compositions used in the present work. Silica/lime ratio and FeO levels have been varied.

TABLE 4.1

Slag	Composition in mol.%				Composition in wt.%			
	SnO	FeO	CaO	SiO_2	SnO	FeO	CaO	SiO_2
A	4·21	31·6	10·1	54·1	10·0	40·0	10·0	40·0
B	4·21	20·9	20·8	54·1	10·3	27·2	21·2	41·2
C	4·24	10·0	31·6	54·2	10·6	13·5	33·2	42·6
D	4·24	20·9	27·5	47·3	8·9	23·3	23·9	44·0
E	4·24	31·7	23·5	40·5	8·7	34·5	19·6	36·8
F	4·24	10·0	51·6	34·1	9·2	11·5	46·4	32·9
G	4·24	20·9	45·1	29·8	8·9	23·5	39·5	27·1
H	4·24	31·7	38·6	25·5	8·7	34·8	33·0	23·4
I	4·24	10·0	23·9	61·9	9·01	11·3	21·1	58·6
J	4·24	31·7	17·8	46·2	8·63	34·4	15·1	41·9

the triangle. Table 4.1 sets out the composition of all the slags used in detail. The temperature of reduction (1340 ± 5°C), the gas flowrate (600 ml/min) and the time of reduction (2 hours) were kept the same while studying the effect of slag composition.

Effect of Silica/lime ratio: This was varied between 0·66 and 5·4 (Fig 4.1) while the FeO content of the starting slag was kept a constant. Figs 4.2, 4.3 and 4.4 show the effect of the silica/lime ratio on the rate of tin removal at different FeO levels. It is clear that the SiO_2/CaO ratio has a significant effect on the rate of tin removal from slags; the low values for the ratio favouring the rate of removal of tin. This effect is seen at all FeO levels in the starting slag.

Figs. 4.5, 4.6 and 4.7 show the effect of silica/lime ratio on the reduction of FeO from tin slags. The graphs are plotted with FeO expressed as a fraction of the initial FeO. The effect of silica/lime ratio on the rate of FeO reduction is similar to that on tin removal (the lower the silica/lime ratio the faster is the reduction of the oxide) but is less obvious because of the scatter of the results and the smaller fraction of FeO reduced.

Effect of FeO level in the starting slag

Keeping the Silica/lime ratio constant, the FeO level in the starting slags was varied. Figs. 4.8 and 4.9 show the SnO and FeO removed as fractions of the initial SnO and FeO contents of the slag, for two different silica/lime ratios. For a given silica/lime ratio, the fraction of the oxide removed does not depend on the FeO level in the starting slag. The SnO content of the slags was the same to begin with and hence the rate of removal of SnO from slags does not depend on the FeO content of the initial slag. However, for the removal of FeO itself (at any given silica/lime ratio) the amount of FeO removed increases with the increase in the FeO content of the starting slag.

Metal Composition

Fig. 4.10 shows the iron contents of the metals

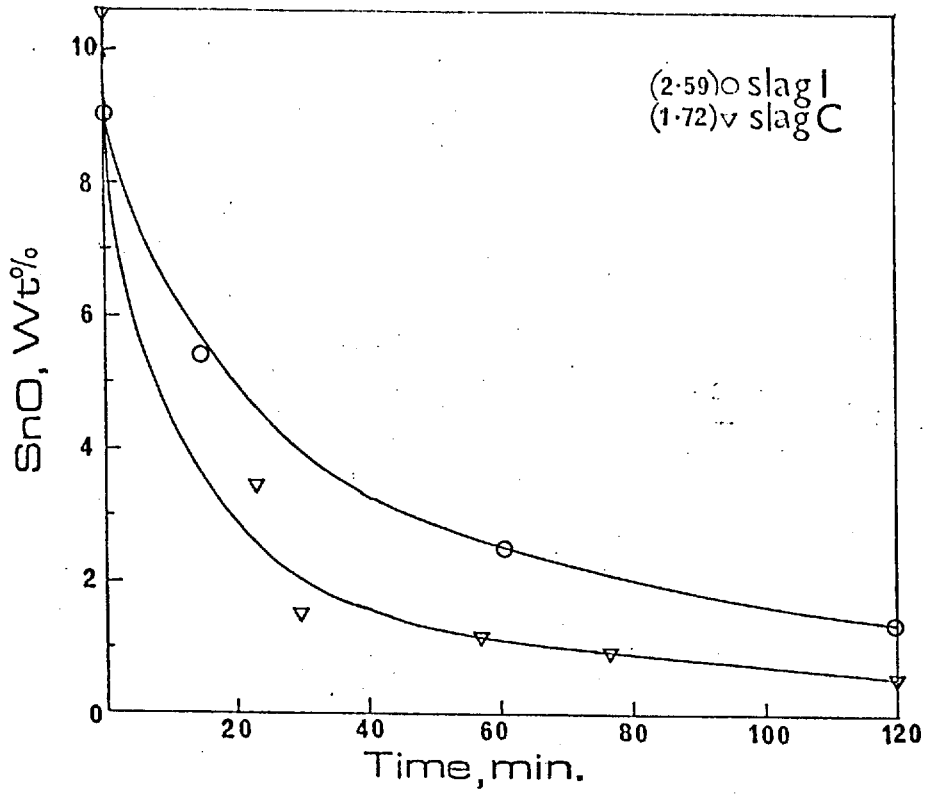

Fig. 4.2: The effect of silica/lime ratio (given in brackets) on tin reduction at constant FeO level, 10 mol.%.

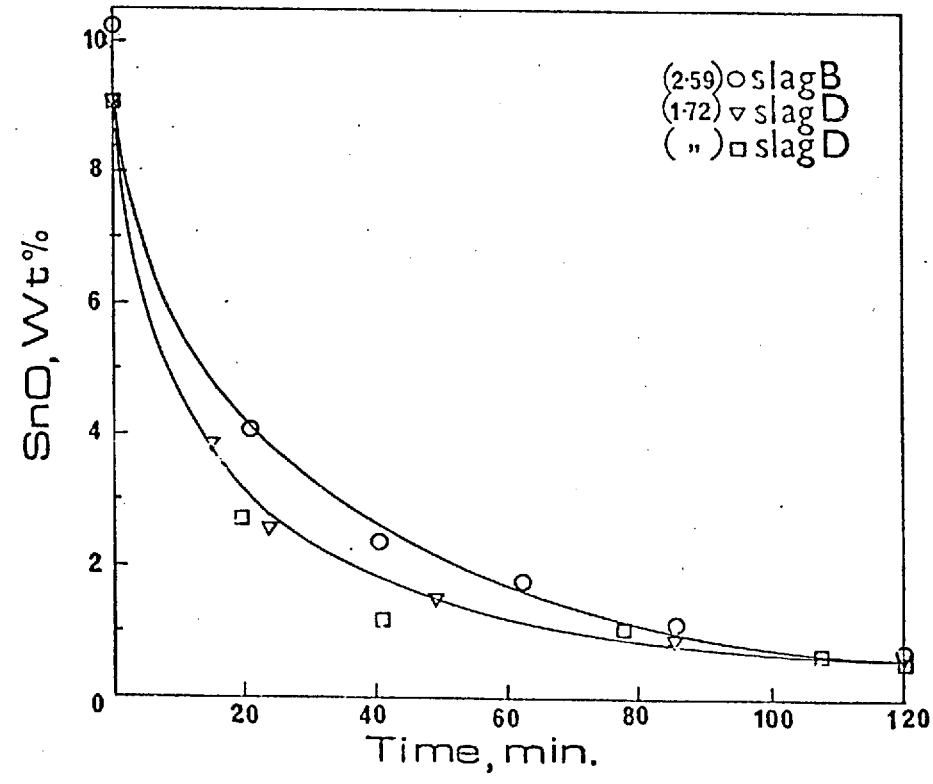

Fig. 4.3: The effect of silica/lime ratio (given in brackets) on tin reduction at constant FeO level, 20·9 mol.%.

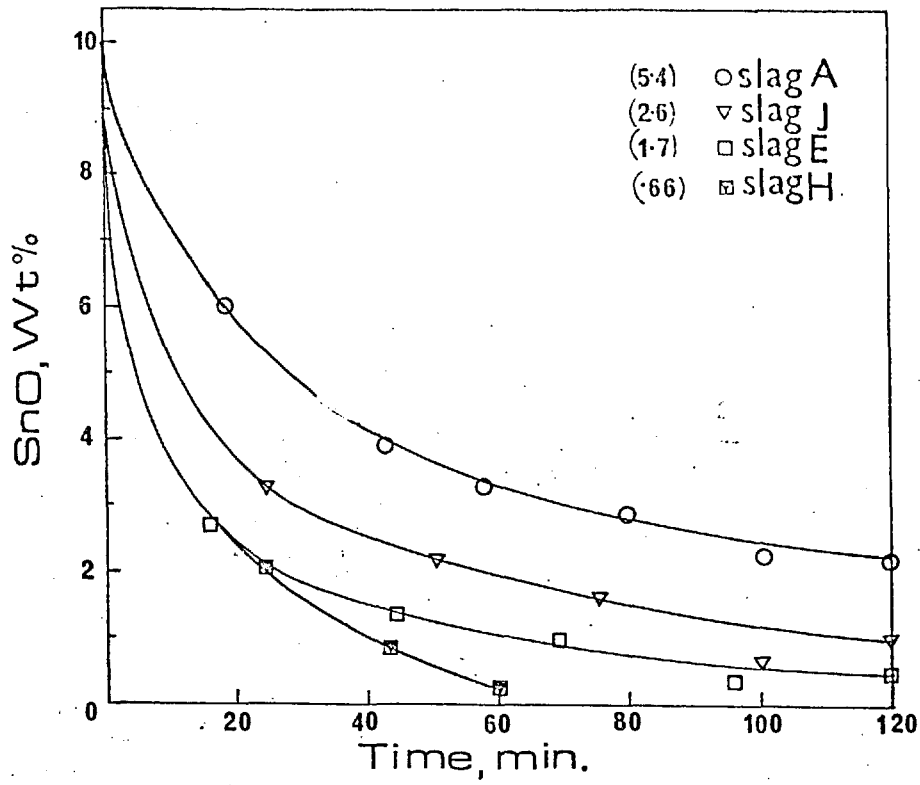

Fig. 4.4: The effect of silica/lime (given in brackets) on tin reduction at constant FeO level, 31·7 mol.%

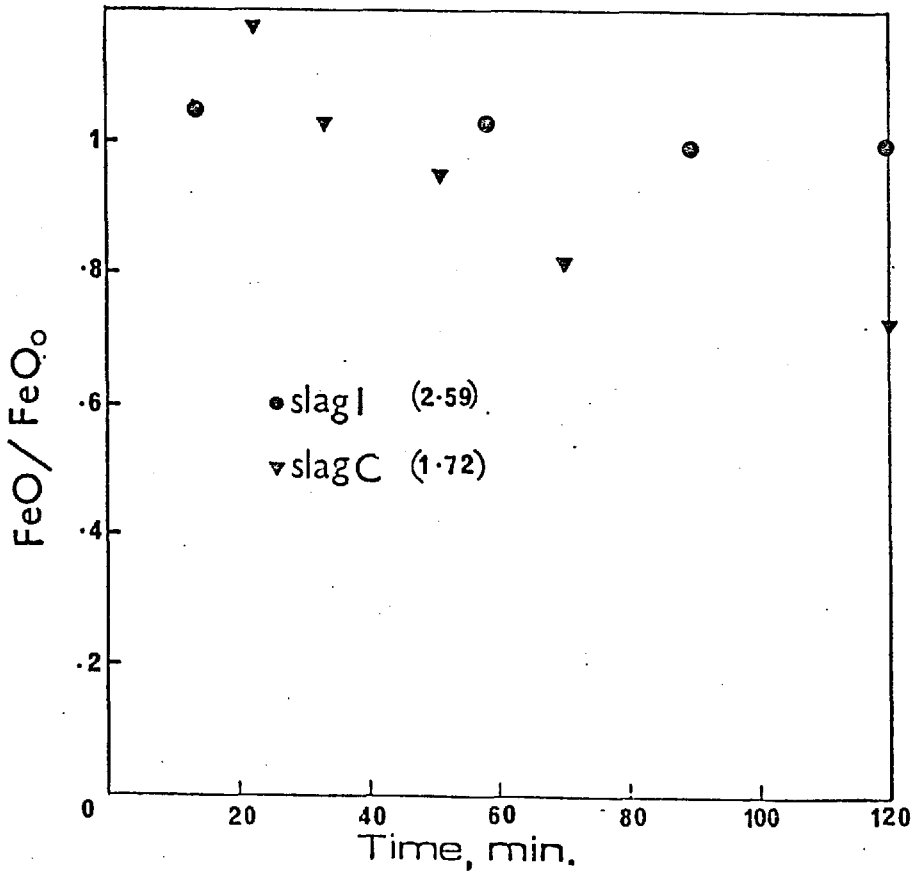

Fig. 4.5: Iron oxide reduction (constant FeO level, 10 mol.%)

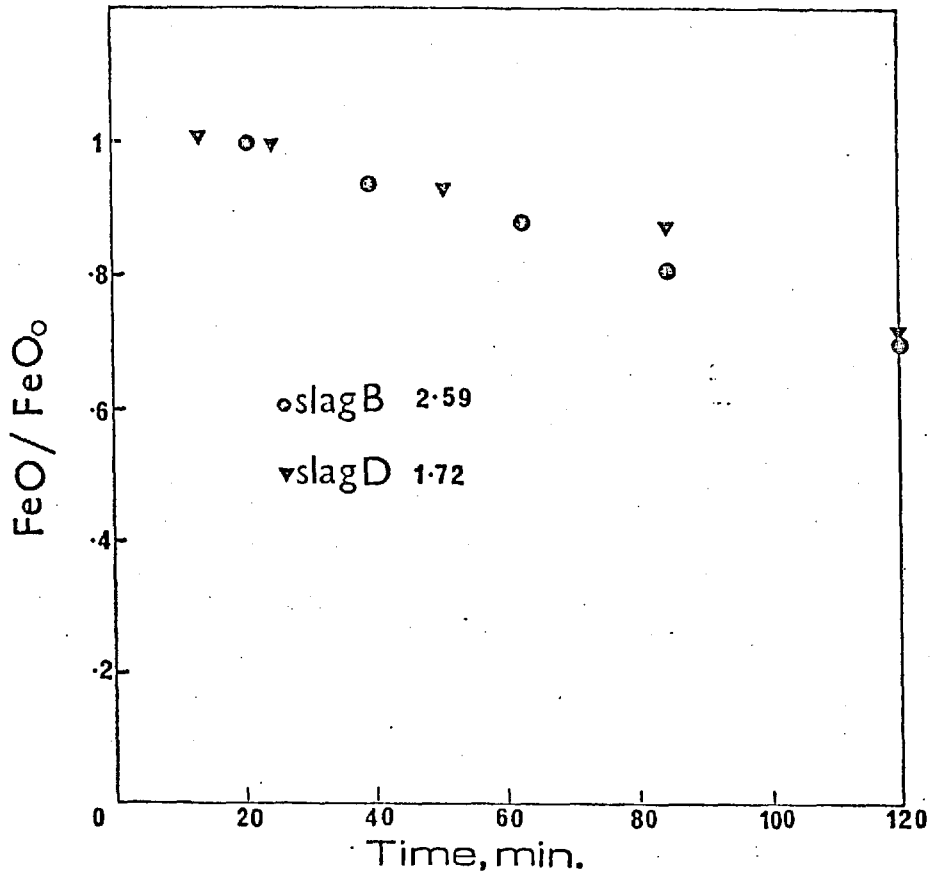

Fig. 4.6: Iron oxide reduction (FeO level, 20·9 mol.%)

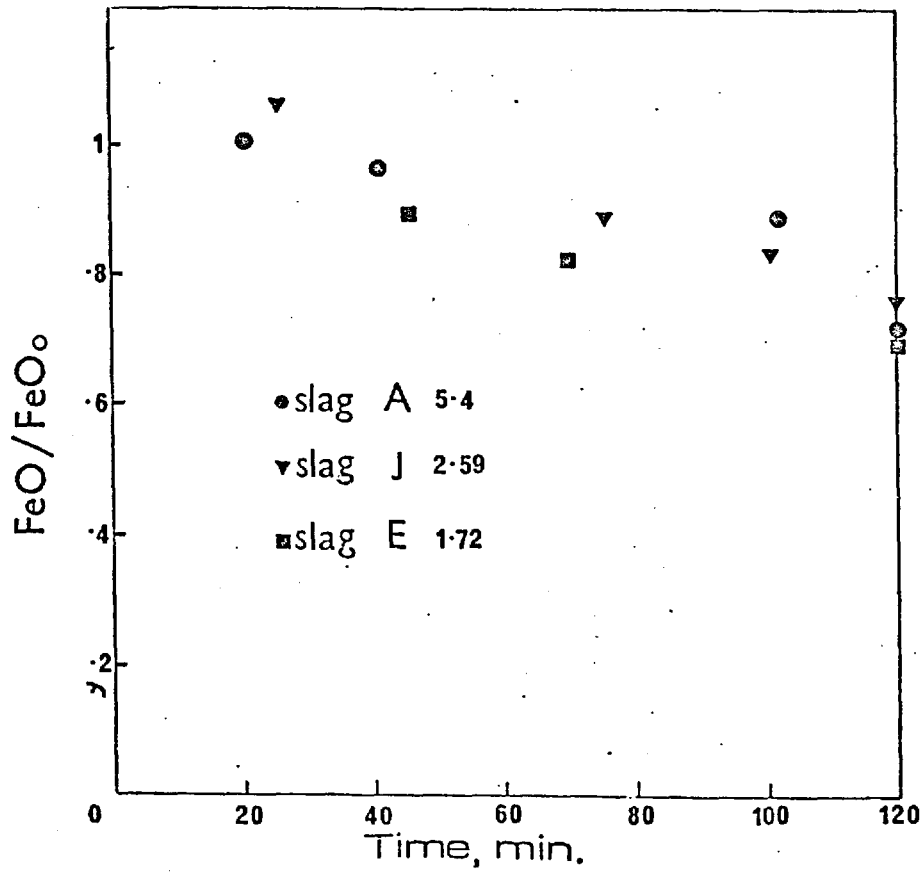

Fig. 4.7: Iron oxide reduction (FeO level, 31·7 mol.%)

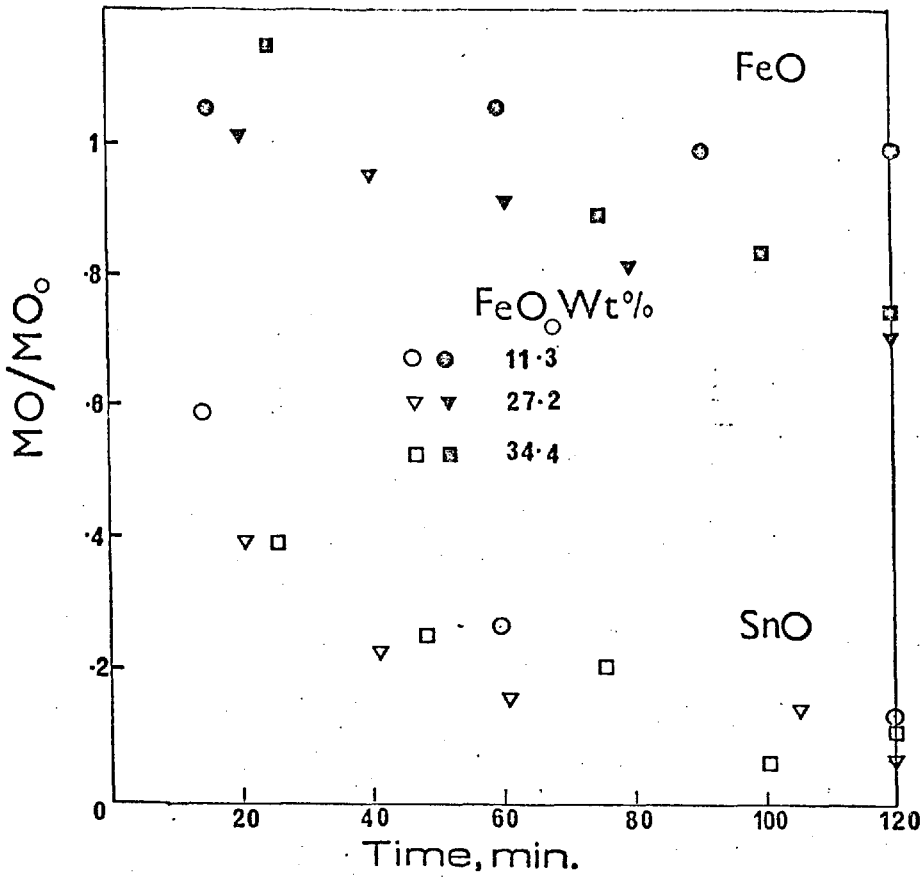

Fig. 4.8: The effect of FeO_o at constant silica/lime ratio (2·59).

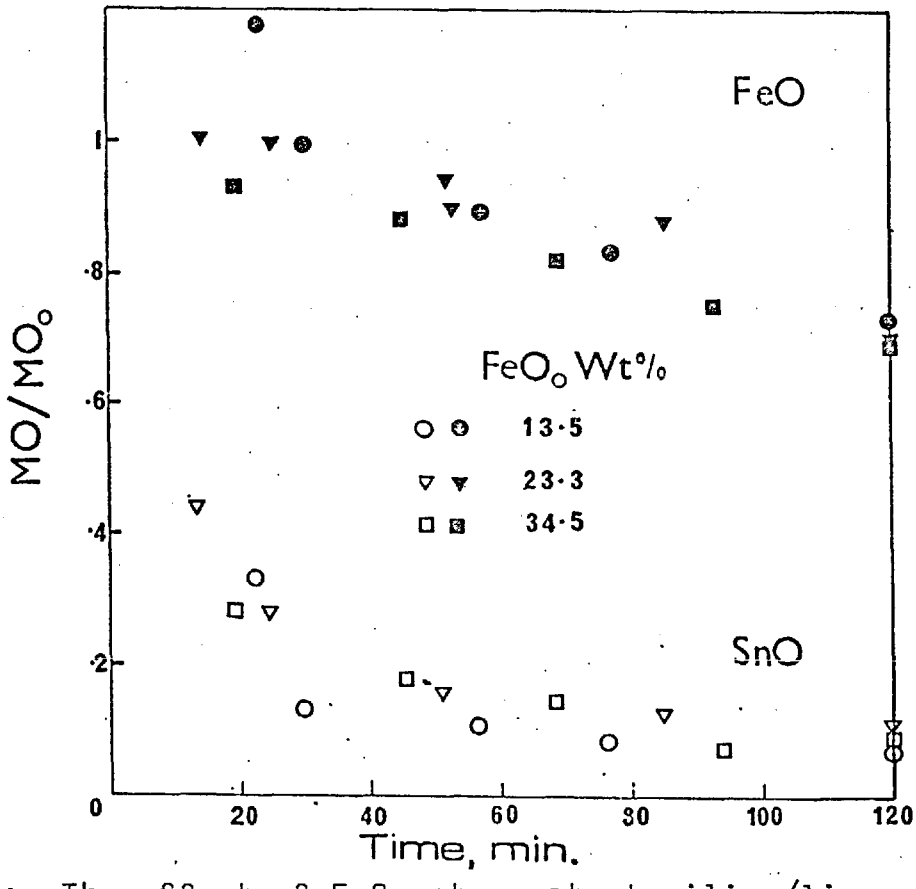

Fig. 4.9: The effect of FeO_o at constant silica/lime ratio (1·72).

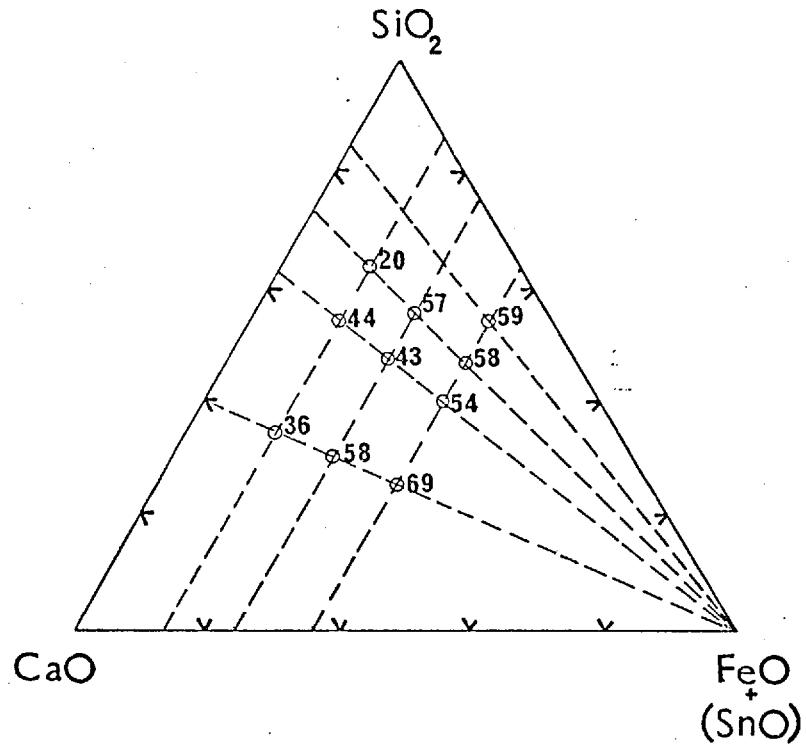

Fig. 4.10: Iron content of metals produced from different slags at 1340°C, 2 hour runs.

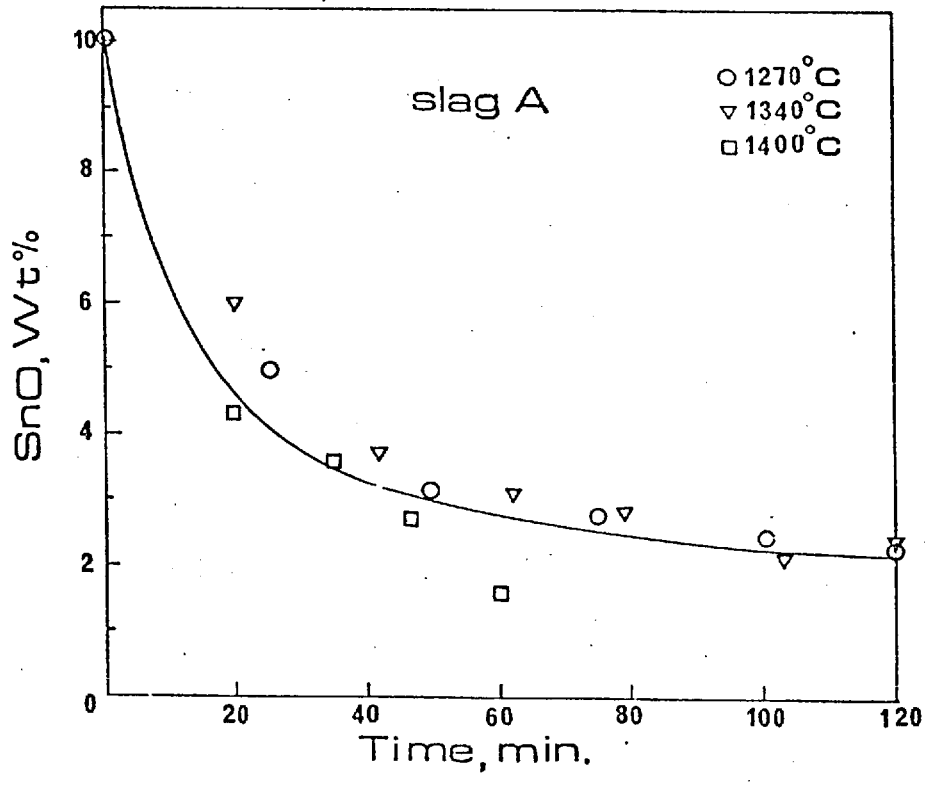

Fig. 4.11: The effect of temperature on the rate of tin removal from slag A.

TABLE 4.2

Results of the pure hydrogen reduction experiments carried out to study the effect of slag composition. All experiments were carried out at 1340°C for two hours with 600 ml/min gas flow rate - see figs. 4.2 - 4.9.

Expt no.	Starting slag wt.% slag	SnO	FeO	$\frac{SiO_2}{CaO}$	Final slag wt.% SnO	FeO	Metal Mass gms.	Fe wt.%	% SnO fumed*
29	A	10·0	40·0	5·4	2·28	28·6	44·1	59·3	27
50	J	8·6	34·4	2·59	1·02	26·3	38·1	57·8	25
28	B	10·3	27·2	2·59	0·65	18·7	41·6	57·4	29
49	I	9·0	11·3	2·59	1·3	11·4	18·3	20·0	16
44	E	8·7	34·5	1·72	0·64	23·9	36·8	54·2	39
43	D	23·3	23·9	1·72	0·47	18·7	29·6	42·5	35
26	C	10·6	13·5	1·72	0·49	9·8	32·7	43·6	28
48	H°	8·7	34·8	0·66	0·26	-	42·7	68·9	40+
46	G°	8·9	23·5	0·66	0·68	-	36·0	58·3	29·5+
45	F°	9·2	11·5	0·66	-	-	21·3	36·4	-

* from mass balance calculations (Appendix 4)

\+ from chemical analyses

\- data not available

° experiments conducted at 1400°C for 1 hour.

produced from different slags. As the initial FeO content of the slag is increased, the iron content of the metal increases as expected. The iron content of the metal decreases as the silica/lime ratio is decreased but then increases again.

Table 4.2 summarises the results of all the experiments carried out to study the effect of slag composition.

4.1.1B: Temperature

Three slags, A, B and C (Fig. 4.1) were selected to study the effect of temperature on the reduction of SnO and FeO. The slags had different silica/lime ratios and FeO levels. Reduction was carried out on slags A and B at 1270°, 1340° and 1400°C. The experiments with slag C could be conducted only at 1340° and 1400°C as at 1270°C the slag was hardly molten. The results are shown in Figs. 4.11, 4.12 and 4.13 for the reduction of SnO for slags A, B and C respectively. The variation of temperature by 130°C has produced no observable change in the tin removal rates at all the compositions studied. Fig. 4.14 shows the effect of temperature on reduction of FeO, the results for all the slags being shown in the same diagram. Temperature has little effect on the reduction of FeO from slags.

4.1.1C: Gas flow rate

The effect of reducing gas flow rate on the rate of tin removal was studied using flow rates of 300 ml/min and 600 ml/min (600 ml/min provided good stirring for the slag melt at all compositions except at very low silica/lime ratio i.e. for slags F, G and H). The slag composition (Slag A), temperature of reduction (1270° ± 5°C) and the times of reduction (2 hrs.) were the same in both cases. The tin removal curves are shown in Fig. 4.15. The metal obtained in the experiment with 300 ml/min flow rate for hydrogen had less iron (30 wt.%) than that from the other experiment (57·2 wt.%).

A three hour experiment was conducted on slag A at 1270°C. The results of that experiment for tin and iron removal rates are shown in Fig. 4.16. It is significant

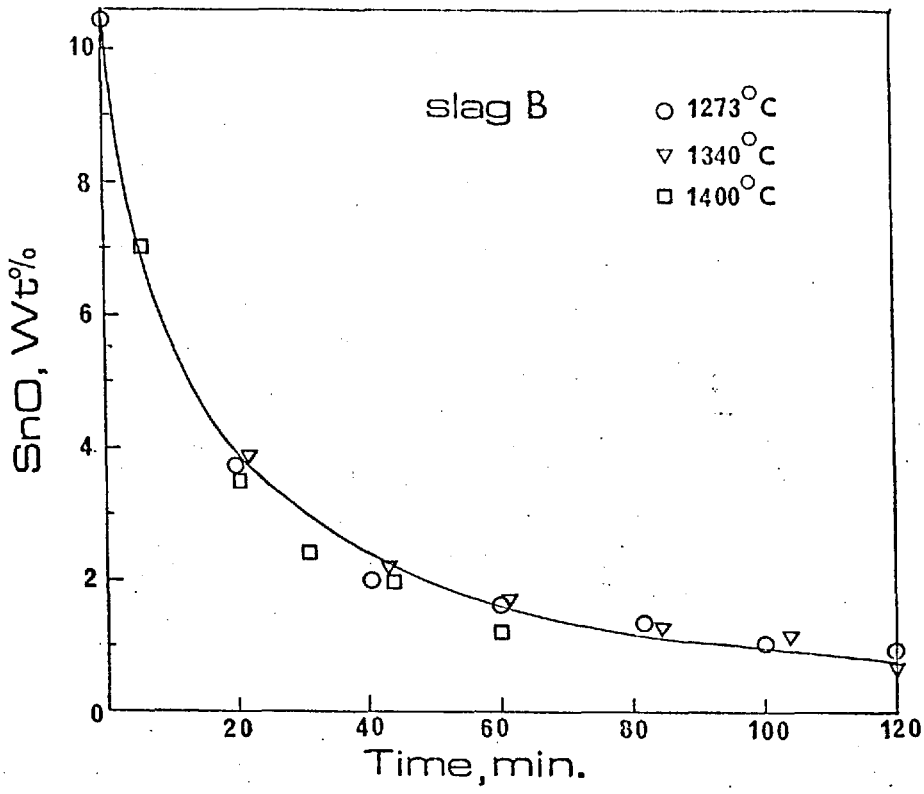

Fig. 4.12: The effect of temperature on the rate of tin removal from slag B.

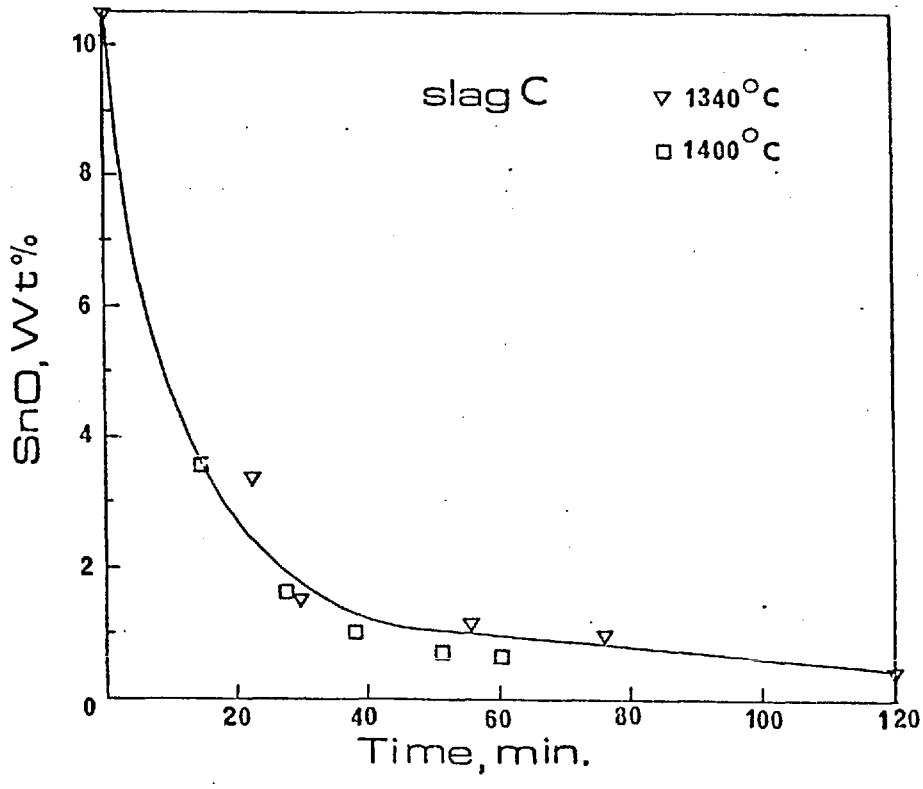

Fig. 4.13: The effect of temperature on the rate of tin removal from slag C.

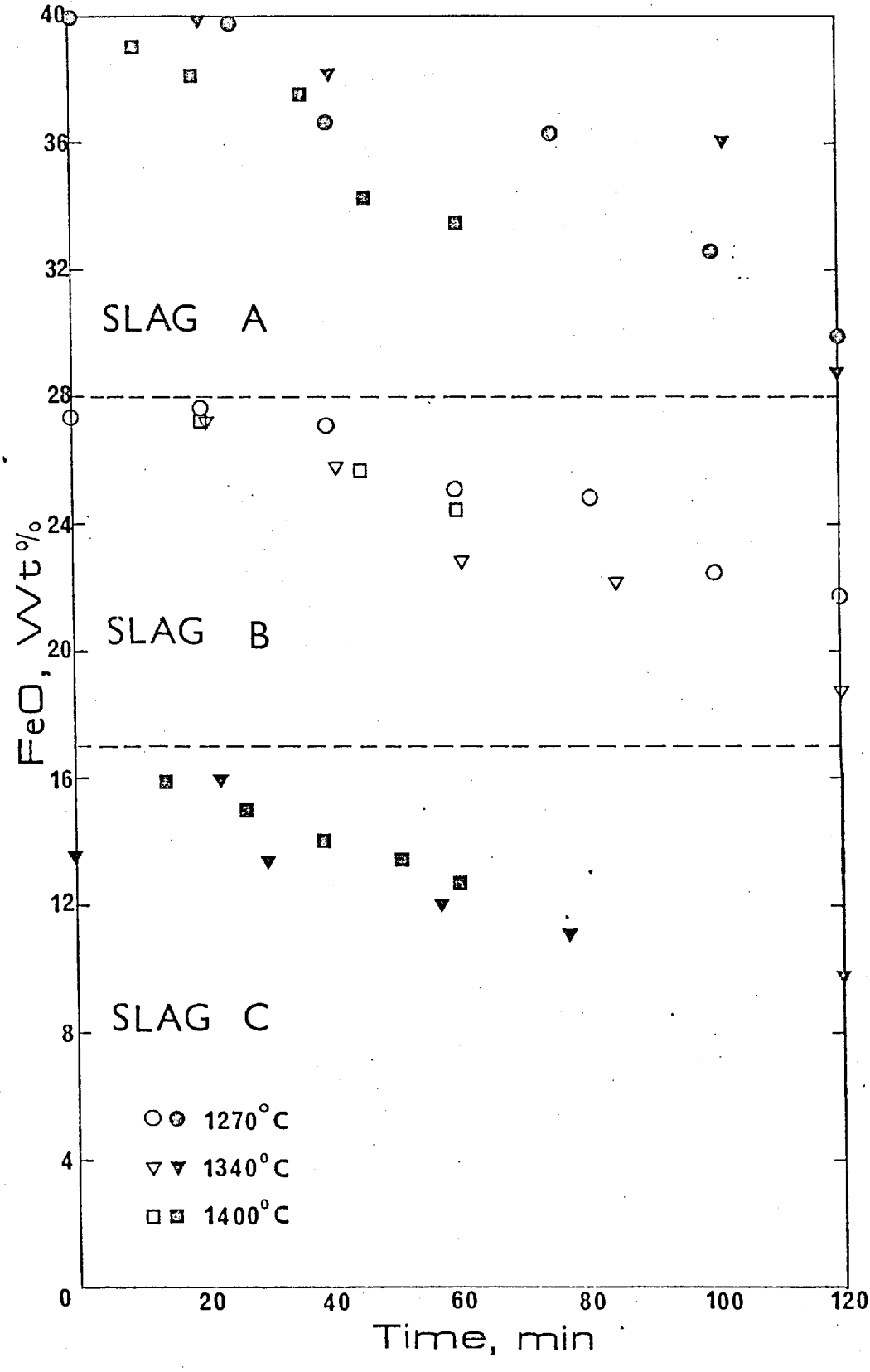

Fig. 4.14: The effect of temperature on the rate of iron oxide reduction.

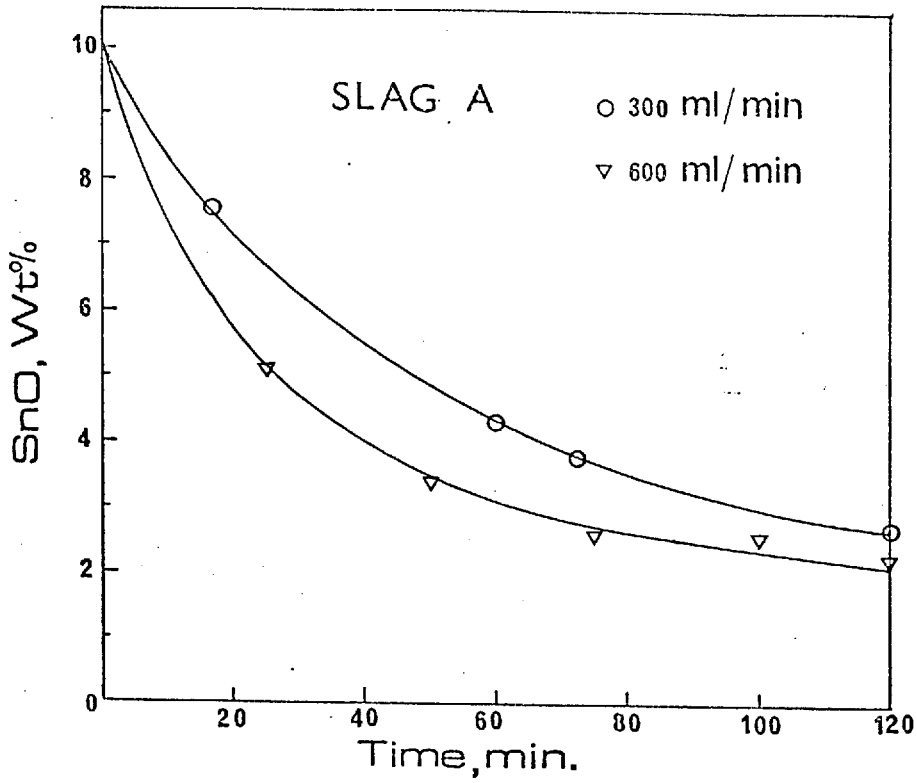

Fig. 4.15: The effect of flowrate on tin oxide reduction at 1270°C.

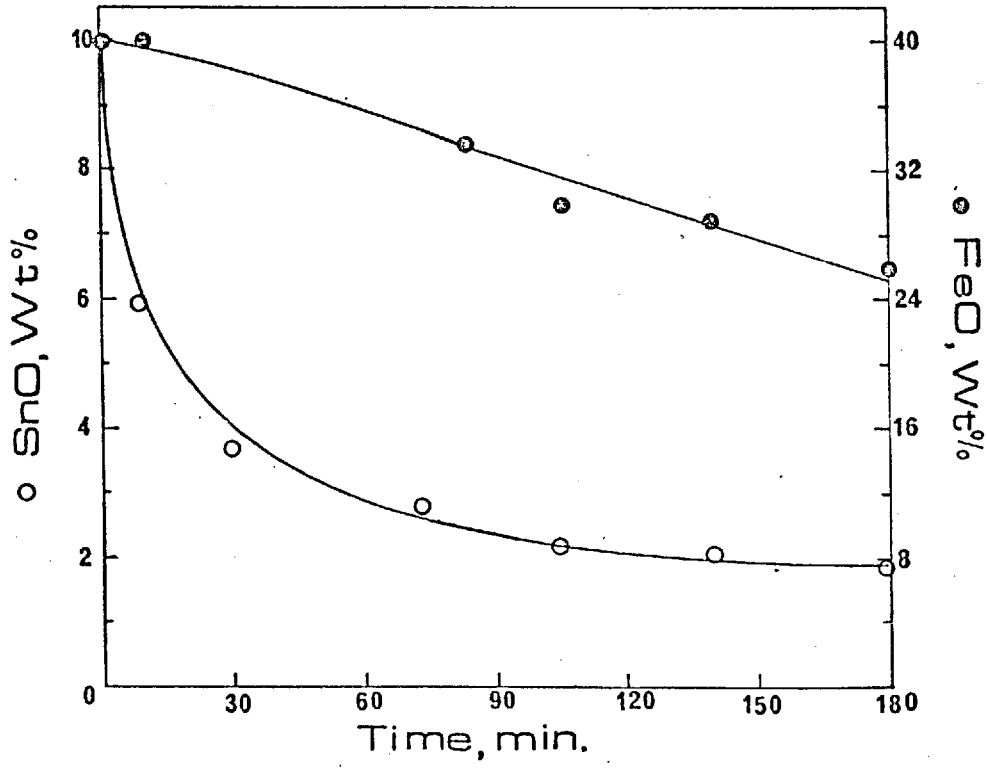

Fig. 4.16: Data for 3-hour run. (Slag A)

TABLE 4.3

Results of the pure hydrogen runs to study the effect of temperature and gas flow rate on reduction. Data for the three hour run is also given.
See figs. 4.11 - 4.16.

Expt. no.	Starting slag wt.%				Final slag wt.%		Metal		% SnO fumed*
	Slag	SnO	FeO	Temp°C	SnO	FeO	Mass gms.	Fe wt.%	
27	A	10·0	40·0	1273	2·22	29·8	47·1	57·2	5+
29	A	10·0	40·0	1340	2·28	28·6	44·2	59·3	27
31	A	10·0	40·0	1400	1·61	33·2	37·8	46·5	29
25	B	10·3	27·2	1273	0·9	21·6	38·5	46·2	30
28	B	10·3	27·2	1340	0·65	18·7	41·6	57·4	29
32	B	10·3	27·2	1400	1·15	24·2	31·9	32·5	31
26	C	10·6	13·5	1340	0·49	9·8	32·7	43·6	28
34	C	10·6	13·5	1400	0·6	12·6	28·1	20·4	22
23●	A	10·0	40·0	1273	2·7	-	32·1	29·9	10+
24Δ	A	10·0	40·0	1273	2·04	26·6	-	69·3	27

* from mass balance calculations (Appendix 4)

\+ from chemical analysis

● gas flow rate 300 ml/min

Δ the three hour run

that after two hours only iron is reduced out of the slag at appreciable rates.

Table 4.3 shows the results of the experiments conducted to study the effects of temperate and gas flow rate on reduction. The results of the three hour run are also included.

4.1.2: Reduction with 10% H_2 (90% N_2) and pure CO:

These experiments were conducted prior to the pure hydrogen runs. The sampling technique and the method of writing mass balance were not yet established. Hence the rate curves could not be drawn and the amount of SnO fumed was calculated from the chemical analyses of the slag and metal. The results for these experiments are not expected to do anymore than serve as a rough comparison for the results of pure hydrogen experiments for the tin recovery.

10% H_2 (+ 90% N_2 runs

Eventhough fourteen experiments were carried out using forming gas only those results which were thought to be reliable are given in Table 4.4. Fig. 4.17 shows the general pattern of tin removal as a function of time. (To put these results in perspective, the results of the reduction run with pure hydrogen on the same slag are shown). In all these experiments the slag had the same composition and the temperatures were similar. As can be seen, the reduction was slow.

Carbon monoxide:

Only one experiment was carried out with pure Carbon monoxide. The slag composition and the temperature were different from those in the hydrogen reduction runs (see Table 4.5). The results are given in Table 4.4. A metal button was produced,but weighed only 10-3 gms. (in contrast, in the pure hydrogen runs,the metal weight was of the order of 40 gms.).

4.1.3: Fume and Metal losses during reduction

Two kinds of tin losses occur in tin smelting

TABLE 4.4

Results of the 10% H_2, pure CO and Ar runs.
see Fig. 4.17

Expt. no.	slag+	Redn. temp. °C	Redn. time hrs.	Gas	Gas flow rate ml/min	SnO in final slag	Metal mass gms.	Metal Fe content wt.%	% SnO fumed*
7	A	1270	1	10%H_2	1000	6·46	-	-	-
8	A	1270	2	10%H_2	1000	5·25	10·6	2·2	12·0
9	A	1270	1	10%H_2	1000	6·86	7·9	1·7	18·3Δ
10	A	1270	2	10%H_2	1000	3·9	8·01	4·3	14
21	A	1270	1	Ar	1000	9·4	-	-	9·3Δ
11	K❶	1300	1	CO	300	5·7	10·3	-	38

* from chemical analyses, as a percentage of initial SnO
\+ see table 4.1
\- data not available
Δ from mass balance
❶ see table 4.5

TABLE 4.5

Composition (wt.%) of slags used in CO reduction and sulfide fuming.

Slag	SnO	FeO	CaO	SiO_2	Al_2O_3
K	18·2	14·6	25·5	33·7	9·00
L	12·0	25·0	11·0	40·0	12·0

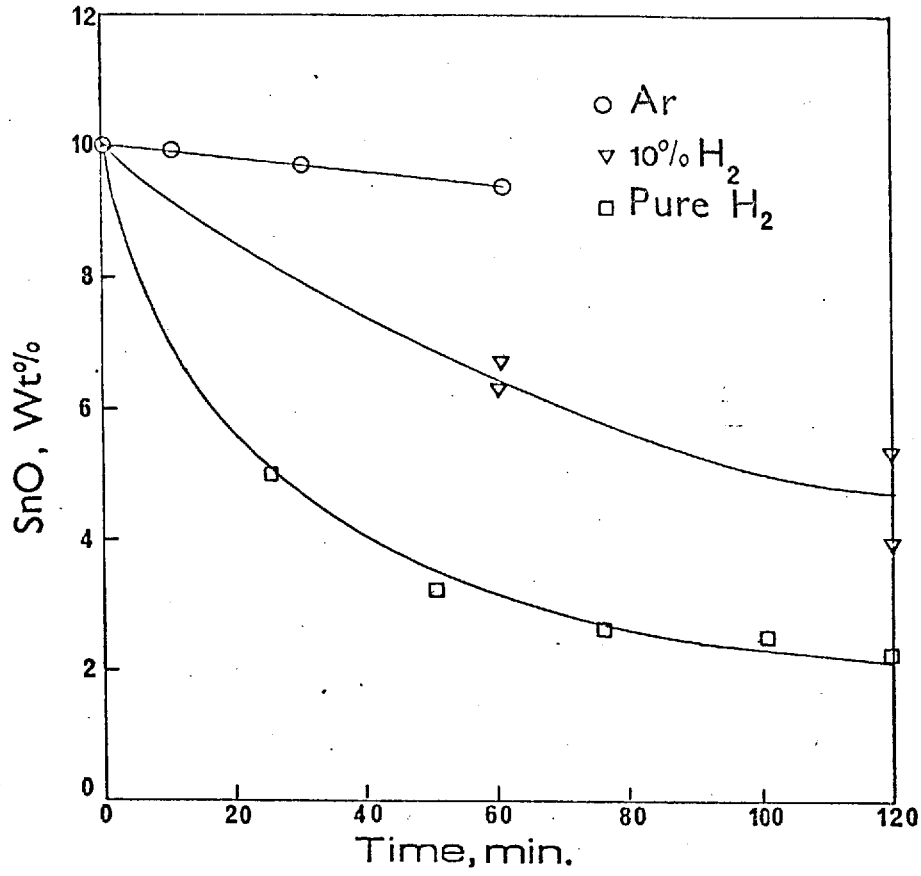

Fig. 4.17: Tin oxide removal from Slag A using different gases at 1270°C.

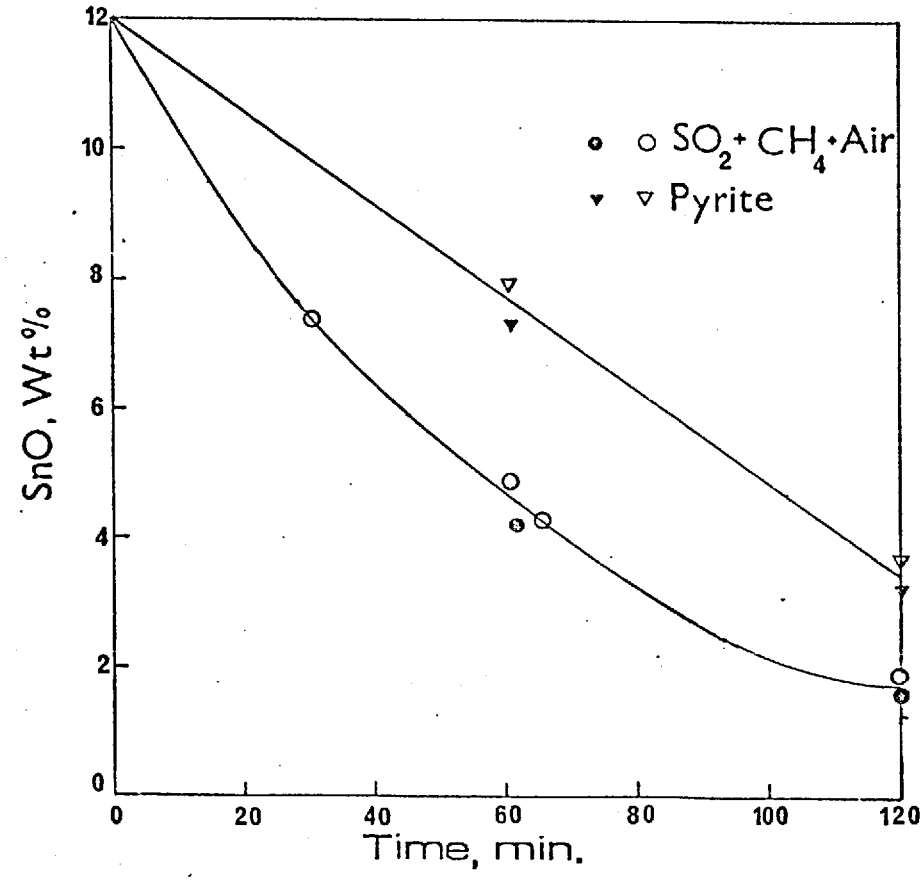

Fig. 4.18: Data for tin sulphide fuming runs.

operations. Tin is lost to the gases as stannous oxide due to the fact that SnO has appreciable vapour pressures at tin smelting temperatures. (This need not be a loss to the smelter if dust-catching equipment is used). The other kind of loss of tin is as metal physically entrapped in slags, due to slow settling of the tiny metal droplets. (The tin chemically lost to the slag is a third, obvious kind of loss).

Mass balances have been written to calculate the amount of SnO fumed from slags during reduction with pure hydrogen. For the experiments with 10% hydrogen and pure CO, the results of the chemical analyses alone were used. The kinetics of fuming of SnO were studied quite separately by bubbling argon through the slag. Quantitative metallography was used to get an idea of the tin losses due to physical entrappment.

4.1.3A: Fume losses

Pure Hydrogen runs

Mass balances were written to calculate fume losses during reduction. All parts of the apparatus susceptible to weight changes were weighed before and after the experiment. The moisture content of the charge was found using a drying column in the gas outlet circuit (Section 3.1.5). Results of the chemical analysis of the metal coupled with the above weight changes were used to calculate the SnO fumed during reduction. (Tables 4.2 & 4.3).

The chemical analyses of the slags were used in addition, to write SnO and FeO balances. This provided a check on the completeness of the separation of the slag and metal phases, the accuracy of the results of the chemical analyses and the different weight measurements involved. Appendix 4 shows a typical set of calculations. The results are tabulated in Table 4.6.

SnO fumed as a percentage of the initial SnO in the slag is roughly around 30% for reduction with pure hydrogen. No definite dependance on temperature or slag composition is seen. It is interesting that in SnO and FeO balances the

TABLE 4.6

Results from mass balances (Appendix 4).
(Two hour runs except expt. no. 24 which was a 3 hr. run).

Expt. no.	Slag	temp °C	SnO fumed %	SnO_i gms.	SnO_f gms.	FeO_i gms.	FeO_f gms.
24	A	1273	27·0	30·0	31·8	119	108
25	B	1273	29·5	30·9	35·5	82	75
26	C	1340	28·1	31·9	31·3	41	45
28	B	1340	29·3	30·9	30·8	82	76
29	A	1340	20·7	29·8	32·2	119	103
31	A	1400	28·5	30·0	35·7	120	103
32	B	1400	31·0	30·9	36·7	82	74
34	C	1400	21·7	31·9	33·9	41	40
43	D	1340	35·5	26·7	31·5	72	64
44	E	1340	38·6	27·0	32·0	103	83
49	I	1340	16·3	27·0	24·7	34	36
50	J	1340	25·1	25·9	27·4	103	95

nature of the discrepancy is complementary.

10% H_2 and pure CO runs

As noted earlier (section 4.1.2) the technique of writing the mass balance was not yet established when these experiments were performed. Thus the results of the chemical analyses were used to calculate the fume losses.

SnO fumed	=	SnO initial slag	-	SnO final slag	+	SnO equivalent of the tin in the metal

all expressed in grams. SnO fume losses calculated as a percentage of the initial slag is shown in Table 4.4. SnO fumed in the 10% H_2 experiments is on an average 10%. However, in the pure CO runs it is much higher, 38% of the initial SnO. These results are not thought to be as reliable as the ones for pure hydrogen runs.

Stannous oxide fuming

Fuming without reduction was studied by bubbling argon at a rate of 1 litre/min (as in 10% H_2 runs), the temperature and the slag composition were also similar to those in the 10% H_2 runs. Argon bubbling through the melt was carried out for 1 hr. and a 'settling period' of ½ hour (as usual) was given. It is significant that no metal beads or button were found. A metal detector was used to confirm the absence of any metal inside the crushed slag pieces.

From chemical analysis it was found that 8·4% of the initial SnO had fumed off. The rate curve for argon fuming is given in Fig. 4.17. The fuming of SnO was extremely slow and the fuming rate was constant.

It can be said from the above that the fume losses were around 30% for pure hydrogen runs, about 15% on an average for 10% hydrogen reduction and nearly 10% of the initial SnO for pure argon bubbling runs. The slag composition and the temperature did not have any effect.

4.1.38: Quantitative metallography

The solidified slags (after reduction) always contained metallic prills at the top surface. (Fig. 3.5). The beads were big, upto 4mm. across, and the centre of the surface always had a collection of droplets which had partly coalesced. Also, during the experiment, the metallic droplets (appearing darker than the slag) were seen floating on the slag surface. In the experiments with viscous slags (slags F, G and H) the process of abrupt appearance of the droplets at the centre of the crucible, their movement towards the walls and the disappearance at the walls was clear. By moving the ceramic gas lance up,higher in the melt, this could be reduced. In all experiments,the lance was kept 1 cm. above the bottom of the crucible. The lance was moved up progressively (in roughly 3 mm steps every 30 mins) as the experiment proceeded. During the settling period (half an hour for all experiments) a collection of the metal droplets at the centre of the slag top surface could be seen.

The slags solidified partly in crystalline and partly in amorphous fashion. The cooled slag around the tin beads at the top surface of the slag had a somewhat different colour than the rest of the slag (and was often glassy). At the slag/crucible interface,the concentration of fairly large (upto 1·5 mm. across) metal droplets was always high. In the experiments with the slags of orthosilicate composition (slags F, G and H) the slags were always found to be powdery after cooling. Metal beads were recovered after sieving the slag powder. From microscopic studies it was found that the powder particles themselves were free of metal.

Metallographic specimens of slag samples taken from the centre of the bulk were prepared (using diamond paste down to $\frac{1}{4}\mu$). Quantitative metallography was used to estimate the amount of the physically entrapped metal. Table 4.7 shows the results. The area % (of the metal in slags) has been converted into SnO equivalents. In experiments 7, 8, 9 and 10, where 10% H_2 was used for reduction and the metal produced was nearly pure tin, the entrapped tin contents were high. Also, the temperatures of reduction and settling

TABLE 4.7

Results of quantitative metallography ($\frac{1}{2}$hr. settling time)

Expt. no.	Slag	reducing gas	temp °C	% SnO▲ equiv.
7	A	10%H_2 ◎	1270	0·4
8	A	10%H_2 ◎	1270	0·61
9	A	10%H_2 ◎	1270	0·61
10	A	10%H_2 ◎	1270	
23	A	pureH_2 ●	1270	0·39
25	B	pureH_2 Δ	1270	0·08
26	C	"	1340	0·02
27	A	"	1270	0·28
29	A	"	1340	0·01
31	A	"	1400	0·01
32	B	"	1400	0·0

▲ SnO equivalent of the physically entrapped metal, in wt.%

◎ gas flow rate 1000 ml/min

● gas flow rate 300 ml/min Δ 600 ml/min

TABLE 4.8

Results of the Sulfide fuming runs◎. See fig. 4.18.

Expt. no.	'S'	SnO wt.%	fume gms.	Matte gms.	FeS matte wt%	Total Sn_i	Total Sn_f
36	SO_2	2·1	44·3	17·7	94·9	42·3	41·5
37	SO_2	1·9	41·9	11·4	-	-	-
40	FeS_2	3·65	44·5	11·8	94·6	42·3	47·2
41	FeS_2	3·49	51·8	16·1	-	-	-
42*	FeS_2	0·26	64·0	29·2	99·44	47·5	51·3

* The four hour run

◎ For initial slag composition see Table 4·5, slag L

were lower, the gas flow rate higher than those in pure hydrogen runs. The entrapped tin contents of slags in pure hydrogen runs were much less. The effect of temperature can be seen.

4.2: Sulfide fuming

Two types of sulfide fuming experiments were carried out. In one case sulfur was supplied continously as SO_2 (with CH_4 + air) to the slag melt while in the other sulfur was added intermittently as pyrite (FeS_2). The slag composition (five component slag with 12 wt.% SnO, see Table 4.5) and the fuming temperature (1300° ± 5°C) were the same in both the cases. The experiments were conducted for two hours and a half an hour settling time (for matte) was given. Both types of experiments were repeated.

Always a matte was obtained whose separation was neither simple nor complete. Chemical analysis was done on slag samples and the final slag, to draw the fuming rate curves. Mass balances (Appendix 4) were written to calculate the amount of fume produced. Some fume deposition on the radiation shields was always seen. The bright, crystalline fume deposit was found to consist wholly of SnS from X-ray diffraction tests.

4.2.1: SO_2 (+ CH_4 + air) bubbling runs

A mixture of SO_2 + CH_4 + air (in the ratio 25:20:55) was bubbled at a rate of 600 ml/min through the melt. Samples were drawn intermittently and analysed. The rate curves are shown in Fig. 4.18 and the results are tabulated in Table 4.8.

4.2.2: Pyrite addition

It was assumed that 80% of the total SO_2 bubbled acted as the source of sulfur in SO_2 bubbling runs and pyrite corresponding to this (6·5 gms. every 20 min.) was added. The pyrite used was not finer than 300 μ, this prolonged its dissolution, made the supply of sulfur slightly more continous and facilitated its addition through the ceramic tube. Argon was bubbled through the melt at a rate of 600 ml/min.

The rate curve for pyrite fuming is shown in Fig. 4.18 along with that for the SO_2 bubbling runs. Fuming due to pyrite addition was slower, but the rate of fuming was almost a constant and did not change with time. A four hour pyrite fuming run was carried out under conditions similar to the two hour runs in every other aspect. The results of all the fuming runs are given in table 4.8.

4.3: Estimation of errors

4.3.1: Chemical analyses

A. Slags: Standard slags were made to find the accuracy of the technique used for the analysis of slags. For the analysis of SnO the error (relative) was ±3·5% at all SnO levels and for FeO it was ±4·5%. Eventhough the error levels were not as low as desirable, they were still low enough for the purposes of this work.

B. Metals and matte: Standard alloys were made to estimate the errors in analysis. The error percentages were found to be the same (3·1% for tin and 3·5% for iron) as in slags. For metals, a higher accuracy would be expected. Presumably segregation while cooling contributed to the high errors. Drillings of the metal specimens were taken from 8 - 12 different places on the metal button to get an average composition. The metal specimens were analysed both for tin and iron so that a check could be made. The sum was always between 97·5 and 101·0%.

Mattes were analysed both for iron and tin, but the sum of the sulfide equivalents was between 95 and 98%. This was presumably because of tin loss due to SnS vaporization during fusion. Thus the compositions of mattes were based on iron analyses. No standard mattes were made to estimate the errors. The errors were assumed to be the same as in slag analyses. Analyses on all samples were carried out twice or more until consistent results were obtained. The reproducibility of the methods used was found to be good.

4.3.2: Mass balances

A. SnO fumed off: The accuracy of the calculations of the

amount of SnO fumed (see Appendix 4) depended on the completeness of slag-metal separation, the accuracy of different weighings and the estimation of the total oxygen removed due to reduction. The slag-metal separation was believed to be effectively complete. (For this purpose, the amount of tin metal entrapped in slag which was very small in comparison with the amount of metal collected was neglected. See tables 4.2, 4.3 and 4.7). The different weighings involved were accurate to 0·01 gm. Thus the error involved in the estimation of SnO fumed was due to the error involved in calculating the amount of oxygen removed due to reduction reactions and this depended on the errors in the analyses of the metal. The total error in the calculation of SnO fumed was ±1·1%.

B. SnO and FeO balances: The accuracy of these balances depended on different weighings, the errors in the calculation of SnO fumed off (for SnO balance only), the chemical analyses of slags and errors in the chemical analyses of the metal. For the SnO balance the relative error was ±4·8% and it was 5·7% for the FeO balance. A similar error level was expected for the SnO balance in the fuming experiments.

The errors incurred in quantitative metallography were not known. Thus the results shown in Table 4.7 are expected to give an idea of order of magnitude only.

CHAPTER 5

DISCUSSION

CHAPTER 5

DISCUSSION

5.1: Thermodynamics of Tin reduction

5.1.1: The equilibrium diagram

The reduction reactions that take place when hydrogen is bubbled through a tin slag are,

$$(SnO) + H_2 = \underline{Sn} + H_2O \quad (21)$$

$$K_{21} = (a_{Sn}/a_{SnO})(P_{H_2O}/P_{H_2}) \quad (22)$$

and

$$(FeO) + H_2 = \underline{Fe} + H_2O \quad (23)$$

$$K_{23} = (a_{Fe}/a_{FeO})(P_{H_2O}/P_{H_2}) \quad (24)$$

These two can be combined to give

$$(SnO) + \underline{Fe} = \underline{Sn} + (FeO) \quad (25)$$

At equilibrium, for reaction (25)

$$(a_{Sn}/a_{Fe}) = K_{25}(a_{SnO}/a_{FeO}) \quad (26)$$

Slag composition can be represented by a plot of a_{SnO} vs a_{FeO} as shown in Fig. 5.1. A line of constant slope from the origin represents a fixed a_{SnO}/a_{FeO} ratio and therefore a fixed a_{Sn}/a_{Fe} ratio (equation 26) at a given temperature. The activity coefficients of tin and iron in the binary are given by (see section 2.2.2)

$$\log \gamma_{Sn} = 0{\cdot}6125N_{Fe}^2 + 0{\cdot}3709N_{Fe}^3 \quad (27)$$

and

$$\log \gamma_{Fe} = 1{\cdot}169N_{Sn}^2 - 0{\cdot}371N_{Sn}^3 \quad (28)$$

Thus a_{Sn}, a_{Fe} and a_{Sn}/a_{Fe} are unique functions of N_{Sn}. Therefore the lines with constant a_{Sn}/a_{Fe} ratio in fig. 5.1 are also the lines of constant a_{Sn} (or a_{Fe}) and N_{Sn} (or N_{Fe}). Fig. 5.2 shows the relationship between N_{Sn}, a_{Sn}, a_{Fe} and wt.% Sn. Along a line of constant a_{Sn}, the oxygen potential is directly proportional to a_{SnO}. From equation (22),

$$pO_2^{\frac{1}{2}} \propto \frac{P_{H_2O}}{P_{H_2}} = K_{21}\,\frac{a_{SnO}}{a_{Sn}} \quad (22\text{-A})$$

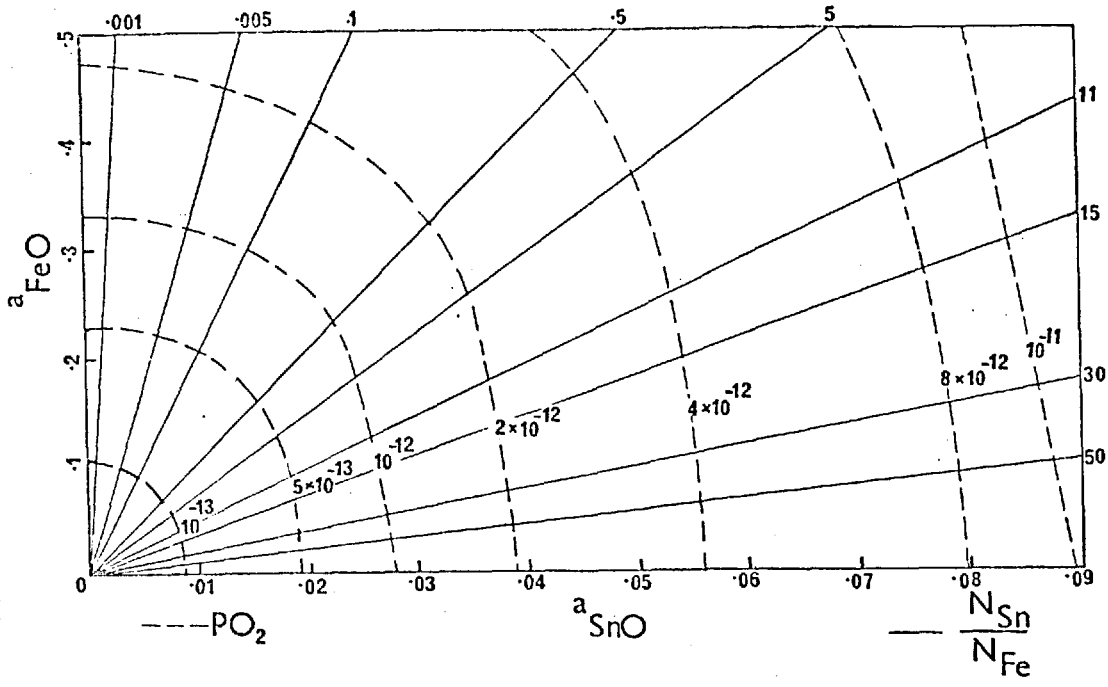

Fig. 5.1: The equilibrium diagram for tin smelting.

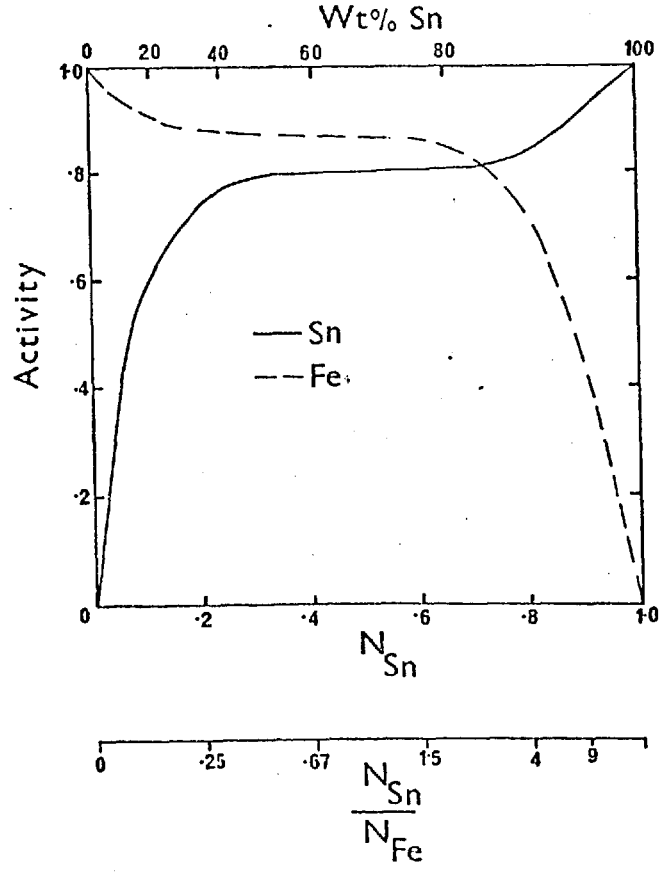

Fig. 5.2: The relationships between composition and activities in the tin-iron binary.

Thus, iso-oxygen potential lines (constant p_{H2O}/p_{H2}) lines can also be constructed on the diagram and these are shown in Fig. 5.1. This displays the equilibrium relationship between the important thermodynamic variables in tin smelting and is an equilibrium diagram.

Such a pictorial display of equilibrium relations has many uses. The simplest of these is as a standard chart. For any given slag composition, Fig. 5.1 can be used to find the equilibrium metal composition. Alternatively, if actual metal and slag compositions are known, it is possible to check rapidly if the system is in equilibrium.

5.1.2: Sequence of reduction

The x-axis in Fig. 5.1 corresponds to the system SnO/Sn (reaction 21) and the y-axis represents the system FeO/Fe (reaction 23). By comparing these two systems it can be seen that for any given $pO_2(p_{H2O}/p_{H2})$ value, FeO exists at a much higher activity than SnO. This means that when reduction of a slag is carried out, FeO remains at high activities (near the starting level) while a_{SnO} is decreased. In other words, active reduction of SnO takes place while little FeO is reduced. However, when a_{SnO} is very low and low oxygen potentials have been reached, reduction of FeO would become important. This is the case as can be seen from figs. 4.2 - 4.16.

Fig. 5.3 is a schematic equilibrium diagram. P is the starting slag composition and Q is the final slag composition. Q can be reached from P by different paths such as A or B. In both cases, the reduction of SnO is predominant initially, (as the slopes are low and a_{SnO} is decreasing more rapidly than a_{FeO}) but more so along A than along B. The path of reduction is decided by the relative magnitudes of $(a_{Sn}/a_{Fe})_{actual}$ and $(a_{Sn}/a_{Fe})_{equilibrium}$. The departures from equilibrium values are important in deciding the actual paths (and hence the sequence) of reduction.

Fig. 5.1 can also be drawn with N_{SnO} and N_{FeO} as

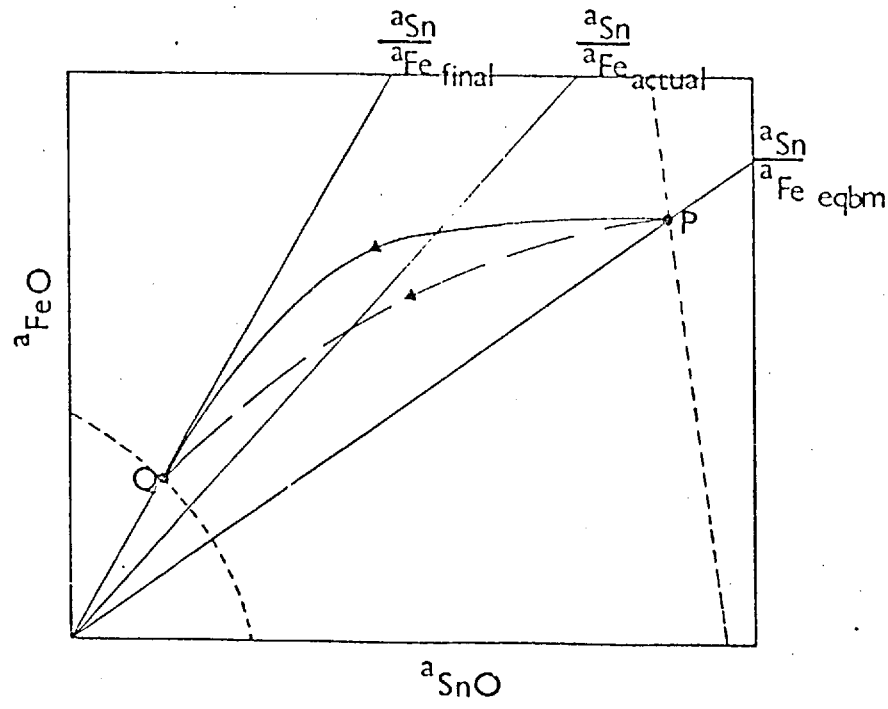

Fig. 5.3: A Schematic equilibrium diagram.

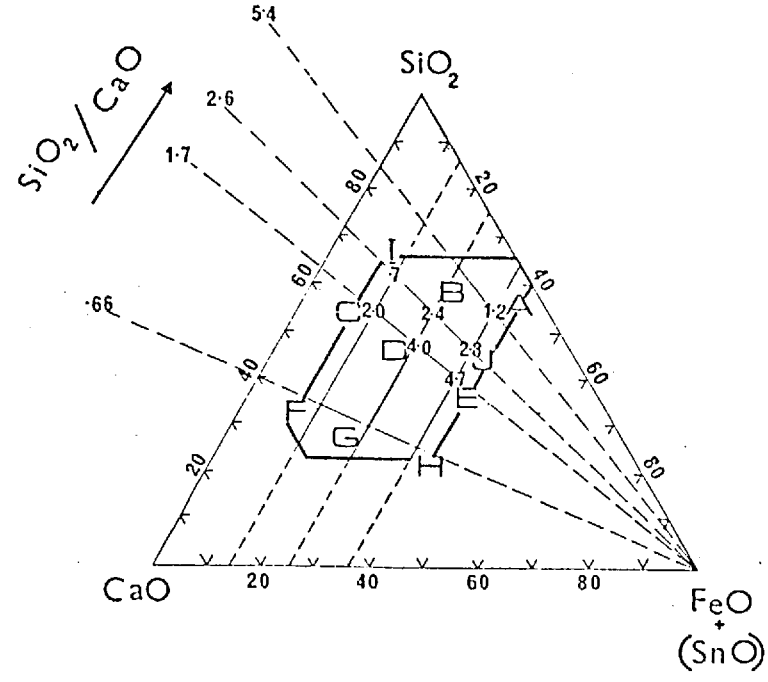

Fig. 5.4: The estimated activity coefficient of SnO in different slags.

coordinates when the activity coefficients are constant. It can then be used to visualise the fluxes involved in mass transport of slag components and their relation to metal composition. This will be discussed later.

5.1.3: Estimation of γ_{SnO}

Assuming that equilibrium between the metal and slag was achieved at the end of every experiment in the present study, γ_{SnO} values have been calculated for different slags. The equilibrium is represented by the reaction (25). Re-writing the expression for the equilibrium constant,

$$K = \frac{a_{Sn}}{a_{Fe}} \cdot \frac{a_{FeO}}{a_{SnO}} \qquad (29)$$

$$= \left(\frac{\gamma_{Sn}}{\gamma_{Fe}}\right)\left(\frac{N_{Sn}}{N_{Fe}}\right)\left(\frac{N_{FeO}}{N_{SnO}}\right) \times \frac{\gamma_{FeO}}{\gamma_{SnO}} \qquad (30)$$

From the chemical analyses of slag and metal the values for N_{Sn}, N_{Fe}, N_{SnO} and N_{FeO} were known. The expressions given by Shiraishi and Bell, Equations (27) and (28), were used to calculate γ_{Sn} and γ_{Fe}. K was calculated from the free energy change of the reaction (25). (See Appendix 2). Thus from equation (30) it was possible to calculate the ratio $\gamma_{FeO}/\gamma_{SnO}$. The slag composition was approximated to the FeO - CaO - SiO_2 ternary by substituting all the SnO (which was low in the final slag) by FeO and this was used to find γ_{FeO} from Bodsworth's[37] work. These γ_{FeO} values, in conjunction with the $\gamma_{FeO}/\gamma_{SnO}$ ratios were used to find the γ_{SnO} values. The results are shown in Fig. 5.4 and tabulated in Table 5.1.

The γ_{FeO} values taken from Bodsworth's work were those determined either for 1305° or 1365°C. They were used as no data were available for 1340°C. Also, they were read off from a graph. Thus the γ_{SnO} values estimated are only approximate. Nevertheless, they clearly demonstrate the trends. At any given FeO level there is an increase in the γ_{SnO} value for a decrease in the silica/lime ratio. An increase in the value of γ_{FeO} can also be seen but this is very much less than that of SnO. (Also the γ_{SnO} increases,

but only slightly with the FeO content). The values shown are lower than those shown in Fig. 2.6. The values shown in Fig. 2.6 were also approximate and sufficient reliable data are not available on this topic to explain the difference. The necessity for experimental determination of tin oxide activity in slags of industrial composition is clear.

The assumption that equilibrium was achieved between the slag and metal at the end of the experiment is thought to be a reasonable one. The reaction rates were low towards the end of a run, particularly that of SnO reduction. Also, Davey and Floyd[12] and Harris and Hallett[31] have shown that equilibrium between the slag and metal is reached in less than 90 minutes of contacting. In their works, the approach to equilibrium was slow (due to poor stirring conditions). Hence, in the present work (where the stirring and mixing of the phases were good) equilibrium must have been achieved in the second hour.

5.1.4: The effect of slag composition on reduction

From the above it is clear that as Silica/lime ratio was decreased, the γ_{SnO} (and to a much lesser degree γ_{FeO}, see Table 5.1) increased. Hence the ratio a_{FeO}/a_{SnO} decreased considerably, requiring a higher a_{Sn}/a_{Fe} value for equilibrium (from Eqn. 29). Thus reduction of SnO took place more intensely. As the FeO level in the slag was increased, at constant silica/lime ratio, the increase in the γ_{SnO} was small and the increase was not much more than that in γ_{FeO} itself. Thus a_{FeO}/a_{SnO} changed in proportion to the FeO concentration as did the rates of FeO reduction and the iron concentration in the metal (Fig. 4.10). The effect of silica/lime ratio on the metal composition is more difficult to predict as the rates of reduction of SnO and FeO and the general levels of SnO and FeO are important.

5.1.5: The Effect of Temperature

From Figs. 4.11 - 4.14 it is clear that the temperature of reduction had little or no effect on the reduction rates of both SnO and FeO at all slag compositions. (The slags A, B and C studied had different silica/lime ratios and

different FeO levels). This lack of effect of temperature on the rates of reduction of SnO and FeO is consistent with the thermodynamics of the system. The equilibrium constants for the reduction reactions (21) and (23) do not vary much with temperature. The value for K_{22} varies from 10·96 to 12·73 and for K_{23} varies from 0·97 to 1·17 as the temperature is raised from 1270° to 1400°C. Temperature had an effect on tin slag reduction with solid reductants in the work reported by Katkov[2]. This was because the stirring and mixing of the phases (which were originally very poor) increased considerably as viscosity decreased with increase in temperature. (The other factor of importance in determining the effect of temperature is the activation energy for the rate controlling step. The results show that this must be low).

5.1.6: The equilibrium model

The principle used in the equilibrium model is that at equilibrium, any slag composition corresponds to a particular metal composition (a_{Sn}/a_{Fe} ratio) and to a particular oxygen potential. Equilibrium between the slag and metal is assumed to develop the model and Fig. 5.5 shows the flow chart for the model. At any given slag composition, the equilibrium metal composition is calculated from eqn. (29) and the equilibrium gas composition is calculated from eqn. (22). To simulate reduction (i.e. to allow for slag composition changes) the p^e_{H2O} can be assumed to be a constant for a given time interval Δt. The amount of reduction that takes place during this Δt time interval is calculated from the conservation eqn.

$$\left.\begin{matrix}\text{moles of}\\ \text{metal}\\ \text{produced}\end{matrix}\right\} = p^e_{H_2O} \times G \times \Delta t$$

As the a_{Sn}/a_{Fe} ratio is known and as this is a unique function of N_{Sn} (see eqns. 27 and 28) the metal composition can be calculated. Thus the resulting slag composition (at the end of Δt) is calculated. This process is continued. Since the slag composition used is always that chosen at the start of a time interval, the p^e_{H2O} calculated will be too high (by a small amount). This problem is overcome in the model by

using a suitable mean slag composition for every time interval.

The results of the model are shown in fig. 5.6. The 'rate' curve shown depends slightly on the Δt value chosen (slightly faster rates are obtained for higher Δt values, but the differences are negligibly small and cannot be made out from the diagram). The equilibrium model predicts a higher rate than the actual rate for SnO in the first forty minutes. However the fact that the slopes of the two rate curves are very similar in the second hour suggests that equilibrium was achieved between the slag and metal by the end of the first hour of reduction.

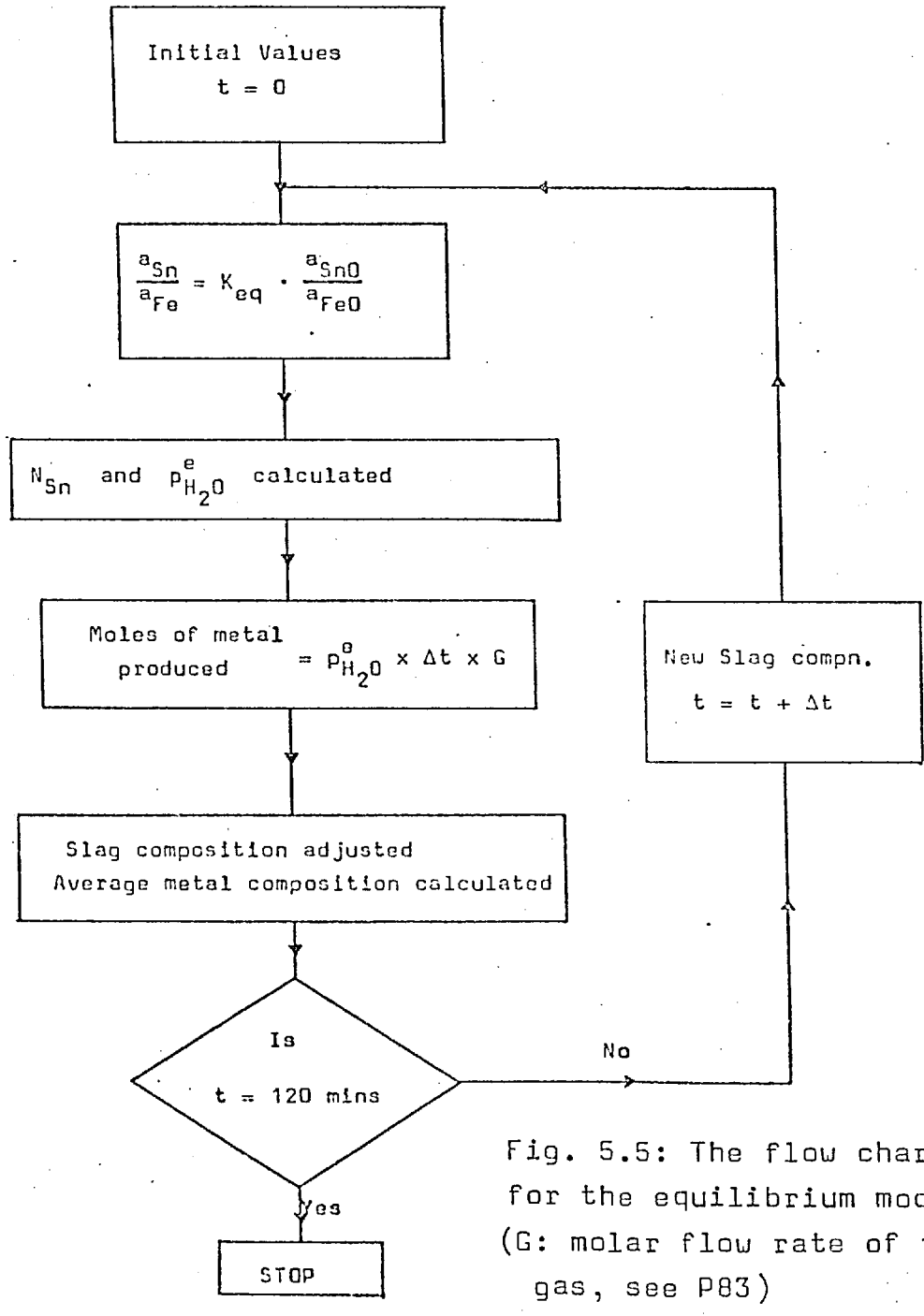

Fig. 5.5: The flow chart for the equilibrium model. (G: molar flow rate of the gas, see P83)

TABLE 5.1 (See Fig. 5.4)

Slag	wt% $(\frac{SnO}{FeO})_f$	Fe_M wt%	$\frac{a_{Fe}}{a_{Sn}}$	$\frac{\gamma_{FeO}}{\gamma_{SnO}}$	γ_{FeO}^{*}	γ_{SnO}
A	0·080	59·3	1·11	0·66	0·79	1·2
B	0·035	57·5	1·08	0·28	0·68	2·4
C	0·050	43·6	1·08	0·41	0·80	2·0
D	0·028	42·5	1·08	0·23	0·92	4·0
E	0·027	54·2	1·08	0·22	1·03	4·7
I	0·114	20·0	1·07	0·92	0·65	0·71
J	0·039	57·8	1·08	0·32	0·9	2·8

* From Bodsworth's [37] work

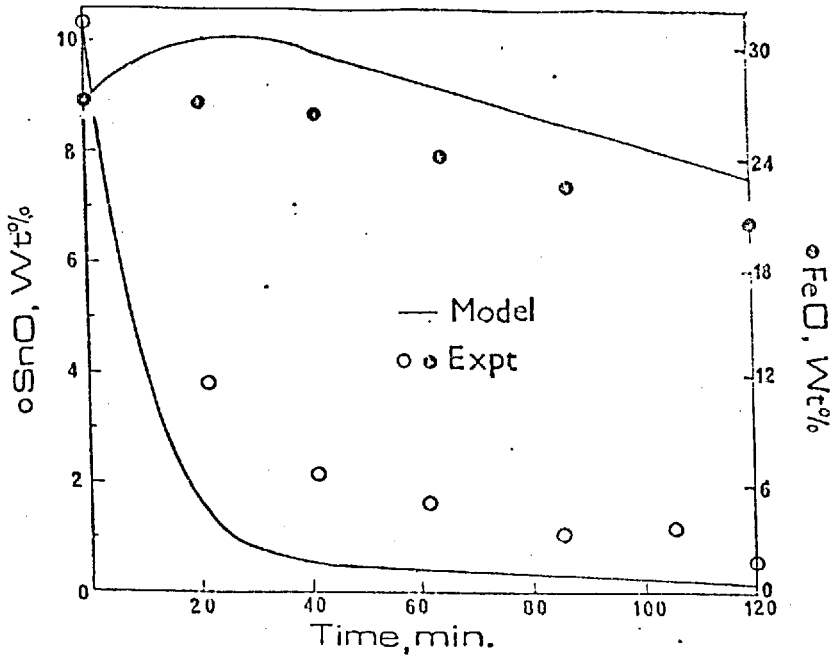

Fig. 5.6: Comparison of results from the equilibrium model and experiment for slag B at 1340°C.

5.2: Kinetics of Tin Reduction

5.2.1: Pure hydrogen runs

The reduction reactions, reactions (21) and (23) are rewritten here.

$$(SnO) + H_2 = \underline{Sn} + H_2O \quad (21)$$

$$(FeO) + H_2 = \underline{Fe} + H_2O \quad (23)$$

The overall rate of the process depends on the rate of chemical reactions and the mass transport of the reactants to and products from the reaction interface. Heat transfer is considered unimportant as the above reactions are not associated with large heat changes. As the nature or form of the initial metal/alloy formed (drop or film) is not known and as the difference in the densities of metal and slag is high, the rate of removal of metal/alloy from the interface is assumed to be fast. (Nucleation of the metal/alloy is not considered). Finally, as pure hydrogen gas was used for reduction, the transport of hydrogen to the gas/slag interface is fast. Thus, the mass transfer of SnO and FeO in the slag to the gas/slag interface and H_2O away from the interface into the gas phase are likely to be important. One or more of these could be rate controlling.

Mass transfer model

When examining the kinetics of a mass transfer controlled process a mathematical model of the process is written and the predictions of the model are compared with the experimental results.[60, 61, 62] The constant factors controlling the mass transfer rate, e.g. mass transfer coefficients and interfacial areas, can either be estimated from first principles or evaluated experimentally using model systems. The latter procedure is more satisfactory.

In the present study, to give an insight into the kinetics of gas/slag reduction reactions, a mass transfer model was developed. Making certain simplifying assumptions, the relevant rate equations, thermodynamic equilibrium relationships and conservation equations were written. A computer programme was written to solve these equations and

the rate curves were drawn. These results were compared with the experimental results. Also, by constructing another programme, parameters to identify the rate controlling step were evaluated.

A. Description

The liquid slag column (of height Z) in the crucible was divided into N elements, each of height ΔZ. At any given instant of time t, $C^b_{SnO(t)}$ and $C^b_{FeO(t)}$ were assumed to remain constant. (See Table 5.2 for the meaning of symbols used). With the time frozen, J_{SnO}, J_{FeO} and J_{H2O} were calculated in each element. The arithmetic mean values of J_{SnO} and J_{FeO} were calculated and were taken as the average reduction rates at time t over the height Z (whole of the slag bath). These rates were assumed constant for a short time interval Δt and the amount of SnO and FeO reduced (amount and composition of the metal produced) in this period were calculated. The slag composition (bulk) was changed to account for this reduction in time Δt and thus the new values for C^b_{SnO} and C^b_{FeO} at $(t + \Delta t)$ were calculated. The process was repeated for another Δt, freezing the time at $(t + \Delta t)$. The new slag composition for $(t + 2\Delta t)$ was found similarly, and the process was continued. The initial slag composition used in experiments was taken as the slag composition for time t equal to zero and by making $\sum\Delta t$ = 120 mins. rate curves were obtained which could be compared with the experimental ones.

B. Assumptions

The following simplifying assumptions were made.

(1) The chemical reactions were fast and equilibrium (for reactions 21 and 23) was achieved at the gas/slag interface.

(2) Only reduction was important and fuming of SnO was not accounted for.

(3) The activity coefficients of SnO and FeO remained constant.

(4) a. p^b_{H2O} value was a constant in any given ΔZ element.

b. C^b_{SnO} and C^b_{FeO} were constant at any given time t.

(5) $p_{H2} + p_{H2O}$ = 1 atm. throughout.

(6) The bubbles were spherical and the change in volume as they rose in the slag bath was negligible.

TABLE 5.2

C	concentration, g mol/cc
p	partial pressure, atm.
J	molar flux, moles/cm^2 sec.
$N_{Sn}N_{Fe}$	atom fractions of Tin and Iron.
K	equilibrium constant
T	Absolute temperature, °K
R	Universal gas constant, atm. moles/cc. °K
Z	height of the slag bath, cm.
N	no. of height elements
G	molar gas flow rate, moles/sec.
A	Cross sectional area of the reactor, cm^2
A_v	gas/slag contact area per unit volume of the bath, sec^{-1}
V_s	Volume of the slag bath, cc.
V	Volemetric gas flow rate, cc/min.
M	moles of metal produced (mean value when used as a subscript)
κ	mass transfer coefficient, cm/sec.
t	time, sec.
z	height of the slag bath at any h^{th} element ($Nz = Z$)
d_b	gas bubble diameter, cm.
d_o	gas lance orifice diameter, cm.
V_b	Volume of the gas bubble, cc.
U_t	terminal velocity of the gas bubble, cm/sec.
ρ	density gm/cc.
σ, γ	Interfacial tension, dynes/cm.
ν	Kinematic viscosity, stoke
$\varkappa$	no. of height elements at any given height ($\sum\varkappa = N$)

(7) 'Surface renewal theory' operated for the mode of mass transfer.
(8) The mass transfer coefficients κ_g and κ_l, were independent of composition of gas and slag respectively. Also, the κ_l value was the same for both SnO and FeO transfer.

Assumption (1) is thought to be reasonable as there is evidence that the chemical reactions were fast. Assumptions (2) and (4) were made to maintain the simplicity of the model. While comparing the results from the model with those from the experiments, fuming could be allowed for qualitatively. Assumption (3) is reasonable as the silica and lime contents, on which γ_{SnO} and γ_{FeO} mainly depend, do not undergo significant changes. Assumption (8) is reasonable as diffusivities in gases are not strong functions of composition for a given binary system[63]. Also, it is reasonable to use the same value of κ_l for both SnO and FeO since their cationic radii and charges are the same in silicate melts (see section 2.3.1) and hence the diffusivities would be nearly the same. Generally for bubble stirred systems, the surface renewal model gives good results and hence assumption (7) is believed to be valid. The change in the bubble volume as the bubbles rose was small because of the shallow bath and could only be estimated very approximately, as the bubble volume at the orifice itself was known only approximately (as the slag properties, viscosity and surface tension used in the calculations were not experimentally determined).

C. Mathematical formulation

The following flux equations are written for SnO, FeO and H_2O

$$J_{SnO} = \kappa_l(C^b_{SnO} - C^i_{SnO}) \quad (31)$$

$$J_{FeO} = \kappa_l(C^b_{FeO} - C^i_{FeO}) \quad (32)$$

$$J_{H_2O} = \frac{\kappa_g}{RT}(P^i_{H_2O} - P^b_{H_2O}) \quad (33)$$

From equations (21) and (23) it is clear that

$$J_{H_2O} = J_{SnO} + J_{FeO} \quad (34)$$

As equilibrium is assumed at the gas/slag-metal interface, the following equilibrium relationships are valid for the interfacial concentrations.

$$K_{21} = (a^i_{Sn}/a^i_{SnO})(p^i_{H_2O}/p^i_{H_2}) \quad (35)$$

and $$K_{23} = (a^i_{Fe}/a^i_{SnO})(p^i_{H_2O}/p^i_{H_2}) \quad (36)$$

A relationship between the fluxes in the slag and the metal composition at the slag/gas interface can be written. As reactions are fast, the ratio J_{SnO}/J_{FeO} represents the actual metal composition and as equilibrium is assumed at the interface, this should be equal to $(N_{Sn}/N_{Fe})^{eq.}$ value. Thus,

$$\frac{J_{SnO}}{J_{FeO}} = \frac{N^i_{Sn}}{N^i_{Fe}} \quad (37)$$

Because of the nature of the expressions for γ_{Sn} and γ_{Fe} (Eqns. 27 and 28), and as the alloy is a binary solution ($N_{Sn} + N_{Fe_i} = 1$), a^i_{Sn}, a^i_{Fe} and N^i_{Fe} are all functions of N^i_{Sn}. a^i_{SnO} and a^i_{FeO} are expressed as functions of C^i_{SnO} and C^i_{FeO} (using the γ_{SnO} and γ_{FeO} values estimated, section 5.1.3). From assumption (5), $p^i_{H2O} = 1 - p^i_{H2}$.

Thus in eqns. (31) - (37), J_{SnO}, J_{FeO}, J_{H2O}, C^i_{SnO}, C^i_{FeO}, p^i_{H2O} and N^i_{Sn} are the only unknowns. The equations represent a set of seven equations with seven unknowns. The method of solution is discussed below.

D. Solution

Equations (31) to (36) can be rearranged to write all the interfacial values and the fluxes in terms of $N^i_{Sn_i}$ and for each value of N^i_{Sn}, a set of interfacial values (C^i_{SnO}, C^i_{FeO} nad p^i_{H2O}) are obtained. Eqn. (37) can then be used to find the unique solution.

Fig. 5.7 is a schematic diagram of the equilibrium (Fig. 5.1) for tin smelting. P is the bulk slag composition

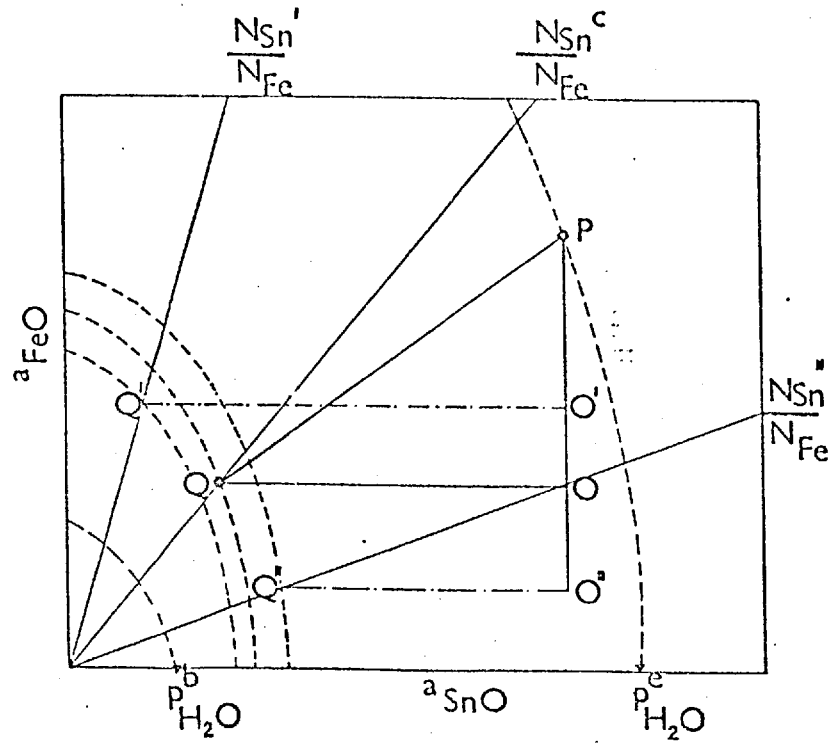

Fig. 5.7: A Schematic equilibrium diagram.

TABLE 5.3

	EXPERIMENTAL					MODEL			
Slag	Slag, wt%		Metal			Slag, wt%		Metal	
	SnO	FeO	Fe wt%	Wt. gms.	fume* loss	SnO	FeO	Fe wt%	Wt. gms.
A	2·3	28·6	59·3	44·2	1·2	2·7	36·7	52·4	42·9
B	0·65	18·7	57·5	41·6	5·0	0·73	26·4	30·7	36·6
C	0·49	9·9	43·6	32·7	7·3	0·66	12·4	18·9	32·7
D	0·47	18·7	42·5	29·6	6·7	0·38	20·4	37·6	36·4
E	0·64	23·9	54·2	36·8	12·8	0·52	29·9	52·1	45·6
I	1·3	11·4	20·0	18·3	5·5	1·49	10·8	14·9	23·8
J	1·0	26·3	57·8	38·1	4·0	0·90	30·5	50·5	42·1

* Tin equivalent of the SnO fumed, gms.

and Q is the interfacial value (to be found). p^e_{H2O} is the partial pressure of H_2O which would be in equilibrium with the bulk slag and p^b_{H2O} is the partial pressure of H_2O in the gas bulk. These two serve as the limiting values and p^i_{H2O} must lie between these two values. PO represents the driving force for FeO and OQ is the driving force for SnO. $(p^i_{H2O} - p^b_{H2O})$ is the driving force for H_2O in the gas phase. Equation (34) then requires,

$$\underset{\left[\begin{array}{c}\text{Total liquid}\\ \text{flux}\end{array}\right]}{K_l\ (PO + OQ)} = \underset{\left[\begin{array}{c}\text{Total gas}\\ \text{flux}\end{array}\right]}{K_g/RT\ (p^i_{H_2O} - p^b_{H_2O})} \qquad (38)$$

When N^i_{Sn} is varied from 0 to 1 and different interfacial concentrations are calculated (using Eqns. 31 to 36) the above condition is always satisfied. The solution required is obtained for that value of N^i_{Sn} for which eqn. (37) is also satisfied.

As N^i_{Sn} is varied from 0 to 1, the N_{Sn}/N_{Fe} equilibrium line in Fig. 5.7 moves in the clockwise direction from the y axis to the x axis. At a value of N^i_{Sn}, corresponding to $(N_{Sn}/N_{Fe})'$ the flux of SnO (O'Q') is higher than it should be (OQ). Also, the flux of FeO is smaller. Thus the actual metal composition, given by J_{SnO}/J_{FeO} is greater than the equilibrium N_{Sn}/N_{Fe}. For a value of N^i_{Sn} greater than the correct value, corresponding to a value such as $(N_{Sn}/N_{Fe})''$, the flux of SnO (O"Q") is less than it should be and the flux of FeO greater. Thus the actual metal composition given by (J_{SnO}/J_{FeO}) would be less than the equilibrium value. The solution is obtained for $(N_{Sn}/N_{Fe})^c$ for which (N_{Sn}/N_{Fe}) is equal to (J_{SnO}/J_{FeO}).

p^b_{H2O} is zero for the first ΔZ element as pure hydrogen was used and p^b_{H2O} is calculated for subsequent height elements. To find the increase in p^b_{H2O} the following conservation equation is used. As total pressure was 1 atm.,

$$\Delta p^b_{H_2O} = J_{H_2O}\ A_v\ \Delta Z\ A/G \qquad (39)$$

At the end of n^{th} height element,

$$P^{b}_{H_2O,\ n+1} = P^{b}_{H_2O,\ n} + \Delta P_{H_2O,\ n} \quad (40)$$

Thus the set of equations (31) - (37) are solved in all the N elements at any given time t. Once $N \cdot \Delta Z$ is equal to Z, the mean J_{SnO} and J_{FeO} were calculated as,

$$J^{M}_{SnO} = \sum^{N} J_{SnO,n}/N \quad (41)$$

$$J^{M}_{FeO} = \sum^{N} J_{FeO,n}/N \quad (42)$$

At the end of the m^{th} time interval,

$$C^{b}_{SnO(m+1)} = C^{b}_{SnO,m} - \left[J^{M}_{SnO,m} \quad A_v \quad \Delta t\right] \quad (43)$$

$$C^{b}_{FeO(m+1)} = C^{b}_{FeO,m} - \left[J^{M}_{FeO,m} \quad A_v \quad \Delta t\right] \quad (44)$$

For the number moles of metal produced,

$$M_{sn(m+1)} = M_{Sn,m} + J^{M}_{SnO,m} \cdot V_s \cdot A_v \cdot \Delta t \quad (45)$$

and $$M_{Fe(m+1)} = M_{Fe,m} + J^{M}_{FeO,m} \cdot V_s \cdot A_v \cdot \Delta t \quad (46)$$

Fig. 5.8 shows the flow chart describing the way the equations are solved.

E. Results

The slag column was divided into 20 height elements and a value of 60 secs. was used for Δt. The values of κ^* and $A_v\kappa_l$ estimated in Appendix 5 were used. Fig. 5.9 shows the predicted and the experimental rate curves for SnO and FeO reduction for slag B. The agreement is generally good, in particular for SnO reduction after 40 mins. Table 5.3 shows the results from the model for other slags. Final slag and metal compositions are given along with the experimental results for comparison. The agreement between the two sets of results is reasonably good.

The values of κ^* and $A_v\kappa_l$ estimated in Appendix 5

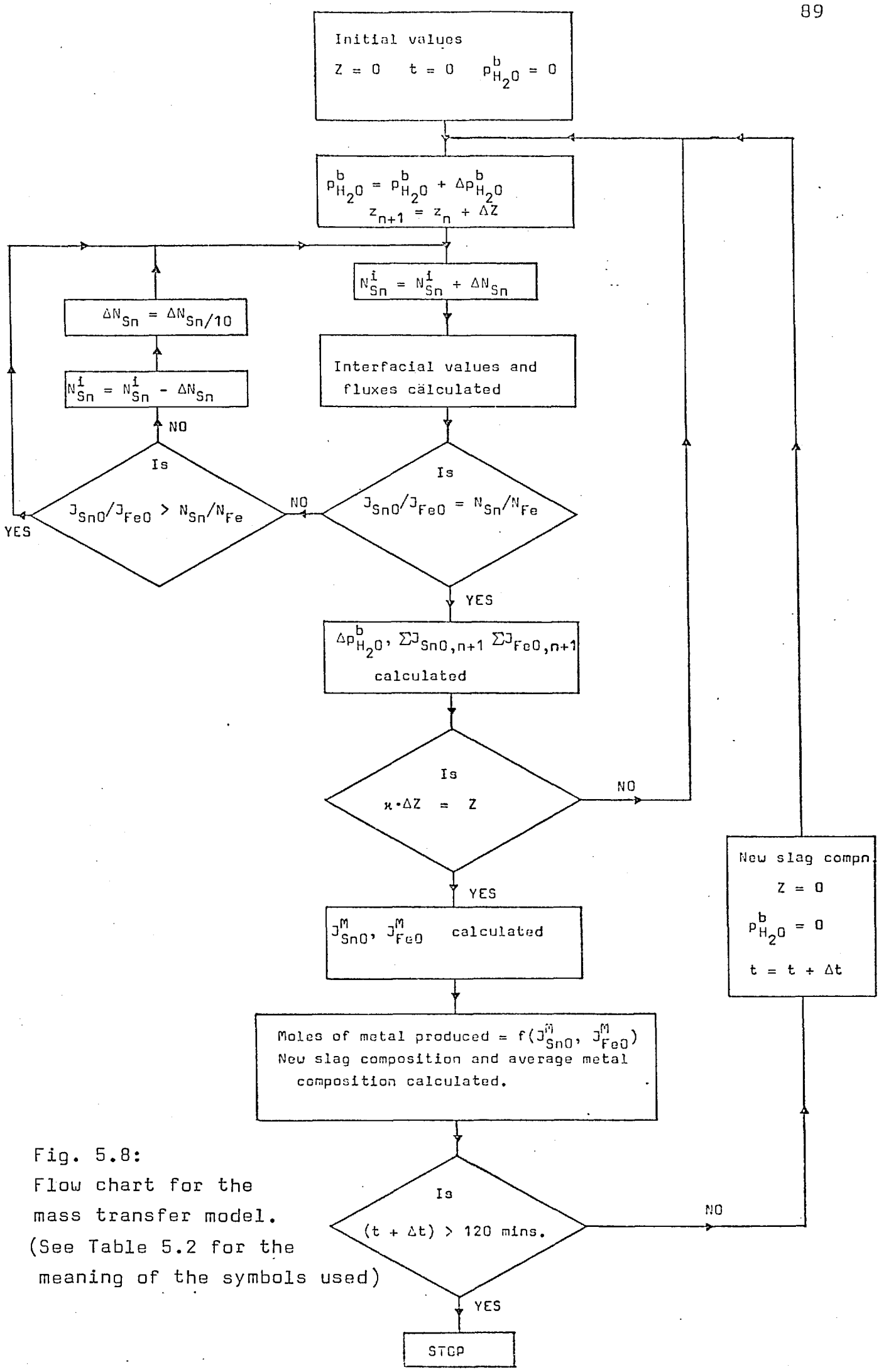

Fig. 5.8:
Flow chart for the mass transfer model.
(See Table 5.2 for the meaning of the symbols used)

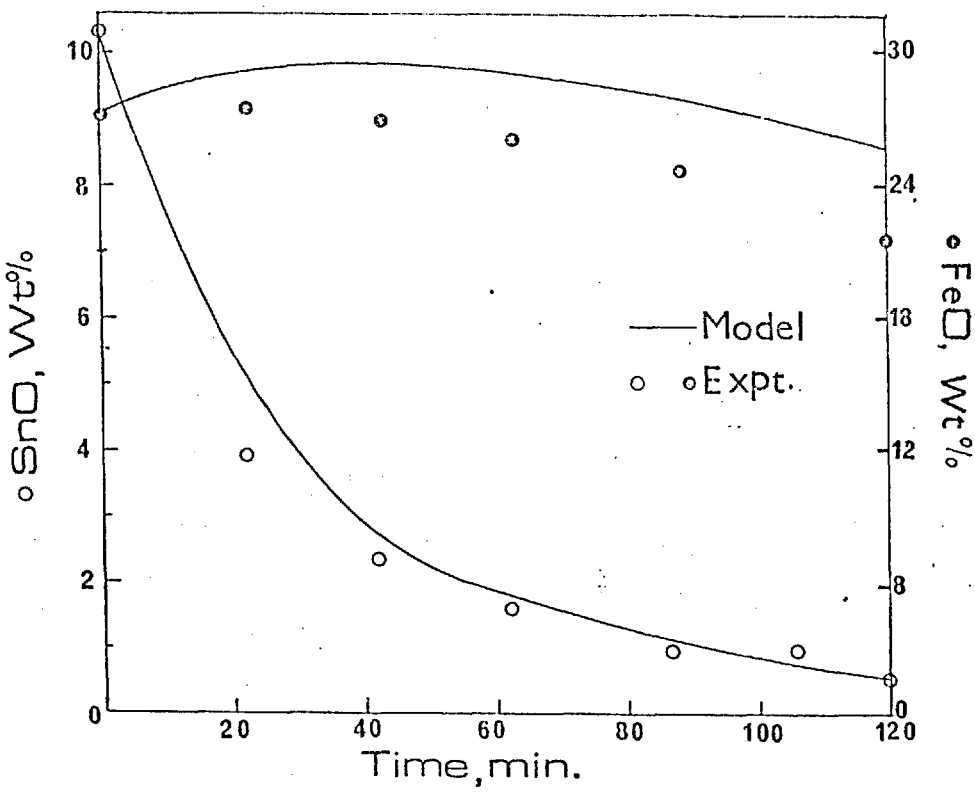

Fig. 5.9: Comparison of results from the mass transfer model and experiment for slag B at 1340°C. (See Table 5·3 on page no. 86 for other slags).

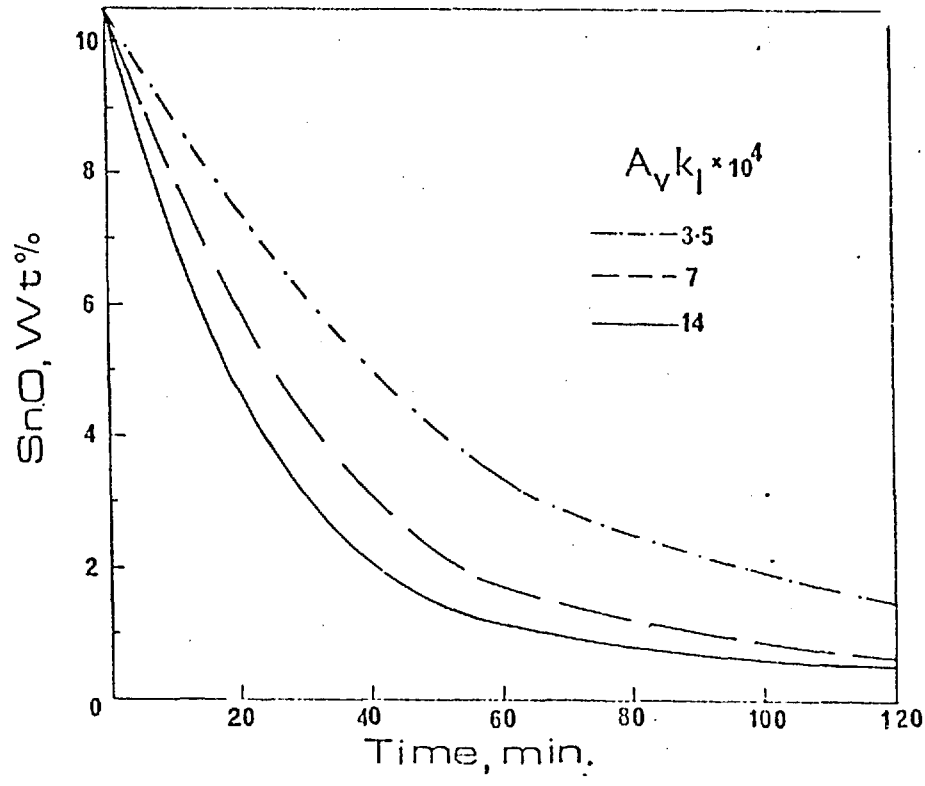

Fig. 5.10: The effect of variation in $A_v k_l$ on the predictions of the mass transfer model.

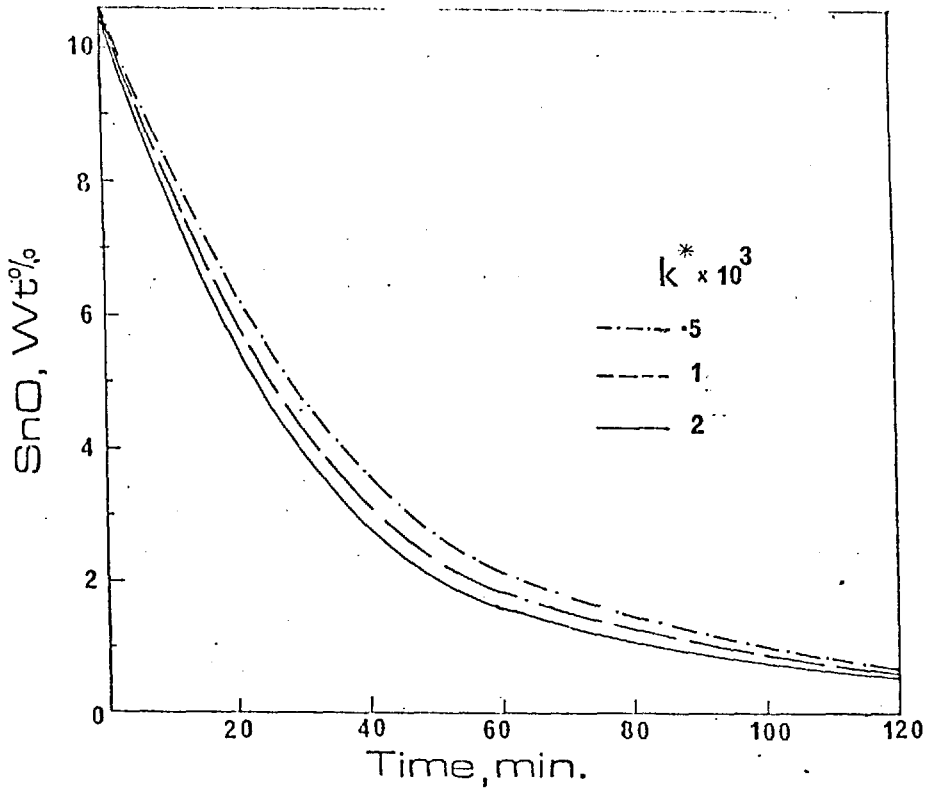

Fig. 5.11: The effect of variation of K* as the predictions from the kinetic model.

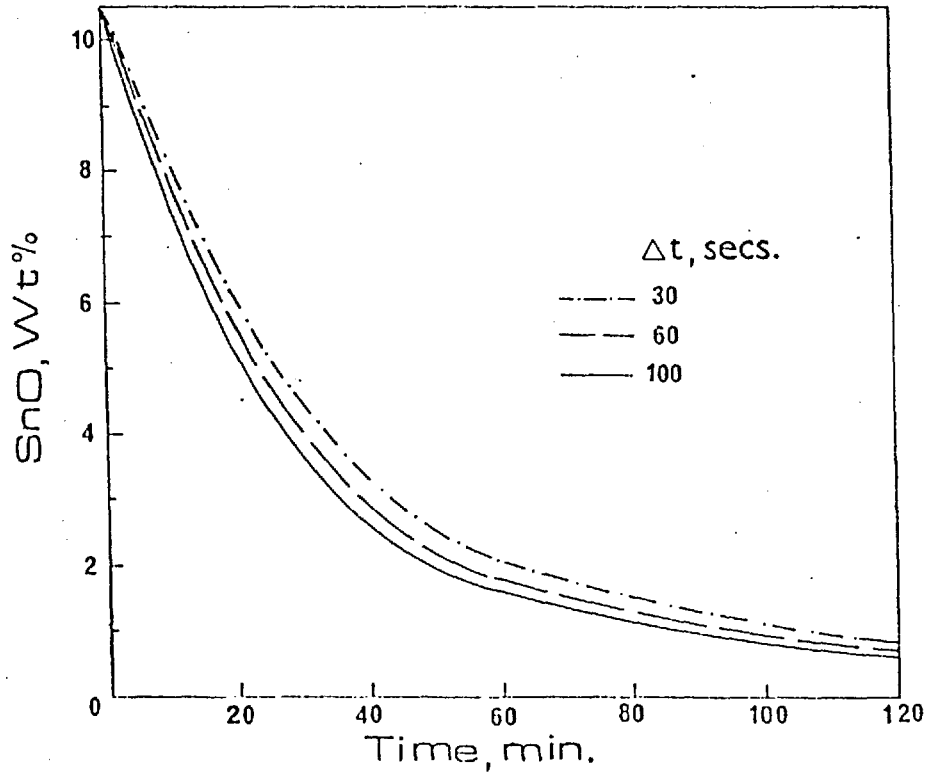

Fig. 5.12: The effect of variation of the magnitude of the time interval on the predictions from the model.

are believed of the correct order of magnitude. (See Appendix 6). κ^* and $A_v\kappa_l$ were varied by a factor of 4 and the changes in the rates due to this are presented in Figs. 5.10 and 5.11. Also, Δt was varied to see if it had an effect on the predictions and this is shown in Fig. 5.12. As can be seen, all the variations in κ^*, $A_v\kappa_l$ and Δt have produced little change.

In figs. 5.13 - 5.16 the variation of interfacial and bulk concentrations with height at different times are shown. C^b_{SnO} and C^b_{FeO} were constant throughout the melt at any time. (See section 5.2.2). The distance between the respective interfacial and bulk concentrations for a species indicates the driving force for that species. (For comparison of the driving forces in the liquid and gas phases, Δp_{H2O} should be multiplied by $7{\cdot}9 \times 10^{-3}$, the κ^*/RT term). The driving force for FeO is always small.

F. Criteria for control

The main resistance to mass transfer could either lie in the gas phase or in the liquid phase. Mixed control is also possible and it is now known that several important gas-liquid metal reactions are mixed transport controlled[71]. Also, consecutive control can occur, where the mode of control changes from one type to another, as was found in copper deoxidation[72]. To decide unambiguously where the control lies, the dimensionless parameters η_l and η_g are used[71]. They are defined as follows.

$$\eta_l = \frac{\text{actual rate}}{\text{Rate calculated assuming liquid phase control}} \qquad (47)$$

$$\eta_g = \frac{\text{actual rate}}{\text{Rate calculated assuming gas phase control}} \qquad (48)$$

Clearly then, the process is liquid phase controlled if η_l is nearly 1·0. If η_l is very small, then the process is far from liquid phase control. Similarly, if η_g is nearly unity, the process is gas phase controlled. Generally an η value

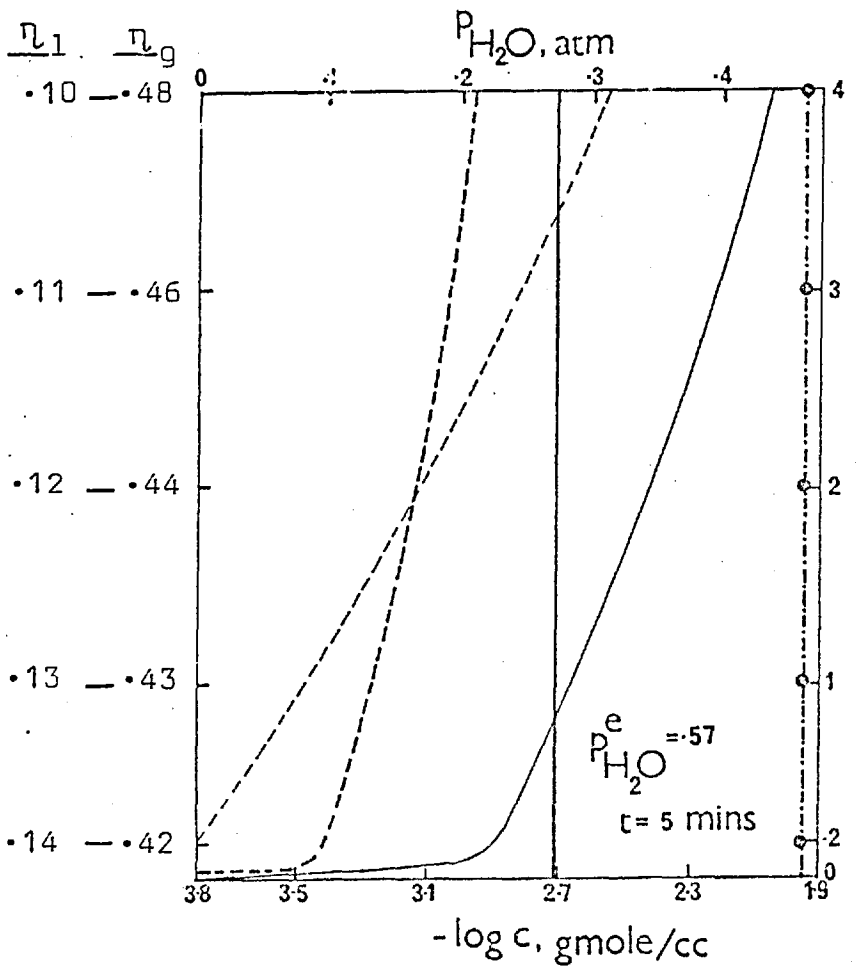

Fig 5·13:

Concentration profiles at different times

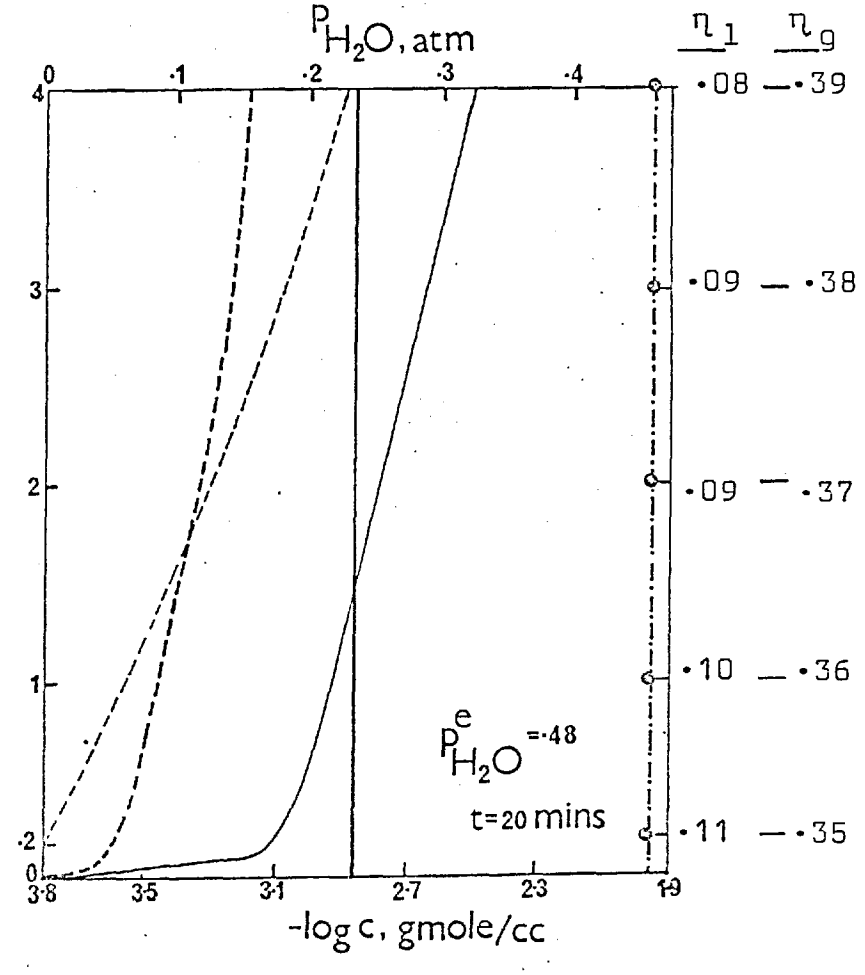

Fig 5.14:

Height, cm.

C^b_{SnO} C^i_{SnO} C^b_{FeO} $P^i_{H_2O}$ $P^b_{H_2O}$ C^i_{FeO}

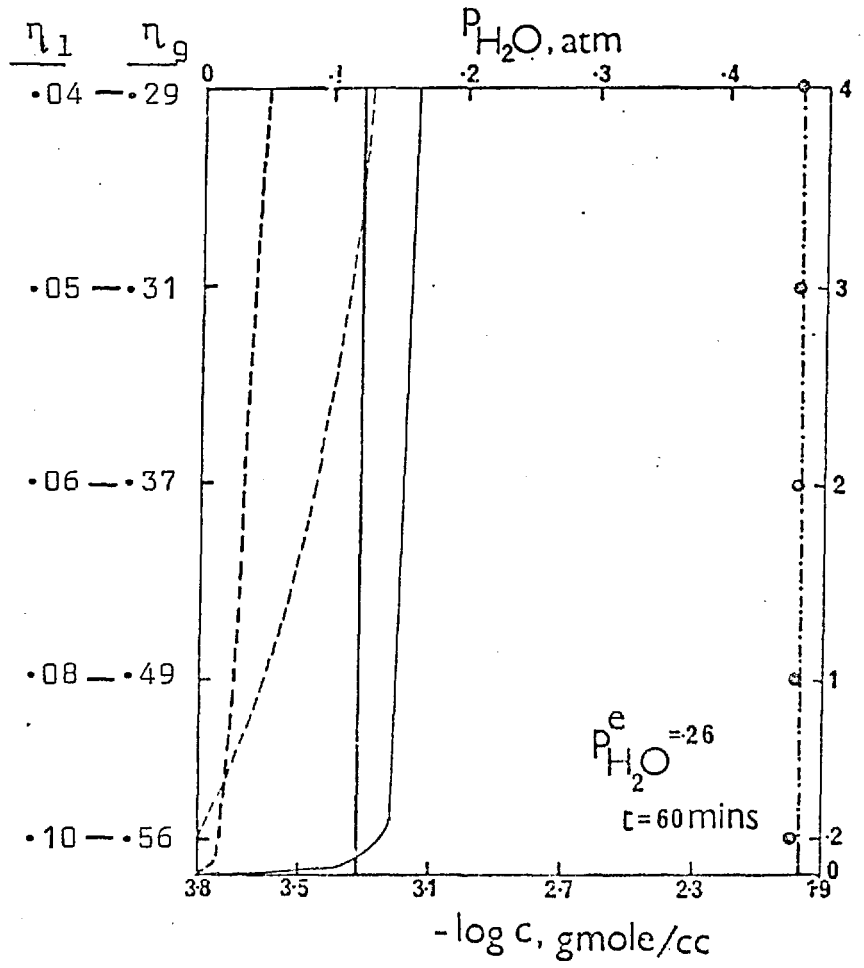

Fig. 5.15:

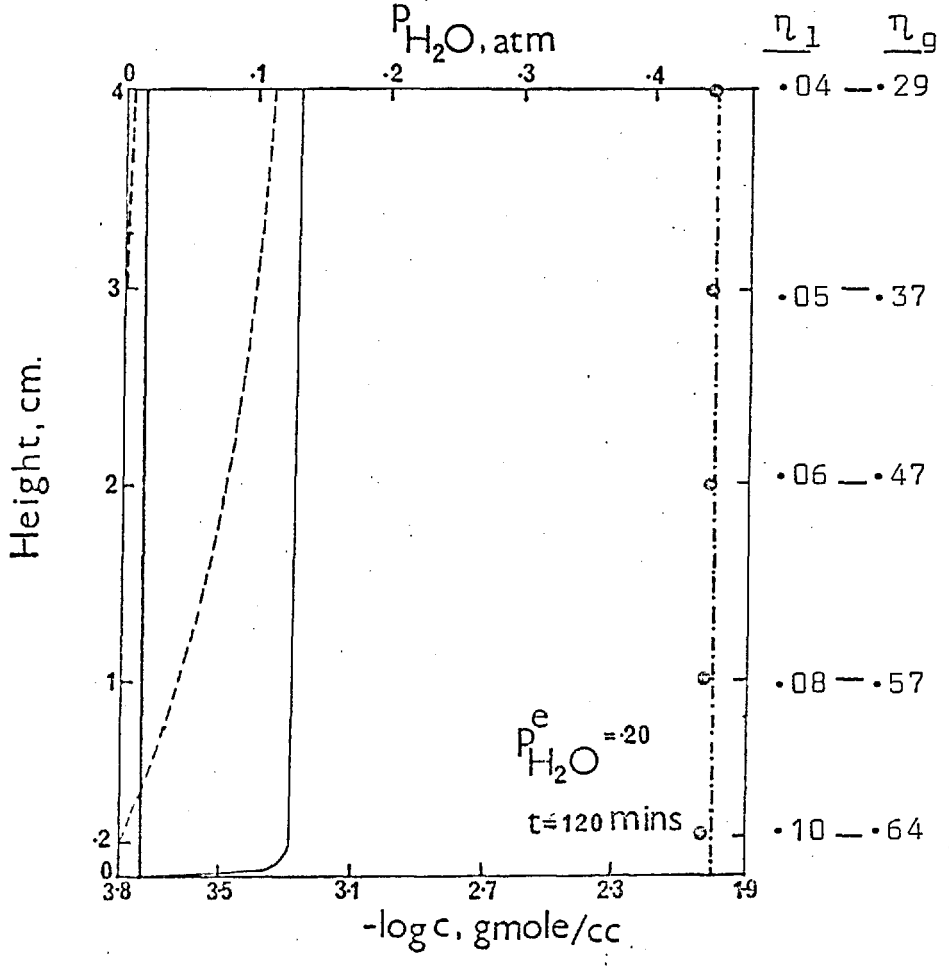

Fig. 5.16:

C^b_{SnO} C^i_{SnO} C^b_{FeO} $P^i_{H_2O}$ $P^b_{H_2O}$ C^i_{FeO}

Concentration profiles at different times

greater than 0·9 is taken to mean rate control in that phase. η values less than 0·9 are taken to mean that transport in the phase considered is not exclusively rate controlling.

To calculate η_l zero gradient is assumed in the gas phase with $p^i_{H2O} = p^b_{H2O}$ (see Fig. 5.17-a). The C^e_{SnO} and C^e_{FeO} in equilibrium with this p_{H2O} are calculated. The fluxes calculated using these values for the interfacial concentrations would be those under liquid phase control conditions.

Then,
$$\eta_l = \frac{\left(C^b_{SnO} - C^i_{SnO}\right) + \left(C^b_{FeO} - C^i_{FeO}\right)}{\left(C^b_{SnO} - C^e_{SnO}\right) + \left(C^b_{FeO} - C^e_{FeO}\right)} \qquad (49)$$

Similarly for calculating η_g, zero resistance is assumed in the liquid phase (Fig. 5.17-b). The p^e_{H2O}, in equilibrium with the bulk liquid is calculated. The rate calculated using this would be the rate under gas phase control conditions.

Then,
$$\eta_g = \frac{\left(p^i_{H_2O} - p^b_{H_2O}\right)}{\left(p^e_{H_2O} - p^b_{H_2O}\right)} \qquad (50)$$

η_l and η_g have been calculated at different levels in the slag melt for different times. These values are shown in Figs. 5.13 to 5.16. η_l values are slightly greater than 0·1 during the initial period and at the bottom of the melt. η_g is always greater than 0·1 but much less than 0·9, decreasing with time for the top of the melt. Eventhough η_l is often lower than 0·1 η_g is also low. Hence the process is mixed transport controlled throughout.

κ^* and $A_v\kappa_l$ were varied; η_l and η_g were calculated for the top of the slag melt. These values are presented in Table 5.4. As expected, increasing the $A_v\kappa_l$ value decreases η_l and increases η_g. The nature of variation in η_l and η_g is of course opposite for the variation of κ^*. But the magnitude of changes in η_l and η_g are very small. This itself is a sign of mixed control[71].

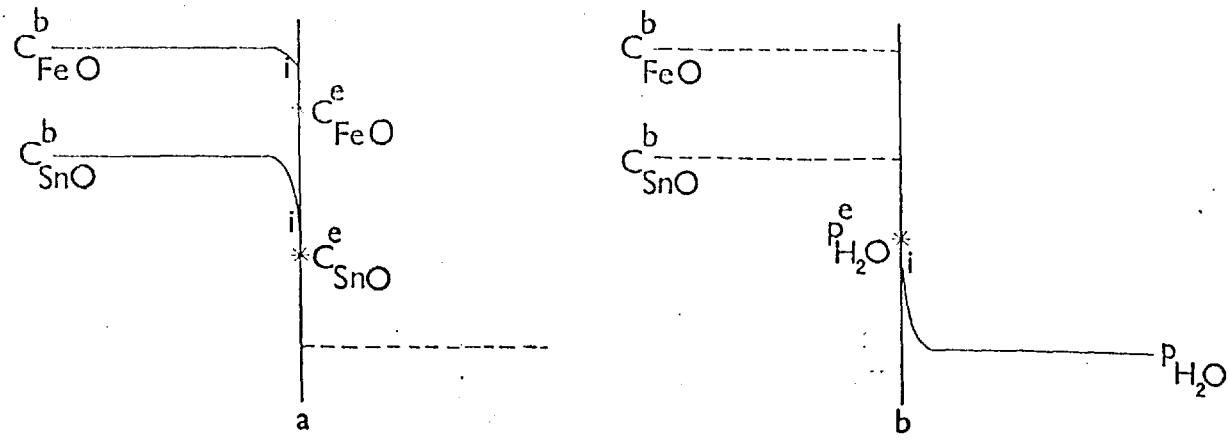

Liquid phase control

Gas phase control

Fig. 5.17: Concentration gradients used for the calculation of η_l and η_g.

TABLE 5.4

Time mins.	$K^* = 1000$				$K^* = 1000$		$A_v k_l = 0.0007$/sec.			
	$A_v k_l = 0.00035$		$A_v k_l = 0.0014$		$A_v k_l = 0.0007$		$K^* = 500$		$K^* = 2000$	
	η_l	η_g	η_l	η_g	η_l	η_g	η_l	η_g	η_l	η_g
10	.13	.26	.06	.64	.09	.44	.08	.64	.11	.27
20	.21	.24	.05	.53	.08	.39	.07	.57	.08	.22
30	.10	.22	.03	.45	.06	.32	.06	.52	.07	.19
40	.09	.20	.02	.40	.05	.30	.05	.48	.05	.17
50	.08	.19	.02	.34	.04	.29	.04	.45	.04	.16
60	.07	.19	.02	.30	.04	.29	.03	.45	.04	.15
70	.07	.19	.02	.28	.04	.29	.03	.47	.03	.11
80	.06	.19	.02	.28	.04	.29	.03	.49	.02	.10
90	.06	.20	.02	.27	.04	.29	.03	.49	.02	.09
100	.07	.23	.02	.27	.04	.29	.03	.49	.02	.09
110	.07	.27	.02	.27	.04	.29	.03	.48	.02	.08
120	.08	.29	.02	.26	.04	.29	.03	.48	.02	.08

The values shown are for the slag(B, 1340°C) top surface.

G. Discussion

The agreement between the results predicted by the model and those found from the experiments is well with in the experimental errors and the errors from the assumptions made to develop the model. The rate of SnO reduction is well predicted by the model (fig. 5.9). The experimental rates are somewhat higher in the first forty minutes due to fuming of SnO. The rate curve for FeO from the model shows the correct trend but the values themselves are lower than the actual values. This perhaps is due to slight inaccuracies in the γ_{FeO} values used. Thus in Table 5.3 the iron content of metals is slightly less than the experimental values.

The lack of variation of rates with changes in $A_v k_1$ and κ^* values is consistent with the fact that the process is mixed transport controlled. This is also reflected in small changes in η_1 and η_g values as $A_v k_1$ and κ^* are varied. The η_1 and η_g values vary depending on the concentration profiles (with height) at any given time. As the gradient for C_{FeO} is very small, most of the resistance to transfer in the liquid phase is due to SnO. All the resistance to transport in the gas phase is due to back diffusion of H_2O.

5.2.2: 10% H_2 runs

From the rate curve for reduction with 10% H_2 (fig. 4.17) it can be seen that reduction was slow. All the experimental conditions were the same as those in pure hydrogen runs for slag A (Table 4.4) except the gas flow rates. Still lower rates would be expected for reduction with 10% H_2 if lower gas flow rates were used.

The mass transfer model was used to predict the kinetics of reduction by 10% H_2. The same methods (as in Appendix 5) were used to estimate $A_v k_1$ and κ^*, and values $1{\cdot}5 \times 10^{-3}$/sec and 755 were used respectively. $(P_{H2} + P_{H2O})$ was assumed equal to 0·1 and the γ_{SnO} and γ_{FeO} values estimated for slag A were used. The rate curve obtained from the model is shown in fig. 5.18 along with the experimental curve. Also, η_1 and η_g were calculated at two

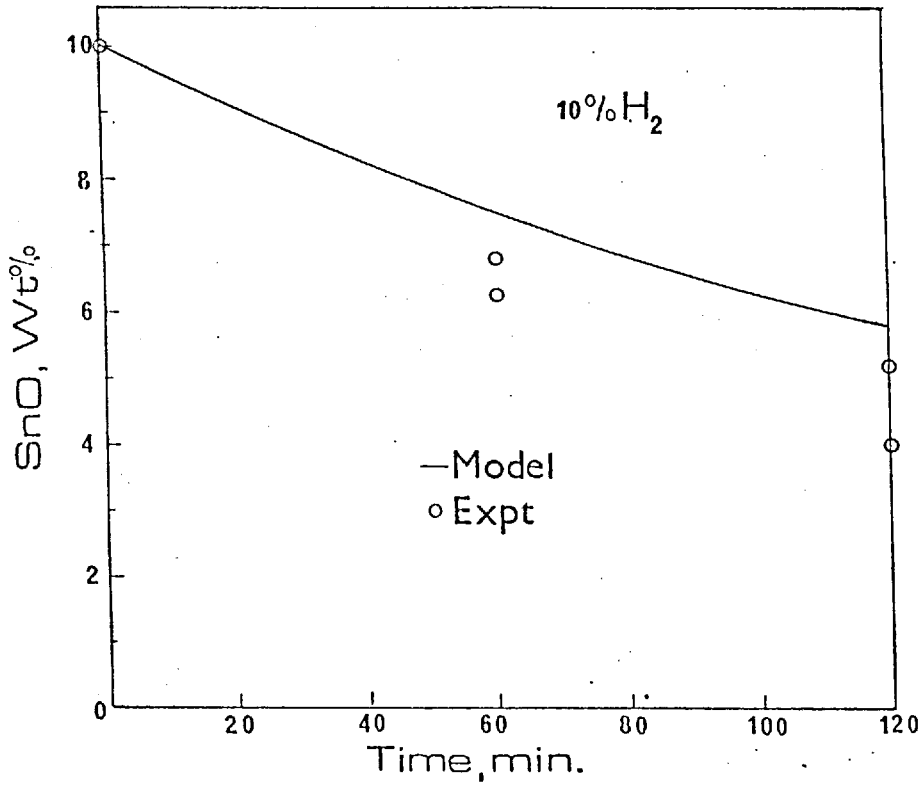

Fig. 5.18: Comparison of results from the mass transfer model and experiments for reduction with 10% H_2

TABLE 5.5

Time mins.	Melt bottom		Melt Top	
	η_l	η_g	η_l	η_g
15	·01	·95	·00	·89
30	·01	·95	·00	1·00
45	·01	·94	·00	·94
60	·01	·94	·00	·88
75	·01	·94	·00	·97
90	·01	·94	·00	·90
105	·01	·94	·00	·84
120	·01	·94	·00	·99

different levels in the slag bath (bottom at Z = 0·2cm, and at the slag melt surface, Z = 4·0cm.) for different time intervals. These are presented in Table 5.5.

The rate predicted by the model is less than the actual reduction rate. Fuming, which was not accounted for in the model, would make a big difference, as, 15% of the initial SnO was removed through fuming while the total SnO removed itself was only ≈ 45%. From Table 5.5 it is clear that the process is gas phase mass transfer controlled. All the η_g values being greater than 0·9 and η_l values nearly zero, this is a good example of gas phase control. Higher gas flow rates would result in better reduction.

5.3: Reduction with pure CO:

Floyd and Thurlby[4] found no reduction of SnO when pure CO was bubbled through a slag melt. Also, the fuming was high (53% of the initial SnO). The CO run was carried out in the present study mainly to check their result. The experimental conditions used were quite different from those in the pure hydrogen runs (see Table 4.4). Metal was produced, though only in a small quantity and the fuming was ≈ 39% of the initial SnO, slightly higher than those in pure hydrogen runs.

In Floyd and Thurlby's experiment the slag composition was different from that in the present study. The SnO, FeO and CaO contents, in wt.%, were 9·42, 30·9 and 11 in their work; as opposed to 18·88, 14·56 and 25·5 in the present work. Thus a_{SnO} in their study must have been lower. Even then, as metal is produced when slag is just held in pure CO atmosphere[47], some tin must have been produced as they bubbled CO through the slag melt (as in the present work). The amount of metal produced was obviously small and as they did not provide any settling time it is possible that a metal pool did not form. This might explain the total lack of reduction with pure CO reported by Floyd and Thurlby.

5.4: SnO fuming

No definite dependence of the amount of tin fumed as

SnO can be seen from Table 4.6 on any variable such as the slag composition of temperature. However, the composition of the gas bubbled through the slag melt seems to have had a marked effect. As the gas composition was changed from pure argon to pure hydrogen via 10% H_2, the percent SnO fumed increased from around 10% to 30%.

From Table 4.6 it can also be seen that varying the time of reduction between 1 and 3 hours had no effect on the total amount of SnO fumed. This means that most of the SnO fuming occurred within the first 20 - 30 minutes. During the experiments fume (appearing dark because of the red hot slag in the background) was seen to evolve in the first 20 - 30 mins. of reduction. Thus fuming during reduction was different from that under an inert atmosphere. In the argon run the fuming rate was constant, see Fig. 4.17 (but the SnO level in the slag did not change much).

All the fuming must have been due to SnO as the vapour pressure of Sn is low (see Fig. 2.2). From powder X-ray diffraction analysis of fume, it has been shown in this laboratory that tin is fumed off as SnO from slags in CO/argon and CO/CO_2 atmosphere[47].

The fundamental aspects of SnO fuming are not well understood. Above 1100°C $SnO_{(l)}$ is the stable phase containing very little (4 mol.%) of $SnO_{2(c)}$ in solution[8]. Thus for fuming of SnO from slags, the formation of $SnO_{(g)}$ from "$SnO_{(l)}$" (dissolved in the slag) is the most likely mechanism. In the present study the polymerization of SnO would not have been important because of the low SnO activity. The volatilization of $SnO_{(l)}$ is highly endothermic (ΔH°_{298} is 65·44 K.cals. the calculations are shown in Appendix 7).

From the results of this study (Table 4.6) it is clear that temperature does not have any effect on total tin removed as fume during hydrogen reduction. The temperature was controlled carefully, within ±5°C and the total variation in temperature was 130°C. The mass balances written had low error levels. (see Section 4.3). Thus

the results are accurate enough to reach the above conclusion.

In their study on SnO fuming from slags, Debroy and Robertson[47] also found that increasing the reducing nature of the atmosphere above the slag resulted in higher fuming. They used CO/Ar and CO/CO_2 mixtures and varied the p_{CO}. The kinetics of fuming were generally slow. At $p_{CO} = 1$ the amount of SnO fumed in three hours was ≈ 22% of the initial SnO and the rate of fuming was roughly constant. In the present study, the amount of SnO fumed in the CO run was nearly 39% in one hour. This difference must have been due to the stirring produced by injection of CO into the melt in the present study. It was also found that almost no SnO fuming took place before the bath was stirred. Debroy and Robertson[47] also found that gas injection through the slag melt increased the vaporization of SnO considerably.

5.5: Quantitative metallography

Physically entrapped tin metal in slags was determined using quantitative metallography. The results are shown in Table 4.7. As can be seen the tin entrapped in slags was very much higher in the case of the 10% H_2 runs than in the pure hydrogen runs. With 10% hydrogen the SnO equivalent of the entrapped tin was always around 0·6 wt.%. In all these experiments the temperature was 1270°C and the gas flow rate was 1 lit/min.

In the results for the pure hydrogen runs the effect of increasing temperature in decreasing the tin loss is clearly seen. For example, for slag B, the SnO equivalent of tin loss was 0·075%, 0·04% and 0·01% at 1273°, 1340° and 1400°C respectively. The gas flow rate of 600 ml/min as compared to 1 lit/min in the 10% H_2 runs could have had an effect in reducing the entrapped tin content of slags. Iron increases the surface tension and density of the alloy, thus facilitating coalescence and sinking of the alloy. Floyd[59] observed less flotation of tin when the iron content of the metal was high. This could have contributed to the decrease in tin entrapped in pure hydrogen runs where the final iron content of the metal was very much higher. If the gas lance

is positioned such that, after a certain reduction time the gas lance is immersed into the newly formed metal pool, metal losses would be considerably increased. In the pure hydrogen runs the gas lance was moved up (in steps of 3mm. every 30 mins.) and this must have contributed significantly to the lower tin entrappment.

Metal beads upto ≈ 4 mm. in diameter were always found at the slag - gas surface. There were fewer smaller beads in the surface at the end of pure hydrogen runs. About 2/3rds of the bead was always submerged in the slag. One such sample was taken and sectioned carefully and using a microscope the contact angle was measured. Rough calculation of the surface tension of the slag is shown in Appendix 8. The value obtained (550 dynes/cm.) was used to calculate the critical diameter above which the metal bead would sink and the critical diameter was calculated to be 7·8 mm. Individual beads bigger than this were never found in practice and hence the value estimated for the surface tension of the slag is thought to be roughly correct.

In the experiments with slags F, G and H, the slags were found to be powdery after cooling. The slags of ortho-silicate composition form dicalcium silicate (Ca_2SiO_4) which undergoes solid - state transformations (at less than 1000°C) involving significant volume changes. Thus when these slags are cooled they become powdery[76]. The slags were analysed by powder x-ray diffraction and shown to contain Ca_2SiO_4. The powdery slag was sieved to separate tiny as well as big metal beads. (Unfortunately, as the whole bulk of the slag had collapsed, it was not possible to distinguish the entrapped metal from that on the surface or at the walls or at the bottom). The slag powder particles were examined under the microscope and found to contain no metal beads.

5.6: Significance of the reduction results to tin smelting practice

It has been shown that temperature of reduction had no effect on reduction rates or on the overall SnO lost as fume. Hence temperatures which give reasonable fluidity for the slag

(probably no more than ≈ 50°C higher than the liquidus temperature) are sufficient. The Silica/lime ratio has an important role to play on reduction and a value of about 1·75 - 2·0 for this ratio seems to be the optimum value (higher values, apart from making the slag viscous, contribute significantly to the contamination of the metal by increasing a_{FeO} excessively, see Fig. 4.10). Regarding the FeO level in the starting slag, as it does not have any effect on the rate of reduction of SnO, the initial FeO content of the slag does not matter. This finding is thought to be significant as this means that ores and slags with high FeO levels can be successfully treated. FeO decreases the melting point of the slag and hence reduction can be carried out at still lower temperatures in high FeO slags. However, the metal obtained would be richer in iron if the FeO level in the starting slag is high. This disadvantage could be easily overcome by tapping the metal early. This point is elucidated below.

Fig. 5.19 shows the results of a typical reduction run. (expt. no. 26, Table 4.2). The first 35 mins. are significant as the tin removal rate was high while that of iron was low. For the 35th minute the tin recovery was 86·24% and the metal, nearly pure tin. However, continued reduction for two hours resulted in an additional tin recovery of 9·04% while the iron content of the metal rose to 43·6%. It can be seen from Fig. 5.20 that beyond 80% recovery of SnO, further recovery would be at the cost of contamination of the metal. The sequence of reduction is important from the metal recovery and iron contamination points of view. The delay in significant reduction of FeO is extremely important as it permits the production of tin which is not grossly debased by iron, at recoveries which are not greatly enhanced by further reduction.

The distribution coefficient (see Section 2.3.2) for different slags is calculated for different stages of reduction and shown for some slags in Fig. 5.21. The values for tin and iron were calculated from mass balances. Again the importance of the initial silica/lime ratio and the time of metal tapping is clear.

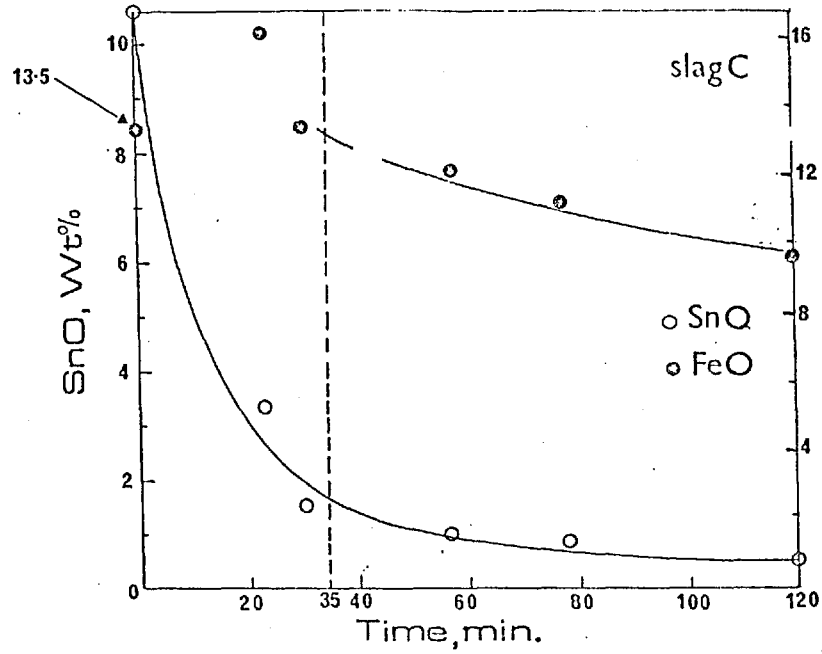

Fig. 5.19: Reduction of slag C at 1340°C; a look at the relative extents of reduction of SnO and FeO at 35 min. and 120 mins.

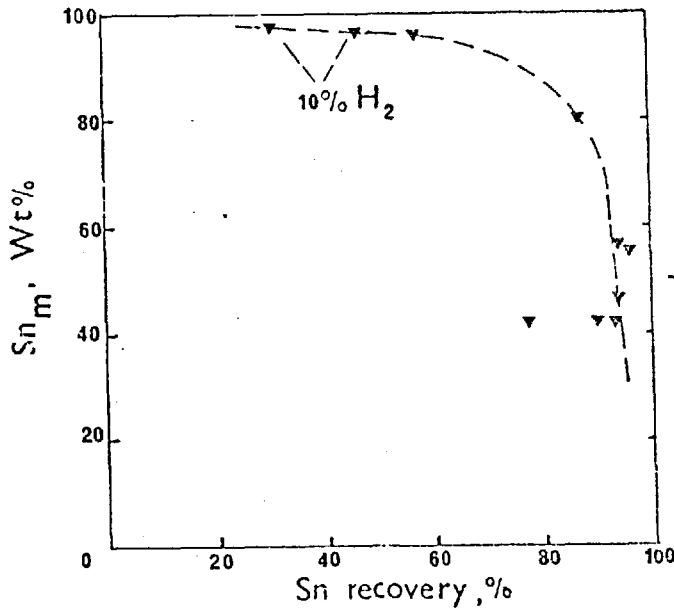

Fig. 5.20: Relationship between the tin content of the metal and the tin recovery

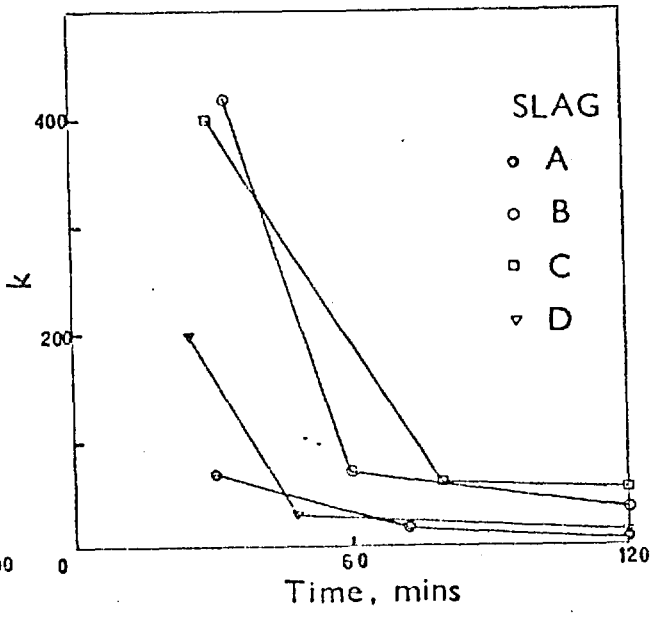

Fig 5·21: The variation of the distribution coefficient with time for different slags.

Reduction with pure hydrogen has been shown to be a mixed transport controlled process and so increasing the driving force in both slag and gas phases and increasing the gas/slag contact area increase the reduction rates. Both these are done by increasing the reducing gas flow rate. Even solid reductants could be used if stirring of the phases is taken care of by some inert or reducing gas bubbling. This would eliminate the gas resistance step. (Also nucleation of product gases would be easy as bubbling through the melt is carried out).

5.7: Stannous sulfide fuming

Tin was recovered from slags in these experiments in the form of SnS by supplying sulfur to the slag melt either as SO_2 (which was subsequently reduced) or as pyrite. The fuming rate curves are shown in Fig. 4.18 (composition of the slag used is given in Table 4.5). The amount of tin fumed was calculated by mass balances (Appendix 4) and the results are tabulated in Table 4.8. Sulfide fuming due to SO_2 bubbling was found to be faster than that due to pyrite addition. The fuming rate decreased as the SnO level dropped in the SO_2 bubbling experiments and was constant in the pyrite addition runs.

In three hours SO_2 bubbling resulted in a tin recovery of 83·3% while it was 70·8% for the pyrite addition runs. The four hour experiment carried out with pyrite addition yielded 97·9% tin recovery. Of the total sulfur supplied, 36·6% in the SO_2 run and 45·4% in the pyrite run were utilized to form the SnS. (In the pyrite addition run the total amount of S supplied was 80% of that in the SO_2 bubbling experiment). Mattes were obtained in all cases and were almost entirely FeS (See Table 4.8). The fume was deposited on the cooler parts of the furnace (notably on the radiation shields). This was analysed by powder x-ray diffraction and was found to consist entirely of SnS.

The following reactions can be expected to take place. The combustion of CH_4 (with the sub-stoichiometric air supplied) will yield CO, H_2 and water vapour. The hydrogen and

CO will react with SO_2 to produce sulfur.

$$\tfrac{1}{2}SO_2 + H_2 = H_2O + \tfrac{1}{2}S_2 \quad (51)$$
$$(SO_2 + CO = CO_2 + \tfrac{1}{2}S_2)$$

This in turn will sulfidise tin and iron.

$$SnO_{(l)} + \tfrac{1}{2}S_2 = SnS_{(g)} + \tfrac{1}{2}O_2 \quad (52)$$
$$(FeO_{(l)} + \tfrac{1}{2}S_2 = FeS_{(l)} + \tfrac{1}{2}O_2)$$

Other reactions can occur, for example the reduction of SnO and FeO by CH_4, H_2 and CO, the formation of H_2S etc. (H_2S was detected during the experiment and the deposition of sulfur on the cooler parts of the apparatus was also observed).

To find the parameters most important for the formation of SnS in the SO_2 bubbling runs, the reactions (51) and (52) are considered. If these reactions predominate, it can be shown that

$$P_{SnS} = K' \, a_{SnO} \, P_{SO_2}^{\frac{1}{2}} \quad (53)$$

For pyrite addition runs the sulfur is generated according to the reaction

$$FeS_2 = FeS + \tfrac{1}{2}S_2 \quad (54)$$

From reactions (52) and (53) it can be shown that

$$P_{SnS} = \frac{K'' \cdot a_{SnO}}{P_{O_2}^{\frac{1}{2}}} \quad (55)$$

assuming unit activity for FeS_2 and FeS (as the matte obtained was almost entirely FeS, see Table 4.8).

Thus in sulfide fuming the activity of SnO and hence the composition of the slag is important. High partial pressure of SO_2 in the SO_2 bubbling runs and a reducing atmosphere in the pyrite addition runs would help too. Temperature might increase the fuming rate as P_{SnS} increases sharply with temperature (See Fig. 2.2). FeS_2 loses a lot of sulfur at temperatures greater than 500°C[77] and hence the nature of addition is extremely important. This is even more

the case if elemental sulfur is used. Entrainment of pyrite powder (not too fine) with a reducing gas blown through the melt would be ideal.

CONCLUSIONS

CONCLUSIONS

1. Reduction of slags containing SnO and FeO with pure hydrogen was shown to be a mixed transport controlled process using the mathematical model developed to study the kinetics of the reduction reactions. The estimated values of $A_v k_1$ and k^* were used in the model and the results of the room temperature experiments confirmed that these were of the correct order of magnitude.

2. The Silica/lime ratio of the initial slag had a significant effect on the rates of reduction: lower values for the ratio resulted in faster reduction due to raised SnO activity.

3. The FeO level in the starting slag had no observable effect on the rate of reduction of SnO. However, high FeO levels resulted in a metal phase richer in iron.

4. The temperature of reduction had no appreciable effect on the reduction rates.

5. Increasing the gas flow rate increased the rates of reduction through an increase in $A_v k_1$.

Thus slags however high in FeO can be treated successfully at low temperatures by reduction with pure hydrogen. By adjusting the Silica/lime ratio of the slag and using high gas flow rates, high reduction rates can be achieved. By tapping the metal at the appropriate time, the contamination of tin by iron can be prevented at little penalty with respect to tin recovery.

6. Reduction with 10% H_2 and pure CO was slow. The former was shown to be a gas-phase controlled process.

7. The fuming of SnO during reduction depended on the reduction potential of the gas used and on the SnO level in the slag. The higher the reduction potential of the gas, the greater was the amount of SnO fumed.

8. The fuming of SnO in inert atmosphere was slow and the nature of fuming was possibly different to that in a reducing atmosphere.

9. The metal losses in slags due to the physical entrappment of tin could be greatly reduced by increasing the temperature of reduction. Lower gas flow rates and moving the gas lance away from the metal pool reduced the tin loss due to physical entrappment.

10. Recovery of tin as sulfides from slags by bubbling SO_2 with reducing gases was faster than the traditional pyrite fuming.

APPENDIX 1

To calculate γ_{Fe} at the miscibility gap composition.

Monotectic temperature:	1401°K (1128°C)
Latent heat of fusion of iron:	3300 cals/mole[51]
Melting point of iron:	1809°K (1536°C)
Solid solubility of tin in α iron:	0·083
Solubility of iron in tin: (at the tin rich end of the miscibility gap)	34·7 at %

Neglecting the difference between the specific heats of liquid and solid iron, the activity of pure solid iron (supercooled liquid iron) is given by

$$\log a_{Fe} = \frac{\Delta H_M (T-T_M)}{4{\cdot}576 T \cdot T_M} \qquad \text{(A1-1)}$$

(all the notations have their conventional meaning)

at 1401°K,

$$\log a_{\text{pure-Fe}} = \frac{3300\ (1401-1809)}{4{\cdot}576 \times 1401 \times 1809} \qquad \text{(A1-2)}$$

$$= -0{\cdot}1163$$

Assuming that Raoult's law holds for the activity of iron in the α phase over the region $N_{Sn} = 0$ to $N_{Sn} = 0{\cdot}083$, the corrected activity for α-iron saturated with tin would be

$$\log a_{Fe} = -0{\cdot}1163 + \log 0{\cdot}917$$
$$= -0{\cdot}1539$$

and $a_{Fe} = 0{\cdot}702$

At the miscibility gap composition ($N_{Fe} = 0{\cdot}347$)

$$\gamma_{Fe} = 0{\cdot}702/0{\cdot}347$$

$$= 2{\cdot}02$$

(If the latent heat of fusion of iron is taken as 3700 cals./mole as Davey and Floyd[12] have, γ_{Fe} would then be 1·95).

APPENDIX 2

To calculate the free energy change of the reaction

$$SnO_{(l)} + Fe = Sn_{(l)} + FeO_{(l)} \qquad (A2\text{-}1)$$

From Section 2.1.2,

$$Sn_{(l)} + \tfrac{1}{2}O_{2(g)} = SnO_{(l)}$$

$$\Delta G^\circ = -63566{\cdot}7 + 20{\cdot}93T \qquad (A2\text{-}2)$$

From reference 51,

$$Fe_{(l)} + \tfrac{1}{2}O_{2(g)} = FeO_{(l)} \qquad (A2\text{-}3)$$

$$\Delta G^\circ = -55620 + 10{\cdot}83T \qquad (A2\text{-}4)$$

(Eventhough equation (A2-4) is strictly valid only above 1808°K, its use at tin smelting temperatures introduces negligible error).

From (A2-2) and (A2-4), the free energy change for (A2-1) is

$$\Delta G^\circ = 7946{\cdot}7 - 10{\cdot}1T. \qquad (A2\text{-}5)$$

The variation of the equilibrium constant for the reaction (A2-1) with temperature is shown below.

T°K	K_{eq}
1523	10·85
1573	11·22
1673	15·14
1773	17·38

APPENDIX 3

Calculation of enthalpy changes for the reduction reactions:

Calculations for the following reactions are for 1543°K (1270°C)

$$SnO + H_2 = Sn + H_2O \qquad (A3\text{-}1)$$

$$FeO + H_2 = Fe + H_2O \qquad (A3\text{-}2)$$

$$SnO + Fe = Sn + FeO \qquad (A3\text{-}3)$$

The sensible heats of all the elements and compounds taking part in the above reactions calculated (see the following pages) are as follows.

Substance	Sensible heat at 1543°K (cals./mol.)
$Sn_{(l)}$	11205·9
$Fe_{(l)}$	15179·1
$H_{2(g)}$	9043·8
$SnO_{(l)}$	-45449·2
$FeO_{(l)}$	-39147·5
$H_2O_{(g)}$	-45930·3

Thus the enthalpy changes for reactions (A3-1), (A3-2) and (A3-3) are 1681·0 cals, -647·5 cals and 2328·5 cals. respectively.

(As the error in the values of heats of formation and heats of fusion are of the order of 500 cals. the error in enthalpy changes are of the same order).

The values for heat capacities, heats of transformation etc. used are given in table A3.1.

$Sn_{(l)}$:

$$\Delta H^{1543}_{Sn(l)} = \Delta H_t + \int_{298}^{504\cdot9} \left(C_{P_{Sn(s)}} \cdot dT\right) + L_f + \int_{504\cdot9}^{1543} \left(C_{P_{Sn(l)}} \cdot dT\right)$$

$$= \underline{11205\cdot9} \text{ cals/mol.}$$

$Fe_{(l)}$: The following are the calculations for the supercooled liquid as, at 1543°K, iron is solid.

$$\Delta H^{1543}_{Fe(l)} = \int_{298}^{1033} \left(C_{P_\alpha} \cdot dT\right) + \Delta H_{\alpha\rightarrow\beta} + \int_{1033}^{1181} \left(C_{P_\beta} \cdot dT\right) + \Delta H_{\beta\rightarrow\gamma}$$

$$+ \int_{1181}^{1674} \left(C_{P_\gamma} \cdot dT\right) + \Delta H_{\gamma\rightarrow\delta} + \int_{1674}^{1809} \left(C_{P_\delta} \cdot dT\right) + L_f$$

$$+ \int_{1809}^{1543} C_{P_L} \cdot dT$$

$$= \underline{15179\cdot1} \text{ cals/mol.}$$

$H_{2(g)}$:

$$\Delta H^{1543}_{H_{2(g)}} = \int_{298}^{1543} \left(C_p \cdot dT\right)$$

$$= \underline{9043\cdot78} \text{ cals/mol.}$$

$SnO_{(l)}$:

$$\Delta H^{1543}_{SnO_{(l)}} = \Delta H^{298}_{formation} + \int_{298}^{m.p.} \left(C_p \cdot dT\right) + \Delta H_f + \int_{m.p.}^{1543} \left(C_p \cdot dT\right)$$

(The same value of C_p is used throughout as no other value is available).

$$= -45449{\cdot}2 \text{ cals/mol.}$$

$FeO_{(l)}$: (Supercooled liquid)

$$\Delta H^{1543}_{FeO_{(l)}} = \Delta H^{298}_{formation} + \int_{298}^{1651} \left(C_{p_{(s)}} \cdot dT\right) + L_f + \int_{1651}^{1543} \left(C_{p_{(L)}} \cdot dT\right)$$

$$= -39331{\cdot}5 \text{ cals/mol.}$$

$H_2O_{(g)}$:

$$\Delta H^{1543}_{H_2O_{(g)}} = \Delta H^{298}_{formation} + \int_{298}^{1543} \left(C_p \cdot dT\right)$$

$$= -45930{\cdot}3 \text{ cals/mol.}$$

TABLE A3-1

Substance	-Heat of formation cal./mol.	Transformation point °K	Heat of Transformation Cal./mol.	Heat capacity $A+BT+CT^{-2}$ cal/deg.°K			Temp. Range °K
				A	$Bx10^{3}$	$Cx10^{-5}$	
Sn_s	-	504·9	1690	4·42	6·3	-	298 - 504·9
Sn_l	-	-	-	7·3(52)	-	-	505 - 1300*
Sn_α	-	286	500	-	-	-	-
α-Fe	-	1033	1200	4·18	5·92	-	273 - 1033
β-Fe	-	1181	220	9·0	-	-	1033 - 1181
γ-Fe	-	1674	210	1·84	4·66	-	1181 - 1674
δ-Fe	-	1809 (m.p.)	3300	10·5	-	-	1674 - 1809
$Fe_{(l)}$	-	-	-	10·0	-	-	m.p. - 1873
H_{2g}	-	-	-	6·52	0·78	0·12	298 - 3000
SnO_s	68350	1273(8)	7000(12)	9·55	3·5(11)	-	298 - 1273*
FeO_s	63200	1651	7400	11·66	2·00	-0·67	298·1651
FeO_l	-	-	-	16·30	-	-	1651 - 1800
H_2O_g	57800	-	-	7·16	2·56	0·08	298 - 2500

Refcrence in brackets: where not mentioned it is ref. 51. * This has been used upto 1543°K and the error involved is small[53,54].

Mass balances

Reduction (Calculations shown are for experiment no. 28)

I. SnO content of the initial slag: 10·3 (wt.%)

II. FeO content of the initial slag: 27·3 (wt.%)

All masses in grams

a. mass of the empty crucible: 259·52

b. mass of the crucible + charge: 558·25

c. mass of the crucible + Slag + metal: 528·10
(Crucible with its contents as it was taken out of the apparatus after reduction).

d. Total mass of the slag samples: 12·20

δ_i. mass of the sample i

e. mass gained by the thermocouple sheath: 0·50

f. mass gained by the ceramic gas lance: -1·50
(-ve for wt. loss)

g. mass gained by the drying column: 0·63
(in the outlet gas circuit to measure the moisture content of the charge)

h. mass of the metal produced: 41·60

Chemical analyses: results (wt.%)

A. Iron content of the metal: 57·51

B. Tin content of the final slag: 0·65

C. Iron content of the final slag: 18·66

D. Tin content of the slag sample i: D_i

E. Iron content of the slag sample i: E_i

SnO fumed (gms.)

i. Total mass loss = C - b = 30·15

j. mass loss due to SnO fumed + mass loss due to O_2 removed due to reduction = i - (d + e + f + g)

= 18·32

k. O_2 removed due to reduction = {oxygen equivalent of iron produced} + {oxygen equivalent of tin produced}

$$= \left(\frac{A}{100} \times h \times 0{\cdot}286\right) + \left(\frac{100-A}{100}\right)(h \times 0{\cdot}135$$

= 9·22 grams

l. SnO fumed = j - k = 9·10 grmas

m. SnO fumed as a percentage of initial SnO = $\frac{1001}{I \times (b - a)}$ = 29·6

SnO balance

n. Total final SnO = SnO in the final slag + SnO equivalent of the tin produced + SnO fumed + Total SnO in slag samples.

$$= \frac{B}{100}(c - a - h) + \left(\frac{100-A}{100}\right)(h \times 1{\cdot}135) + 1 + \Sigma_i\left(\frac{Di}{100} \times \delta_i\right)$$

= 30·81 grams

o. Total initial SnO = I x (b - a) = 30·9 grams

FeO balance

p. Total final FeO = $\frac{C}{100}(c - a - h) + \frac{A}{100}(h \times 1{\cdot}286) + \frac{1}{100}\Sigma_i E_i \delta_i$

= 75·7 grams

q. Total initial FeO = II x (b - a) = 81·9 grams

Fuming (Calculations shown are for a pyrite addition experiment, no. 40)

A. Tin content of the initial slag = 12·0 (wt.%)

All masses in grams

a. mass of the empty crucible = 249·25

b. mass of the crucible + charge = 644·74

c. mass of the crucible + reaction products = 617·23

d. mass gained by the gas lance = 1·27

e. mass gained by the thermocouple sheath = 1·50

f. total sample mass = 18·24

g. mass gained by the drying column = 0·98
(moisture content of the charge)

h. total mass of the pyrite added = 39·00

l. mass of the matte produced = 11·80

m. Initial slag mass = b - a = 395·49

n. Final slag mass = c + d + e + f - a - l = 377·19

o. Fume produced = m + h - n - l - g = 44·52

Tin balance

from chemical analyses,

p. Tin content of the final slag = 3·5 (wt.%)

q. Tin content of the matte = 4·25 (wt.%)

r. Total final tin = Tin in final slag + Tin in matte + Tin fume (assuming all fume was SnS)

= 48·76

s. Total initial tin = 47·45

APPENDIX 5

Estimation of $A_v k_1$ and κ^*

a. Bubble diameter

As the orifice Reynold's number was low (2.22) the balance between the buoyancy and surface tension forces can be used to calculate the bubble diameter.

$$\frac{\pi}{6} \cdot d_b^3 \cdot g(\rho_{slag} - \rho_{gas}) = \pi \, d_0 \, \sigma_{slag} \qquad (5\text{-}1)$$

(See Table 5.2 for the meaning of the symbols used). A value of 500 dynes/cm. for σ_{slag} is considered reasonable. Taking a value of 3 gms/cc for ρ_{slag} (d_0 = 0·4cm), d_b^3 = 0·349cc or d_b = 0·70cm.

Bubble generation at an orifice in viscous liquids was studied in a classical investigation by Davidson and Schuler[64] and they give the following expression for the bubble volume.

$$V_b = (4\pi/3)^{\frac{1}{4}} \cdot (15\nu V/2g)^{3/4} \qquad (5\text{-}2)$$

Using a value of 0·66 St. for ν, d_b calculated would be 0·68cm. Thus a value of 0·7cm is used.

b. Residence time

Grace etal[65] give the generalized correlation between Reynolds number, Morton number and Eotvos number ($gd_b^2\Delta/\sigma$) for freely rising bubbles in liquids. This was used to calculate the Re_b as 200 and 100. For values of 1p and 2p for slag viscosity, the terminal velocities were equal to 71·6 cms/sec. Sometimes the following expression is also used for finding the terminal velocity of a rising bubble in liquids[66].

$$U_t = \left[\frac{4(\rho_l - \rho_g) g \, d_b}{3\rho_l \cdot f}\right]^{\frac{1}{2}} \qquad (5\text{-}3)$$

Using a value of 1·0 for f the friction factor, (as Re_b was 100) U_t would be 30·3 cm/sec. A value of 50 cm/sec. has been used. Thus for the slag bath of 4 cm, the residence time is 0·08 sec.

c. A_v value

A_v is the total slag/gas contact area per unit volume of the slag bath.

Total gas/slag area = Surface area of a bubble × Total number of bubbles

= Surface area of a bubble x frequency of bubble generation × residence time of a bubble

$$= 4\pi r^2 \times \frac{V}{V_b} \times t_e \qquad (5\text{-}4)$$

$$= 6{\cdot}85 \text{ cm}^2,$$

For the slag bath of 100 cc volume, $A_v = 0{\cdot}069/\text{cm}$.

d. κ_l and κ_g values

For both SnO and FeO, the same value of κ_l is used. As surface renewal theory operates (section 5.2.2) κ_l is given by

$$\kappa_l = 2(D/\pi t_e)^{\frac{1}{2}} \qquad (5\text{-}5)$$

A value of 5×10^{-5} cm^2/sec for Diffusivity in slags is considered reasonable[29,67]. Using that value $\kappa_l = {\cdot}0096$ cm/sec. A value of 0·01 cm/sec is used.

Eqn. (5-5) can also be used to calculate κ_g if the diffusivity of H_2O in H_2 at 1543°K is used. Using the methods given by Perry[63], the diffusivity of H_2O in H_2 at 1543°K was estimated to be 7·55 cm^2/sec. This gives a value of 10·96 cm/sec for κ_g. A value of 10·0 cm/sec is used.

Thus for $A_v\kappa_l$ a value of 7×10^{-4}/sec and for κ^* (κ_g/κ_l) a value of 10^3 are used.

APPENDIX G

Room temperature experiments

Room temperature experiments were carried out on the NH_3-cyclohexanol system to determine $A_v K_1$ independently in a system known to be controlled by mass transfer. This system was chosen as NH_3 has a high solubility in cyclohexanol (1·26 mole of NH_3 in 1 lit. of liquid at S.T.P)[73] and cyclohexanol has a reasonably high viscosity (60 c.p.) at 25°C[74].

The same apparatus (similar refractory crucibles and gas lances as those in the high temperature experiments) was used. Pure NH_3 was bubbled at 600 ml/min (same molar flow rate as in the H_2 reduction runs) through 100 ml of cyclohexanol. After the required 'reaction time' the solution was analysed for its ammonia content. The ammonia was completely desorbed by passing N_2 through the cyclohexanol and was collected in a standardized HCl solution. By back titrating the HCl solution (against Borax) the NH_3 absorbed was calculated. The curve for absorption against time is shown in fig. A6-1.

A total of nine absorption runs were carried out but owing to deterioration of cyclohexanol (becoming yellow in colour) some were rejected. Also, the value of the saturation solubility for NH_3 in cyclohexanol given in the literature was found to be incorrect. From the rate curve the value of $A_v K_1$ was found to be $9{\cdot}6 \times 10^{-4}$ sec^{-1}. This is roughly comparable to that for Fe^{2+} and Sn^{2+} in slags at 1300°C[29,67].

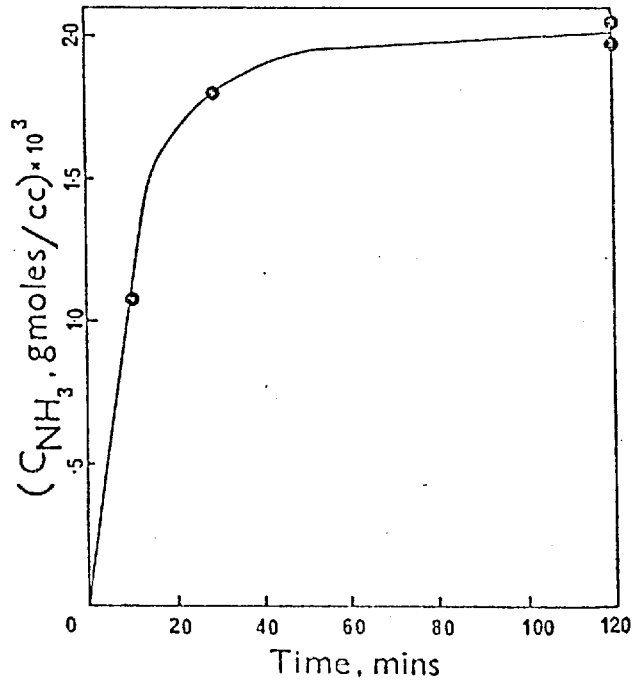

Fig. A6-1, absorption of NH_3 in cyclohexanol at 25°C.

APPENDIX 7

Calculation of Heat change for the SnO fuming reaction $SnO_{(l)} = SnO_{(g)}$

$$\tfrac{1}{2}\,SnO_{2(s)} + \tfrac{1}{2}\,Sn_{(s)} = SnO_{(g)} \quad : \quad \Delta H^{\circ}_{298} = 73{\cdot}5\ (\pm 2{\cdot}1)\ \text{K.cals.}^{15} \qquad (1)$$

$$Sn_{(s)} + O_2 = SnO_{2(s)} \quad : \quad \Delta H^{\circ}_{298} = -138{\cdot}82\ (\pm{\cdot}8)\ \text{K.cals.}^{11} \qquad (2)$$

$$Sn_{(s)} + \tfrac{1}{2}\,O_2 = SnO_{(s)} \quad : \quad \Delta H^{\circ}_{298} = -68{\cdot}35\ (\pm{\cdot}2)\ \text{K.cals.}^{11} \qquad (3)$$

$$SnO_{(s)} = SnO_{(l)} \quad : \quad \Delta H^{\circ}_{298} = 7\ \text{K.cals.}^{12} \qquad (4)$$

From (3) and (4),

$$Sn_{(s)} + \tfrac{1}{2}\,O_2 = SnO_{(l)} \quad : \quad \Delta H^{\circ}_{298} = -61{\cdot}35\ \text{K.cals.} \qquad (5)$$

Multiplying (2) by $\frac{1}{2}$ and subtracting from (5),

$$\tfrac{1}{2}\,Sn_{(s)} + \tfrac{1}{2}\,SnO_2 = SnO_{(l)} \quad : \quad \Delta H^{\circ}_{298} = 8{\cdot}06\ \text{K.cals.} \qquad (6)$$

From (6) and (1),

$$SnO_{(l)} = SnO_{(g)} \quad : \quad \Delta H^{\circ}_{298} = 65{\cdot}44\ \text{K.cals.} \qquad (7)$$

Perhaps the error in the ΔH°_{298} of reaction (7) is as high as 5 K.cals. But it can be said that the fuming of SnO is strongly endothermic.

APPENDIX 8

Calculation of surface tension of the slag:

The slags removed from the furnace contained metal beads at the top surface. One such sample was taken and sheared to measure the contact angle. The two angles measured gave values of 20° and 60° for Φ and θ respectively.

A force balance gives

$$\gamma_{S/G} = \gamma_{S/M} \cos\theta + \gamma_{M/G} \cos\Phi \qquad (A6\text{-}1)$$

$$= \gamma_{S/M} \cos 60 + \gamma_{M/G} \cos 20$$

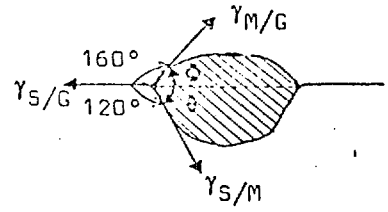

Fig. A6-1
Metal bead at the slag top surface.

$\gamma_{M/G}$ for tin is 600 dynes/cm[68]. However, for $\gamma_{S/M}$, Antonov's approximate rule[69] used by Turpin and Elliott[70] is used, according to which,

$$\gamma_{AB} = | \gamma_A - \gamma_B |$$

Thus $$\gamma_{S/M} = (\gamma_{M/G} - \gamma_{S/G}) \qquad (A6\text{-}2)$$

Using equation (A6-1) in (A6-2) and the value of $\gamma_{M/G}$ as 600 dynes/cm. gives $\gamma_{S/G}$ equal to 576 dynes/cm. However, using $\gamma_{S/M} = (\gamma_{S/G} - \gamma_{M/G})$ gives a value of 528 dynes/cm. Thus a value of 550 dynes/cm. seems appropriate.

This may be checked by calculating the critical diameter for the metal bead to sink into the slag. This is done by making a force balance on the bead.

Weight of the bead = Buoyancy force + Surface tension force of the slag.

$$\frac{4}{3}\pi r_b^3 \cdot \rho_{Tin} \cdot g = f \cdot \frac{4}{3}\pi r_b^3 \rho_{slag} \cdot g + 2\pi r_b \cdot \gamma_{S/G}$$

where f is the fraction of the bead (≈ 2/3rds) immersed in the slag. Taking a value of 3 gms/cm for ρ slag, r_b would be 3·9 mm. From practice this is found to be the case. Thus a value of 550 dynes/cms for the surface tension of tin slags seems correct.

ACKNOWLEDGEMENTS

I wish to express my gratitude to Dr D.G.C. Robertson for his advice, encouragement and supervision during the course of the research work and in the production of this thesis. I am also grateful to him and Prof. F.D. Richardson for the financial assistance received during the period of this research.

I would like to thank Mr P.A. Wright, on whose suggestion the sulfide fuming experiments were carried out, for permitting the results of those experiments to be included in the thesis. My sincere appreciations are due to Dr J. Williamson for the X-ray diffraction analyses, Dr R.J. Tait for the supervision in the first four months of this work and Dr T. Debroy and Mr A. Narayanan for useful discussions and help received during this work.

I thank the technicians of the Chemical Metallurgy Laboratory for their co-operation and help during the chemical analyses. I am grateful to Mr D.S. Conochie for proof reading and Miss Suzanne Tait for typing the thesis.

S.R. Chandrashekar

REFERENCES

1. KENWORTHY, H., STARLIPER, A.G., and FREEMAN, L.L.
   U.S. Bureau of Mines, Report of Investigations 5327

2. KATKOV, O.M.
   Tsvet. Metally., 1967, 8, P45

3. DAVEY, T.R.A.
   Australian Mining, 1966(9), 58, P28

4. FLOYD, J.M. and THURLBY, J.A.
   Australian Mining, 1972(8), 64, P72

5. CARBO NOVER, J. and RICHARDSON, F.D.
   Trans I.M.M., 1972, 81, C63,

6. SPANDAU, H. and KOHLMEYER, E.J.
   Z. Metallk, 1949, 40, P374

7. BEREZKINA, L.G., ERMAKOV, N.I. and CHIZIKOV, D.M.
   Zn. Neorg. Khim., 1964, 9, P1760
   Russ. J. Inorg. Chem., 1964, 9, P53

8. SESHADRI, S.K.
   Ph.D. Thesis, University of London, 1973

9. KESSELITZ, B. and KOHLMEYER, E.J.
   Z. Metallerz, 1933, 30, P185

10. SLONIMSKII, B.I. and TSEIDLER, A.A.
    Tsvet. Metally, 1959, 15, P173
    Chem. Abstr., 1960, 54, 20723

11. WRIGHT, P.A.
    'Extractive Metallurgy of Tin', Elsevier, 1966, P228

12. DAVEY, T.R.A. and FLOYD, J.M.
    Proc. Aust. I.M.M., No. 219, P1

13. ELLIOTT, J.F. and GLEISIER, M.
    'Thermochemistry for Steelmaking', Vol. I, 1960

14. KOZUKA, Z., SIAHAAN, O.P. and MORIYAMA, J.
    Chemical Abstract, 1968, 68, 81899

15. COLIN, R., DROWART, J. and VERHAEGEN, G.
    Trans. Faraday Soc., 1965, 61, P1364

16. KELLOGG, H.H.
    Trans. A.I.M.E. 1966, 236, P602

17. COCHRAN and FOSTER
    J. Electrochem., 1962, 109, P144

18. PLATTEUW, J.C. and MEYER, G.
    Trans. Faraday Soc., 1956, 52, P1066

19. TIN RESEARCH INSTITUTE
    'Equilibrium data for Tin alloys', Greenford 1949

20. CAMPBELL, A.N., WOOD, J.H. and SKINNER, G.B.
    J. Am. Chem. Soc., 1949, 71, P1729

21. MILLS, K.C. and TURKDOGAN, E.T.
    Trans. A.I.M.E., 1964, 230, P1202

22. DAVEY, T.R.A.
    Trans. I.M.M., 1967, 76, P65

23. KOKOVSKII, I.A. and SMIRNOV, N.S.
    Izv. Akad. Nauk SSSR otd. Techn. Nauk., 1957 (11), P44

24. SHIRAISHI, S.Y. and BELL, H.B.
Trans. I.M.M., 1968, 77, C104

25. SHIRAISHI, S.Y. and BELL, H.B.
Trans. I.M.M., 1970, 79, C120

26. DAVEY, T.R.A.
Trans. I.M.M., 1967, 76, C278

27. SHELLEY, T.R. and SHELLEY, R.
Trans. I.M.M., 1973, 82, C54

28. LATHE, F.E.
Can. I.M.M. Trans., 1950, 54, P95

29. SZEKELY, J. and THEMELIS, N.J.
'Rate phenomena in Process Metallurgy' 1971

30. HIGGINS, R. and JONES, T.J.B.
Trans. I.M.M., 1963, 72, P824

31. HARRIS, J.H. and HALETT, G.D.
Proc. Aust. I.M.M., 1967(9), P75

32. SESHADRI, S.K.
Ph.D. Thesis, University of London, 1973, P131

33. GIMMELFARB, A.A.
Russ. Met., 1968, 2, P42

34. MAKATO KATO and SUSUMU MINOWA
Trans. Iron and Steel Inst. of Japan, 1969(1), 9 P31

35. WATANABE, M.
Japan Sci. Rev. Ser., 1950, 1, P67

36. CHIZIKOV, D.M. and KOZANOV, E.I.
Izv. Akad. Nauk. SSSR, 1948, P223

37. BODSWORTH, C.
J. Iron and Steel Inst., 1959, 193, P3

38. BISWAS, A.K. and RANKIN, W.J.
Proc. Aust. I.M.M., 1974(3), 249, P5

39. FINK, C.G. and MANTELL, C.L.
Engg. and Mining Journal, 124(18), P686

40. FLOYD, J.M.
Presented at the Institute of Fuels Conference, Adelaide, Nov. 1974.

41. DAVEY, T.R.A.
Aust. Mining, 1969 (Aug), P62

42. FLOYD, J.M.
Fourth world conference on Tin, Kuala lumpur, 30 Oct. - 5 Nov. 1974

43. GNALOVSKII, E.S. et al
Tsvet. Metally, 1970(5), 43, P27

44. KOSTELOV, V.V. and GRINEVICH, I.N.
Tsvet. Metally, 1962(10), 35, P39

45. KOSTEZOV, V.V. et al
Tsvet. Metally, 1966(8), 39, P41

46. DECROLY, C., GHODSI, M. and WINAND, R.
Trans. I.M.M., 1967, 76, C259

47. DEBROY, T. and ROBERTSON, D.G.C.
Private communication

48. POGGI, D., MINTO, R. and DAVENPORT, W.G.
J. Metals, 1969(11), P40

49. MINTO, R. and DAVENPORT, W.G.
Trans. I.M.M., 1972, 181, C36

50. KATKOV, O.M. and EUSEEV, A.P.
Tsvet. Metally, 1973(4), P17

51. KUBASHEWSKI, O., EVANS, F.L.L. and ALCOCK C.B.
'Metallurgical Thermochemistry' 1967

52. KELLY, K.K.
U.S. Bureau of Mines, Bulletin 476, 1949

53. FEBER, R.C., HERRICK, C.C. and LEHENION
J. Chem. Thermodynamics, 1969(2), 1, P169

54. TIN RESEARCH INSTITUTE
Private communication, 1977

55. RICHARDSON, F.D.
'Physical Chemistry of Melts' Vol II, 1976

56. SHELLEY, T.R. and CHARLES, J.A.
Trans. I.M.M., 1970, 70, C259

57. SHELLEY, T.R. and CHARLES, J.A.
Trans. I.M.M., 1974, 83, C18

58. BARRETT, M.F, HOWIE, F.H. and SAYCE, I.G.
Trans. I.M.M., 1975, 84, C18

59. FLOYD, J.M.
Trans. I.M.M., 1973, 82, C51

60. BRADSHAW, A.V.
Trans. I.M.M., 1970, 79, C281

61. HILLS, A.W.D.
'Heat and Mass transfer in Process Metallurgy', I.M.M., 1968

62. WARNER, N.A.
'Advances in Extractive Metallurgy', I.M.M., 1967

63. PERRY, R.H.
Chemical Engineer's Handbook, 1963

64. DAVIDSON, J.F. and SCHULER, B.O.G.
Trans. Inst. Chem. Engrs., 1960, 38, P145

65. GRACE, J.R., WAIREGI, T. and NGUYEN, T.H.
Trans. Inst. Chem. Engrs., 1976, 54, P167

66. CHITTA R. NANDA and GORDEN H. GEIGER
Met. Trans. 1971(4), 2, P1101

67. RYZHONKOV, D.I. and FILIPPOV, S.I.
Steel in U.S.S.R., 1971(11), P841

68. GROSSE, A.U.
J. Inorg. Chem., 1964, 26, P1349

69. DEFAY, et al
Liege Deosoer, 1951, 52, P161

70. TURPIN, M.C. and ELLIOTT
J. Iron and Steel Inst., 1966(3), P217

71. DEBROY, T., EL-KADDAM, N.H. and ROBERTSON, D.G.C.
Met. Trans. B, 1977(6), 8, P271

72. THEMELIS, N.J. and SCHMIDT, P.R.
Trans, A.I.M.E., 1967, 239, P1313

73. International Critical Tables
Vol. 3, P264

74. International Critical Tables
Vol. 7, P218

75. BIRD, R.B., STEWART, W.E. and LIGHTFOOT, S.I.
'Transport Phenomena' 1960

76. MUAN and OSBORN
'Phase equilibria among oxides in Steelmaking', 1965

77. WRIGHT, P.A.
'Extractive Metallurgy of Tin' 1966